Impact of repetitive particle exposure and latent viral infection on lung immunity and diseases

von

Eva Marie Günther

Inaugural-Dissertation zur Erlangung der Doktorwürde
der Tierärztlichen Fakultät der Ludwig-Maximilians-Universität
München

Impact of repetitive particle exposure and latent viral infection on lung immunity and diseases

von
Eva Marie Günther

aus
Lindau am Bodensee

München 2025

Aus dem Veterinärwissenschaftlichen Department der Tierärztlichen Fakultät der Ludwig-Maximilians-Universität München

Lehrstuhl für Molekulare Tierzucht und Biotechnologie

Arbeit angefertigt unter der Leitung von:

Univ.-Prof. Dr. Eckhard Wolf

Angefertigt am Institut für Lungengesundheit und Immunität (LHI)

Helmholtz Zentrum München

Mentoren:

Dr. Tobias Stöger und Prof. Dr. Heiko Adler

Gedruckt mit Genehmigung der Tierärztlichen Fakultät

der Ludwig-Maximilians-Universität München

Dekan:	Univ.-Prof. Dr. Reinhard K. Straubinger, Ph.D.
Berichterstatter:	Univ.-Prof. Dr. Eckhard Wolf
Korreferent:	Priv.-Doz. Dr. Bianka Schulz

Tag der Promotion:

26. Juli 2025

Für meine Eltern

TABLE OF CONTENTS

TABLE OF FIGURES

ABBREVIATIONS

ACTUB	Acetylated alpha tubulin
AD	Antibody diluent
AQP5	Aquaporin 5
AT1	Alveolar type 1 cell
AT2	Alveolar type 2 cell
BAL	Bronchoalveolar lavage
BALF	Bronchoalveolar lavage fluid
BCA	Bicinchoninic Acid
BSA	Bovine serum albumin
CB	Carbon black
CK18	Cytokeratin 18
CMV	Cytomegalovirus
CNP	Carbonaceous nanoparticle
COPD	Chronic obstructive pulmonary disease
DNA	Deoxyribonucleic acid
EBV	Epstein-Barr virus
EHV-5	Equine herpesvirus 5
ELISA	Enzyme-linked immunosorbent assay
EMPF	Equine multinodular pulmonary fibrosis
FBS	Fetal bovine serum
FVC	Forced vital capacity
H&E	Haematoxylin and Eosin
HIER	Heat induced epitope retrieval
HOPX	Homeodomain only protein homeobox
i.n.	intranasal
i.p.	intraperitoneal
IAD	Inflammatory airway disease
iBALT	inducible bronchial associated lymphoid tissue
IF	Immunofluorescence staining
IgM	Immunoglobulin M
IHC	Immunohistochemistry staining
IPF	Idiopathic pulmonary fibrosis
IVC	Individually ventilated cages
Krt8	Keratin 8
KSHV	Kaposi's sarcoma-associated herpesvirus
LPS	Lipopolysaccharide
MAPK	Mitogen-activated protein kinase
MHV-68	Murine gamma herpesvirus 68
miRNA	Micro ribonucleic acid
MLI	Mean alveolar linear intercept
MMC	Mitomycin C
MMF	Medetomidine-Midazolam-Fentanyl anesthesia mixture
mRNA	Messenger ribonucleic acid
NK-cell	Natural killer cell
NKG2D	Natural-killer receptor group 2, member D
NP	Nanoparticle
ORF4	Open reading frame 4
ORF50	Open reading frame 50
ORF73	Open reading frame 73
PBS	Phosphate-buffered saline
PFA	Paraformaldehyde
PFU	Plaque Forming Units
PM_{10}	Particles smaller than 10 µm
$PM_{2.5}$	Particles smaller than 2.5 µm
qPCR	Quantitative polymerase chain reaction
RCF	Relative centrifugal force
RNA	Ribonucleic acid
RPM	Rounds per minute
RSV	Respiratory syncytial virus
s.c.	subcutaneously
SD	Standard deviation
Sftpb	Surfactant protein C
Sftpc	Surfactant protein C

SPB	Surfactant protein B
SPC	Surfactant protein C
Tuba1a1	Alpha tubulin
TUNEL	TdT-mediated dUTP-biotin nick end labeling
UFP	Ultrafine particle
vUNG	viral uracil DNA glycosylase
WHO	World health organization
αSMA	Alpha smooth muscle actin

I. INTRODUCTION

With a total alveolar surface area of approximately 70 m^2, the lungs are the largest part of the body that is in constant contact with the environment [1]. The average adult human exchanges 0.5 liters of air per breath, known as tidal volume. At a breathing rate of 12 times per minute, this results in a total volume of 6 liters passing through the lungs within one minute [2]. To enable effective gas exchange, a huge as well as very thin surface area is obligatory. The less than 2 µm thin air-blood barrier does not provide space for mucus or cilia as physical barriers against inhaled pathogens and other harmful agents [3]. This means that people inhale and exhale thousands of liters of air every day; air, that can contain various pathogens and ambient particles that are potentially harmful to lung health.

Herpesviruses are omnipresent in our society and in the animal world. More than 90% of adults worldwide are infected with at least one herpesvirus [4]. This is due to the fact, that herpesviruses do have the unique ability to establish lifelong latency within a host. Once infected, the host's immune system is unable to completely eliminate the virus as various viral mechanisms lead to an immune evasion of the host's response [5]. During latency, virus and host immune response stay in a certain balance [6]. This can get disrupted by several triggers like stress, UV-light, hormonal imbalance, co-infections or just immunosuppression, which can lead to viral reactivation and production of infectious particles [7].

One proposed trigger for viral reactivation is pulmonary exposure to carbonaceous nanoparticles [8,9]. The World Health Organization (WHO) estimates that 6.7 million deaths per year are linked to air pollution and that 99.9% of people worldwide live in areas where air quality standards are exceeded.

In view of these omnipresent challenges for lung health it is of great importance to investigate and understand the interaction between latent herpesvirus infection and ambient particle exposure in respiratory diseases.

1. Herpesviruses

1.1. Taxonomy

Orthoherpesviridae is the designation of a family of enveloped, spherical viruses with a linear, double-stranded DNA genome ranging in sizes from 125 to

241 kilobase pairs. Herpesviruses have coevolved with their hosts and are thus highly adapted to them [10]. They play a significant role in disease progression for humans, horses, cattle, pigs, cats, dogs and poultry [11]. The family of Herpesviridae includes three subfamilies: Alpha, Beta and Gamma herpesvirinae, with their main common characteristic to establish lifelong latency in host cells. For most alpha herpesviruses for example, latent infection occurs in the peripheral nerval system. Herpes simplex virus 1 and 2 and varicella zoster virus are the three members of alpha herpesviruses infecting humans, Marek's disease virus, infectious bovine rhinotracheitis virus, canine herpesvirus, equine abortion virus or feline herpesvirus are just some of the many amongst various other species [12]. Human beta herpesviruses include human cytomegalovirus (CMV) and human herpesvirus 6 and 7, with a latency tropism in hematopoietic stem cells. The species-specific beta herpesviruses in animals include, amongst others, suid herpesvirus 2, rhesus cytomegalovirus and murine cytomegalovirus [12]. With an establishment of latency mainly in B-lymphocytes, gamma herpesviruses are especially species- and cell-specific. Human members are Epstein-Barr virus (EBV) and human herpesvirus 8, also known as Kaposi's sarcoma-associated herpesvirus (KSHV). Sheep-associated malignant catarrhal fever virus, porcine lymphotropic herpesvirus 1, 2 and 3, equine herpesvirus 2 and 5 and murine gamma herpesvirus 68 (MHV-68) are only some important members of gamma herpesviruses in different animal species [12].

1.2. Life cycle

In an example of the human gamma herpesvirus Epstein-Barr virus, we can observe four stages in the life cycle of herpesviruses: primary infection, lytic replication, latency, and reactivation. Following primary infection in oropharyngeal epithelial cells and B-cells [13] with attachment and fusion of the herpesvirus envelope with the cell membrane, lytic replication of viral DNA takes place in the nucleus. With a well-orchestrated sequence of viral gene transcription, mRNA translation and replication of the circulated viral DNA, assembled virions are released from infected cells and can spread horizontally to other epithelial or B-cells [11]. The paradigm of herpesviruses is to establish lifelong latency. In this state, the viral genome is stored as extrachromosomal DNA plasmids, in case of EBV mainly in circulating memory B-cells, and only a few viral genes are expressed [14]. Besides periodic reactivation, different stimuli can induce reactivation and lead to reentering

into the lytic replication with production of lytic virus. Apart from well-known reactivation triggers like differentiation of B-cells into plasma cells [15] or activation of B-cells through cytokines or T-cell interaction [16,17], additional extrinsic factors might cause reactivation. As described by Stöger and Adler, these "novel" triggers of herpesvirus reactivation play an equally important role regarding human and animal health and include for example pulmonary exposure to environmental particles [7].

1.3. Epidemiological relevance

"Einmal Herpes, immer Herpes" is a German saying emphasizing the fact, that the host immune system is unable to eliminate this pathogen completely. The peculiarity of latency leads to a massive seroprevalence worldwide with more than 90% of human populations carrying at least one type of herpesvirus [4]. Several studies performed in different areas worldwide could show a high seroprevalence for different herpesvirus species. 97.9% of samples from blood donors living in Qatar and originating from different countries like Egypt, Syria, Jordan, Pakistan or India were tested seropositive for EBV capsid antigens [18]. Similar numbers could be observed in a study including samples from 4 different populations in Uganda, Singapore and Nancy [19] and in another study in southern India [20]. Regarding all herpesvirus families, Virgin et. al summarized the high estimated percentages of people being infected, with EBV and CMV being the most prevalent between 80 and 90% [21]. Not only among humans, within the whole animal world herpesvirus infections play a huge role. In horses, cattle, dogs and cats for instance, different herpesviruses are detectable amongst several populations worldwide [22-25]. This global and ubiquitous infection pattern emphasizes the importance to investigate interactions between latent gamma herpesvirus infections and different triggers, co-infections and extrinsic factors, that could lead to reactivation and disease outbreak or progression.

1.4. Murine gamma herpesvirus 68 as small animal model

As described beforehand, gamma herpesviruses do have a strict species specificity and therefore make studies on EBV or KSHV regarding human infection, reactivation and disease progression difficult. Murine gamma herpesvirus 68 (MHV-68) is a widely used small animal model helping to understand pathogenesis and viral behavior better. MHV-68 is largely homologue to the genome of EBV and

KSHV [26], forming a robust model for gamma herpesvirus research.

Intranasal infection of laboratory mice with MHV-68 leads to a primary productive infection in alveolar epithelial and mononuclear cells in the lungs within the first week. Infected B-lymphocytes spread infectious virus to the whole body leading to splenomegaly, thymus enlargement and pulmonary cell infiltrations ten days after infection. At this timepoint, viral antigens are hardly detectable anymore. Latency establishes two weeks after infection, mainly in B-cells of the spleen but additionally in pulmonary epithelial cells and macrophages. This state of latency persists throughout the life of a host, with the possibility to reactivate following exogenous stimuli or a general immunosuppression. Reactivation leads to the production of infectious virus and restarts the circle of viral spread and infection, although distinct in some features from the acute infection phase [27-30].

2. Ambient particles

2.1. Air pollution as a health risk

Air pollution is considered an important human and planetary health burden linked to cardiovascular and pulmonary diseases. Data of the WHO from 2019 show that 99% of the world's population are living in regions exceeding the WHO global air quality guidelines, resulting in an inevitable pulmonary stress. Recently, the council of the European Union published a statement to align air quality standards more closely with the ones from WHO and reduced existing threshold limits drastically. Accordingly, the Global Burden of Disease Study 2019 estimates 6.67 million premature deaths related to household and ambient air pollution [31].

Pulmonary air pollution exposure is similarly relevant in pets. A study conducted with stray dogs in Mexico City in 2001 used canines as sentinels to investigate the effect of chronic air pollution exposure on the lung. This study revealed particle laden macrophages and ultrafine particles in epithelial cells, endothelial cells and interstitial macrophages in the lungs of those dogs [32]. Another study on stray dogs from 2022 could also show relevant particle deposition in the lungs of those animals associated with pulmonary lesions [33]. In addition, indoor air pollution can exacerbate airway diseases in pets like cats and dogs [34] and environmental particle exposure is associated with a higher risk of lung cancer in dogs [35]. Increased air pollution exposure declines the athletic performances of race horses [36] and is

associated with lower airway inflammation in horses [37].

2.2. Inhaled particles

Besides carbon monoxide, ozone, nitrogen dioxide and sulfur dioxide, particulate matter (PM) is emitted to the environment and the main component of ambient particles. PM is defined by the WHO as "a mixture of solid and liquid particles in the air that are small enough not to settle out in the Earth's surface under the influence of gravity, classified by aerodynamic diameter" [38]. This classification includes particles smaller than 10 µm (PM_{10}), smaller than 2.5 µm ($PM_{2.5}$) and ultrafine particles smaller than 0.1 µm, also referred to as nanoparticles (NPs) or ultrafine particles (UFPs) (**Figure 1**). Depending on their aerodynamic size, deposition of inhaled particles in the respiratory tract varies. PM_{10} particles deposit mainly in the large conducting airways and at bifurcations, whereas fine particles, like $PM_{2.5}$, can reach deeper into the lungs and deposit within the whole respiratory tract, particularly in small airways and alveoli. The smallest particles with sizes less than 100 nm can easily deposit in the alveolar region and due to their high surface area show highest pulmonary toxicity, compared to bigger particles [39,40].

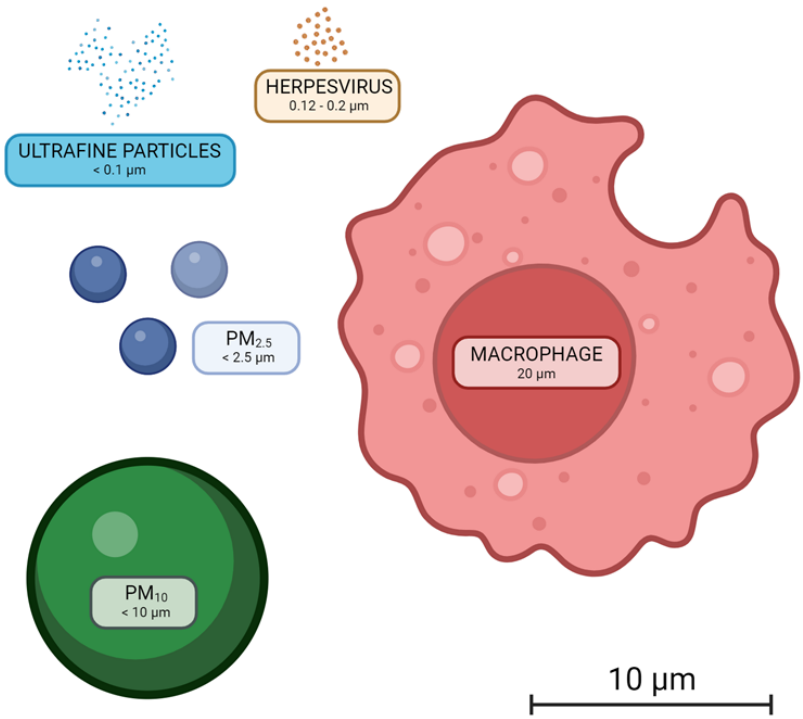

Figure 1 *Illustration of the sizes of PM_{10}, $PM_{2.5}$ and ultrafine particles in reference to herpesvirus particles and a macrophage.*

Adapted from [41]. Created with Biorender.

In general, the lungs are equipped with various defense mechanisms to avoid deposition and retention of harmful substances. The first line of defense is physical translocation. Alveolar macrophages engulf solid particles through phagocytosis and move gradually towards the mucociliary escalator. Mucus is then transported in an upstream direction towards the upper airways by ciliated bronchial cells and the inhaled particles get cleared from the lungs. For the smallest particle sizes, phagocytic clearance is slow and ineffective, which can lead to pulmonary accumulation and retention of nondegradable particles. Those NPs are also able to interact with epithelial cells and translocate into the interstitium and subsequently into the blood or lymphatic circulation, depending on characteristics like size, charge, or coating. Subsequently, the particles can be distributed to different organs and lymph nodes and accumulate in those secondary tissues [42].

2.3. Carbonaceous nanoparticles in the lung

Carbon black (CB), also referred to as carbonaceous nanoparticle (CNP) in this thesis, is a nanosized material consisting of over 95% elemental carbon. Primary spherical particles between 10 and 20 nm form bigger aggregates and agglomerates. Approximately 15 million metric tons CB are produced annually by partial combustion or thermal decomposition of hydrocarbons under controlled conditions and are used for the production of automobile tires, non-tire industrial rubber and to a smaller proportion for products like plastics, ink or paints [43-45]. Potential pulmonary exposure occurs within the production and handling of CB as well as to a smaller amount within the downstream manufacturing industries [45].

Inhalation of those carbonaceous particles smaller than 100 nm is described to induce an acute neutrophilic inflammation in mouse lungs [46,47]. In one study, our research group could observe an accumulation of neutrophil granulocytes in bronchoalveolar lavage (BAL) samples as early as 12 hours after particle exposure. This transient inflammation was completely resolved within 7 days. Particles were already taken up by alveolar macrophages within the first 3 hours after exposure, with 90% of recovered BAL alveolar macrophages being particle laden after 12 hours. Although pro-inflammatory cytokine release and gene expression induction in the lung was highest 12 hours after CNP exposure, alveolar macrophages were, according to the gene expression, not involved in this increase. In contrast, alveolar type 2 cells (AT2s) got activated and expression of the neutrophil chemoattractants Cxcl1 and Cxcl5 was induced [48]. As alveolar

epithelial cells are the first to get into contact with CNPs in the lung, the response or injury of AT2s could be an initial driver for acute neutrophilic inflammation.

3. Chronic lung diseases in association with virus infection and nanoparticle exposure

Viral infections as well as pulmonary nanoparticle exposure can be linked to the development and progression of different chronic lung diseases. According to the Global Burden of Diseases, Injuries, and Risk Factors Study 2019, chronic lung diseases count as the third leading cause of deaths worldwide after cardiovascular diseases and cancer. With 454 million cases worldwide, the prevalence has increased since 1990. Chronic obstructive pulmonary disease (COPD) for example accounts for the majority of deaths from chronic lung diseases, meanwhile Asthma has the highest prevalence [49]. In the following section, relations between the most important lung diseases like idiopathic pulmonary fibrosis (IPF), COPD, Asthma and lung cancer with viral infections and air pollution will be discussed in detail.

3.1. Idiopathic pulmonary fibrosis

Idiopathic pulmonary fibrosis is a chronic, progressive interstitial lung disease of unknown cause, characterized by progressive lung scarring and interstitial pneumonia associated with dyspnea and worsening of lung function. It has a prevalence of around 10 to 60 cases per 100,000 people and affects primarily older adults. Prognosis for patients is poor with a median survival of 3 to 5 years without treatment. Martinez et al. propose a pathogenetic model of how the complex disorder develops. Genetic susceptibility, ageing and environmental factors are the main drivers leading to epigenetic reprogramming and aberrant alveolar epithelial cell activation and injury. Secretion of different mediators induces migration, proliferation and activation of fibroblasts and myofibroblasts. These fibroblasts secrete extracellular matrix components, which in addition contain growth factors and lead to a positive feedback loop between fibroblast activation and matrix stiffness. This results in stiff lungs with decreased volume and gas exchange [50,51].

Environmental exposures and chronic viral infections are amongst others listed as risk factors for developing IPF.

In view of these factors, there are several studies conducted showing that herpesviruses can be detected in lung tissue of IPF patients more often than in

healthy control patients. Especially DNA of gamma herpesviruses EBV and KSHV and beta herpesviruses CMV and human herpesvirus 6 are found in IPF patients, suggesting a relation between viral infection and the occurrence of this lung disease [52-55].

In domestic animals, an association between the equine IPF equivalent and so called equine multinodular pulmonary fibrosis (EMPF) and an infection with equine herpesvirus 5 (EHV-5) is described in horses. EHV-5 is frequently isolated in horses suffering from EMPF and Williams and colleagues could even show that an experimental infection with EHV-5 induces lung fibrosis in horses, with similar features to EMPF [56-61].

In addition to that, exposure to air pollution can be linked to a decline in lung function, exacerbations and even increased mortality in patients suffering from IPF. A study in the US examined the forced vital capacity (FVC), a measurement for lung function, of 135 IPF patients within a timeframe of six years and correlated the rate of decline in FVC with the average particulate matter concentration at each patient's residential address. There was a significant association between higher PM_{10} concentrations and the rate of decline in FVC [62]. Another study, conducted by Johannson and colleagues in 2018 shows an overall lower lung function in IPF patients associated with higher air pollution exposures [63]. Low baseline lung function, disease progression and higher mortality were also linked to $PM_{2.5}$ exposure within parts of a cohort study with 6683 patients [64]. Accordingly, long-term exposure to air pollutions like $PM_{2.5}$ and PM_{10} can act as a risk factor for exacerbations in patients suffering from IPF [65].

3.2. Chronic obstructive pulmonary disease

As described above, COPD is the third leading cause of death worldwide, leading to 3.23 million deaths in 2019 according to the WHO. Chronic lung inflammation and persistent and often progressive airway obstruction characterize this heterogeneous disease. The presence of chronic symptoms, such as cough and sputum production, is indicative of a chronic bronchitis. A hypersecretion and overproduction of mucus by goblet cells as well as impaired elimination narrows the airways and leads to reduced airflow [66]. This can be associated with another leading cause of impaired lung function, namely chronic enlargement of the alveoli, which is termed pulmonary emphysema. Chronic inflammation and oxidative stress

in the alveoli can lead to a loss of elastic recoil and destruction of alveolar septa resulting in an enlargement of the alveolar airspace [67]. This enlargement causes a reduction in respiratory surface area for gas exchange and reduced lung function.

Cigarette smoke is known as the leading cause of COPD, but also occupational and ambient air pollutions as well as pulmonary infections are reported as risk factors for COPD.

For instance, EBV DNA has been detected in the sputum of COPD patients. In this study, stable patients (68) and COPD patients with acute exacerbation (136) were compared to 16 smokers without obstructions. In only one case of non-obstructed smokers EBV DNA could be detected, but around 47% of stable and exacerbation COPD patients were tested positive for EBV in their sputum [68]. In addition, EBV and CMV antigens could be detected using immunofluorescence staining on lung biopsies. Interestingly, the proportion of patients with EBV or CMV antigens in the epithelium was between 68 and 84% in COPD patients in comparison to 6 to 12% in healthy never or former smokers [69].

A cohort study conducted between 2000 and 2018 in the United States assessed the association between long-term exposure to air pollutants and progression of emphysema. They reported a significant increase in emphysema, assessed using computed tomography imaging, associated with higher ambient concentrations of $PM_{2.5}$ and black carbon, amongst others, in 10 years [70]. Liu and colleagues could associate high $PM_{2.5}$ and PM_{10} concentrations with an increased COPD prevalence in a cross-sectional study conducted in southern China. In addition, a decrease in respiratory lung function was likewise linked to higher ambient particle concentrations [71]. There is evidence, that air pollution contributes to prevalence of COPD and lung function to some extent.

3.3. Asthma

Asthma is a chronic inflammatory disease of the respiratory tract. Hallmarks are bronchial hyperreactivity and variable obstruction of the airways. The disease affects 262 million people worldwide and leads to 455 thousand deaths, according to the Global Burden of Diseases, Injuries, and Risk Factors Study 2019. Symptoms include wheeze, cough, shortness of breath and chest tightness. Main drivers for those symptoms are bronchial muscle spasm, mucus hypersecretion and mucosal edema. Asthma is caused by a combination of genetic and environmental factors,

mainly by immunologic responses to allergens. Amongst various others, exposure to air pollution as well as viral infections are listed as risk factors for the development of asthma [72].

A small study from 2021 examined the composition of the pulmonary virome in sputum samples of asthma patients and healthy participants. Interestingly, herpesviruses, especially EBV and CMV, were more abundantly found in the samples of asthma cases than control samples. Herpesvirus abundance showed correlation with asthma severity and lower lung function [73]. Blood samples of patients with asthma and age-matched control people were tested for CMV DNA in a study in Poland. CMV was detected in 41.5% of asthma patients and 13.3% of control subjects. Its occurrence was associated with an increased risk for asthma and lower lung function [74].

Equine asthma is comparable to human asthma referring to symptoms and pathology. In a case-control study including 24 horses with equine asthma and 14 healthy control animals with comparable stabling environments, there was a significant correlation between asthma and detection of equine herpesvirus 2 [75].

More attention is given to studying how air pollution affects asthma patients. Asthma onset in children can already be connected to ambient ozone, $PM_{2.5}$ and nitrogen dioxide exposure [76] and even perinatal exposure to UFPs can be linked to asthma onset [77]. $PM_{2.5}$ can also be associated with asthma exacerbations in children [78-80] and worsening of morbidity [81].

A similar study was also performed for horses. High $PM_{2.5}$ exposure could be associated with an increase in granulocytes in the lower respiratory tract [37].

Taken together, environmental challenges, such as viral infection and particle exposure can be linked to onset and exacerbation of asthma in human and animals.

3.4. Lung cancer

Lung cancer is the leading cause of cancer deaths. Environmental factors such as infections or air pollution have been demonstrated to elevate the risk of cancer development. Indeed, the International Agency for Research on Cancer has classified EBV, KSHV, outdoor air pollution and PM as carcinogenic risks for humans.

Epstein-Barr Virus and Kaposi’s sarcoma-associated virus are known to cause

several neoplasms outside the lungs, including Hodgkin Lymphoma, Burkitt Lymphoma, diffuse large B-cell lymphomas and, as the name states, Kaposi's sarcoma. In the lung, EBV has been detected in bronchoalveolar lavage fluid of patients with bronchogenic carcinoma, supporting the idea of the lung as potential EBV reservoir [82]. Furthermore, EBV has been identified in various forms of lung cancer in multiple studies [83-86]. However, it is essential to consider the limitations of these findings, including the relatively small sample sizes and the rarity of EBV detection in cancerous tissues.

In domestic animals, no such correlation was identified until now.

In contrast, there is a substantial body of evidence indicating a correlation between long-term exposure to ambient particles and the incidence and mortality of lung cancer [87-91]. A meta-analysis conducted by Ciabattini and colleagues included 18 high-quality studies. They report a relative risk for lung cancer incidence and mortality of 1.16 for an increase of 10 $\mu g/m^3$ in $PM_{2.5}$ exposure and 1.23 for PM_{10} [92].

A retrospective study in dogs could also show an increased risk of lung cancer in dogs with higher particle burden in the lungs [35]. This suggests a similar correlation in animals as stated in humans.

3.5. Interplay between virus infection and particle exposure in chronic lung diseases

It is of greater interest to elucidate the interplay between ambient particulate matter and viral infections on human health, rather than to investigate the effects of these ubiquitous hazards separately. The majority of research attention in this field has recently been directed towards the spreading and mortality of SARS-CoV-2 infection in relation to air pollution. Numerous studies indicate that air pollution represents an important risk factor for both, infection with SARS-CoV-2 and the development and mortality of COVID-19 [93-97]. One recent publication describes the cellular mechanisms involved by combining $PM_{2.5}$ exposure and SARS-CoV-2 infection *in vitro*. Apparently, $PM_{2.5}$ increases the infectability and internalization of SARS-CoV-2 in human lung cells by increasing the expression of angiotensin converting enzyme 2 [98]. Furthermore, research is being conducted into other acute respiratory pathogens, including influenza virus and respiratory syncytial virus (RSV). First of all, ambient particles can act as a carrier for viruses as influenza to

reach deep into the lungs [99,100]. Epidemiological studies highlight the increase in influenza transmission and illness associated with increased ambient particles, such as $PM_{2.5}$ [101-104]. Similar relations could be found for RSV, suggesting an influence of the inhalation of air pollution on infection and hospitalization [105-107].

In contrast to these acute viral infections, herpesviruses stay in the host cells in a latent and silent state. It is unlikely that air pollution will affect the infection rate at this stage; however, there is a possibility that it may lead to the reactivation of dormant viruses. Furthermore, it has been suggested that latent viral infections can influence the immune microenvironment, increasing susceptibility to external harms. Few studies underline an effect of inhaled particles on herpesvirus reactivation. A cohort study in China linked solid fuel use with an increased risk of EBV seropositivity and activation [108]. In another Chinese study, miRNAs of EBV, KSHV and CMV were associated with short-term exposure to elemental carbon, but not PM_{10} and $PM_{2.5}$ [109].

Given the complexity of the lung, it is vital to gain a deeper understanding of the interactions and relationships between different external hazards challenging the pulmonary immune system.

4. Aim of the thesis

The objective of this thesis was to gain a more profound understanding of the potential pulmonary health risks associated with the interaction between latent herpes viral infections and chronic exposure to particles in the lung. Research question was, if chronic particle exposure of latently with herpesvirus infected lungs might cause progressive lung inflammation and alveolar injury with subsequent development of chronic lung diseases.

A study conducted in our research group was the first to describe this topic within a mouse model in 2017. Pulmonary nanoparticle exposure of mice, latently infected with MHV-68, resulted in a signature comparable to the acute infection phase. Lytic viral protein production as well as an elevated inflammatory response suggested a reactivation of latent virus in the lungs [8]. A follow-up study was able to target mechanistic processes and include a repeated particle trigger for viral reactivation. Two subsequent nanoparticle exposures to MHV-68 infected mice had progressive effects on mouse lungs. Inflammation signatures were progressively increasing

within the two-time exposure pattern and emphysema-like injury could be detected one week after the repetitive NP exposure. Reactivation of MHV-68 was mainly associated with $CD11b^+$ macrophages and was found to be p38 mitogen-activated protein kinase (MAPK) dependent. In addition, p38 inhibition abrogated viral reactivation upon CNP exposure in mice [9].

Despite the advances in this field, a comprehensive understanding of chronic effects on lung health and inflammatory as well as immunoregulatory mechanisms following particle-triggered viral reactivation remain unclear. This study aimed to add more knowledge to this important topic. To do so, the aforementioned MHV-68 mouse model was expanded to mimic an environmental chronic-like exposure to NPs with a five-time administration of particles. The aim was to explore differences between sole particle or virus effects and the interplay of both on inflammation, immunity, and lung health. In addition, gradual influences of the repetitive, chronic-like exposure on infected lungs were in focus.

Therefore, the first step was to compare overall pathohistological changes and differences between treatment groups. Following the first step, more detailed information about cellular communication through chemokines, cellular infiltrations and structural adaptations should be gained. In addition to these animal experiments, an *in vitro* model was established. Three-dimensional immunocompetent lung organoids were used to investigate cellular communication and reactivation in a simplified setup.

II. MATERIALS AND METHODS

1. Materials

1.1. Nanoparticles

Spherical carbonaceous nanoparticles (CNP, Printex90) from Degussa, Frankfurt, Germany were used in *in vitro* and *in vivo* experiments.

1.2. Devices

Device	Company
Autoclave machine	Systec, Linden, Germany
Bioruptor Probe sonication	Diagenode SA, Seraing, Belgium
Brightfield microscope	Olympus, Tokyo, Japan
Cell incubator	Thermo Fisher Scientific, Waltham, MA, USA
Centrifuge 1k15	Sigma Laborzentrifugen
Centrifuge 5430	Eppendorf, Hamburg, Germany
Centrifuge universal 32R	Hettich
Chemical workflow hood	Köttermann, Uetze, Germany
Cytospin3 cytocentrifuge	Shandon, PA, USA
Decloaking chamber	BioCare Medical, Concord, CA, USA
Disperser, T 10 basic ULTRA-TURRAX®	IKA, Staufen im Breisgau, Germany
Fine weight balance	Mettler-Toledo, Giessen, Germany
Fluorescent Tecan Reader	Tecan, Maennedorf, Switzerland
Histostar Tissue Embedding Station	Thermo Fisher Scientific, Waltham, MA, USA
Ice machine	Buchner Labortechnik, Pfaffenhofen, Germany
Light Cycler 480	Roche, Basel, Switzerland
LSM 880 confocal microscope	ZEISS, Oberkochen, Germany
Luminex 200 instrument	Luminex Corporation, Austen, TX, USA

system	
MACS® MultiStand	Miltenyi Biotec, Berigsch Gladbach, Germany
NanoDrop® ND-1000 spectrophotometer	Thermo Fisher Scientific, Waltham, MA, USA
Olympus fluorescent microscope	Olympus,Tokyo, Japan
Optical microscope	ZEISS, Oberkochen, Germany
PCR Cycler nexus gradient	Eppendorf, Hamburg, Germany
QuadroMACS™ Separator	Miltenyi Biotec, Berigsch Gladbach, Germany
Shaker	Coulter Electronics, Luton, UK
Slide Scanner (Axio Scan 7)	ZEISS, Oberkochen, Germany
Slide Scanner (NanoZoomer-SQ)	Hamamatsu Photonics, Hamamatsu, Japan
Sonication water bath	Bandelin, Berlin, Germany
Spectrophotometer DS-11	DeNovix, Wilmington, DE, USA
Thermo Cycler	Eppendorf, Hamburg, Germany
Ventilation hood	Thermo Fisher Scientific, Waltham, MA, USA
Vortex mixer	Scientific Industries, Karlsruhe, Germany
Water bath	Lauda, Koenigshofen, Germany

1.3. Software

Product	**Company**
BioPlex Manager 6.1 software	Luminex Corporation, Austen, TX, USA
Computer Assisted Stereological Toolbox (newCAST) software	Visiopharm, Hoersholm, Denmark
GraphPad Prism 10	GraphPad, San Diego, CA, USA
Light Cycler 480 software	Roche, Basel, Switzerland
Magellan Software	Tecan Group, Maennedorf, Switzerland
ZEN 2010-Digital Imaging for Lightmicroscopy Software	Zeiss

1.4. Consumables

Product	Company
Cell culture plate (6, 12, 24 & 96 well plate)	Greiner Bio-One, Kremsmünster, Austria
Cell culture T25 and T75 flask	Greiner Bio-One, Kremsmünster, Austria
Cover slips 24x50	Menzel-Gläser, Braunschweig, Germany
Falcon Cell Strainers (100 µm, 40 µm)	Corning Science, Corning, NY, USA
Falcon tube (15 ml, 50 ml)	Corning Science, Corning, NY, USA
Glass bottle & lid for NPs preparation	Carl Roth, Karlsruhe, Germany
Gloves Kimtech Purple Nitrile	Kimberly Clark, Dallas, TX, USA
Gloves Nitril NextGen	Meditrade, Kiefersfelden, Germay
Microcentrifuge tube (1.5 ml, 2 ml)	Eppendorf, Hamburg, Germany
Nunc™ Lab-Tek™ II Chamber Slide™ System (8-well)	Thermo Fisher Scientific, Waltham, MA, USA
Pipette (10 µl, 20 µl, 100 µl, 200µl, 1000 µl)	Eppendorf, Hamburg, Germany
Pipette (5 ml, 10 ml, 25 ml, 50 ml)	Greiner Bio-One, Kremsmünster, Austria
RNase-free microcentrifuge tube (0.5 ml, 1.5 ml)	Eppendorf, Hamburg, Germany
Tips (10 µl, 20 µl, 200 µl, 1000 µl)	Starlab, Hamburg, Germany
Tips with filters (10 µl, 20 µl, 200 µl, 1000 µl)	Biozol, Eching, Germany; Starlab, Hamburg, Germany
Tissue Kimtech	Kimberly Clark, Dallas, TX, USA
Superfrost Plus Adhesion Microscope slides	Menzel-Gläser, Braunschweig, Germany

1.5. Chemicals and reagents

Chemicals and reagents	Company
0.25% Trypsin EDTA (1x)	Gibco; Thermo Fisher Scientific, Waltham,

	MA, USA
0.4% Trypan Blue	Gibco, Thermo Fisher Scientific, Waltham, MA, USA
30% Hydrogen peroxide (H_2O_2)	Merck, Darmstadt, Germany
4% Paraformaldehyde Solution	Thermo Fisher Scientific, Waltham, MA, USA
Acetone	Merck, Darmstadt, Germany
Agarose	Sigma-Aldrich, St. Louis, MO, USA
Amphotericin B	Gibco; Thermo Fisher Scientific, Waltham, MA, USA
Bovine Pituitary Extract	Sigma-Aldrich, St. Louis, MO, USA
Bovine Serum Albumine	Merck, Darmstadt, Germany
Chloroform	Merck, Darmstadt, Germany
Cholera Toxin	Sigma-Aldrich, St. Louis, MO, USA
DAKO fluorescence mounting medium	Agilent Technologies, Glostrup, Denmark
Dispase	Corning Science, Corning, NY, USA
DMEM medium	Sigma-Aldrich, St. Louis, MO, USA
DMEM/F-12 medium	Gibco; Thermo Fisher Scientific, Waltham, MA, USA
DNaseI	AppliChem, Darmstadt, Germany
Dulbecco's phosphate-buffered saline (DBPS)	Gibco, Thermo Fisher Scientific, Waltham, MA, USA
Ethylenediaminetetraacetic acid (EDTA)	Merck, Darmstadt, Germany
Tween® 20	MP Biomedicals, Eschwege, Germany
Entellan mounting solution	Merck, Darmstadt, Germany
Ethanol 99.9%	Sigma-Aldrich, St Louis, MO, USA
Fetal bovine serum (FBS)	Sigma-Aldrich, St. Louis, MO, USA
Giemsa Methylenblue	Merck, Darmstadt, Germany
Glasgow-MEM medium	PAN Biotech, Aidenbach, Germany

Glucose	AppliChem, Darmstadt, Germany
GlutaMAX	Gibco; Thermo Fisher Scientific, Waltham, MA, USA
Haematoxylin solution	Merck, Darmstadt, Germany
HEPES	Gibco; Thermo Fisher Scientific, Waltham, MA, USA
HIER Citrate Buffer pH 6.0	Zytomed Systems, Berlin, Germany
HIER T-EDTA Buffer pH 9.0	Zytomed Systems, Berlin, Germany
Hygromycin B	Invitrogen; Thermo Fisher Scientific, Waltham, MA, USA
Insulin-Transferrin-Selenium-Sodium Pyruvate (100x)	Gibco; Thermo Fisher Scientific, Waltham, MA, USA
L-glutamine, 200mM (100x)	Gibco; Thermo Fisher Scientific, Waltham, MA, USA
Matrigel, Growth factor reduced	Corning Science, Corning, NY, USA
May-Grünwald Solution	Merck, Darmstadt, Germany
Methanol	Merck, Darmstadt, Germany
Methyl cellulose	Merck, Darmstadt, Germany
Mitomycin C	Sigma-Aldrich, St. Louis, MO, USA
Non-essential amino acids (NEAA)	Gibco; Thermo Fisher Scientific, Waltham, MA, USA
Penicillin Streptomycin	Gibco; Thermo Fisher Scientific, Waltham, MA, USA
peqGOLD TriFast®	Peqlab, VWR international, Radnor, PA, USA
Recombinant mouse EGF	Sigma-Aldrich, St. Louis, MO, USA
Retinoic Acid	Sigma-Aldrich, St. Louis, MO, USA
Rho-associated kinase inhibitor (Y-27632)	Sigma-Aldrich, St. Louis, MO, USA
Rodent Block M	BioCare Medical, Concord, CA, USA
RPMI-1640 medium	Gibco; Thermo Fisher Scientific, Waltham, MA, USA

TRIS Wash Buffer, 20x	Zytomed Systems, Berlin, Germany
Triton X-100	Thermo Fisher Scientific, Waltham, MA, USA
Tryptose phosphate broth	Gibco; Thermo Fisher Scientific, Waltham, MA, USA
Ultrapure water	Invitrogen; Thermo Fisher Scientific, Waltham, MA, USA
Xylene	Carl Roth, Karlsruhe, Germany

1.6. Antibodies and Beads

Antibodies and Beads	**Host**	**Company**
CD31 MicroBeads		Miltenyi Biotec, Bergisch Gladbach, Germany
CD326 (EpCAM) Microbeads		Miltenyi Biotec, Bergisch Gladbach, Germany
CD45 MicroBeads		Miltenyi Biotec, Bergisch Gladbach, Germany
Pro-SPC	Rabbit	Sigma-Aldrich, St. Louis, MO, USA
Acetylated alpha Tubulin (ACTUB)	Rabbit	Abcam, Cambridge, UK
Polyclonal MHV-68 antiserum	Rabbit	Described before in [110]
Keratin 8 (KRT8)	Rat	Developmental Studies Hybridoma Bank (DSHB), Iowa City, IA, USA
Aquaporin 5 (AQP5)	Rabbit	Calbiochem, Merck, Darmstadt, Germany
Alpha smooth muscle actin (SMA)	Rabbit	Abcam, Cambridge, UK
HOPX (E-1)	Mouse	Santa Cruz Biotechnology, Dallas, TX, USA
CD8	Rabbit	Abcam, Cambridge, UK
NKG2D	Rabbit	Biozol, Eching, Germany
Granzyme B	Rabbit	Cell Signaling, Danvers, MA, USA

1.7. Primer Sequences

Target gene	Forward Primer (5' – 3')	Reverse Primer (5' – 3')
MHV-68 Orf50	GGAATTTCTCAGCGATGGCCTCT	CCTCTTTTGTTTCAGCAGAGACTCCA
MHV-68 Orf73	CTGGACTCCTCATCACCTT	TGTCTGAGCGTCTTCCAC
L8	CAGTGAATATCGGCAATGTTTTG	TTCACTCGAGTCTTCTTGGTCTC
Actb	TCCATCATGAAGTGTGACGT	GAGCAATGATCTTGATCTTCAT
Sftpc	AGCAAAGAGGTCCTGATGGA	GAGCAGAGCCCCTACAATCA
Sftpb	AGGCTATGCCACAGGCAATG	CAGGTGATGTGGGCATCCTG
Aqp5	CTACTTCACCGGCTGTTC	CTTTGACCACAGCCACAC
Krt8	ACATCGAGATCACCACCTACC	GGATGAACTCAGTCCTCCTGA
Tuba1a	AAGGAGGATGCTGCCAATAA	GCTGTGGAAAACCAAGAAGC

1.8. Kits

Kit	Company
RNeasy Plus Mini Kit	Qiagen, Venlo, Netherlands
Rabbit-on-Rodent AP Polymer	BioCare Medical, Concord, CA, USA
Bio-Plex Pro Mouse Chemokine Panel 31-plex	BioRad Laboratories, Hercules, CA, USA
LightCycler 480 SYBR Green I Master	Roche, Basel, Switzerland
TUNEL assay kit-BrdU-red	Abcam, Cambridge, UK
Vulcan fast red chromogen kit	Zytomed Systems, Berlin, Germany
BCA Protein assay kit	Thermo Fisher Scientific, Waltham, MA, USA
Mouse Keratin, type 1 cytoskeletal 18 (KRT18) ELISA kit	Cusabio, Houston, TX, USA

Mouse Keratin, type 1 cytoskeletal 18 fragment (K18-Asp396) ELISA kit	Cusabio, Houston, TX, USA

1.9. Animals

Wildtype C57BL/6J mice were used in all *in vivo* experiments and purchased from Charles River Laboratories (Sulzfeld, Germany). 7-week-old mice had at least one week after shipping to acclimatize to their new housing and were housed in individually ventilated cages (IVC) under specific pathogen free conditions. Three to four animals were housed in one cage (Tecniplast Greenline GM 500, 501 cm² floor space) with a 12/12 - hour light cycle. The barrier animal rooms were fully air-conditioned, with 20 - 24°C temperature and 45 - 65% humidity. Animals had ad libitum access to sterile filtered water and a standard diet for rodents (Altromin 1314). To improve housing conditions, the cages were equipped with laboratory animal bedding (wood fiber/wood chips; Lignocel Select Fine, SAFE), autoclaved nesting material (Arbocel Crinclets, SAFE), plastic mouse houses and wooden bricks. Cages were changed weekly, and mice were controlled daily.

Hygiene monitoring was carried out at least four times a year in accordance with the current FELASA recommendation. In the animal housing areas equipped with IVC systems, exhaust dust from the IVC ventilation units was tested for all FELASA-listed pathogens using PCR. In addition, animals with clinical abnormalities were examined using classical examination methods (bacteriology, parasitology, pathology).

All animal experiments were performed according to German legislation for the protection of animals and were approved by the government of Upper Bavaria (permit number: ROB-55.2-2532.Vet_02-22-76).

2. Methods

2.1. Particle dispersion preparation

For *in vitro* as well as *in vivo* experiments, carbonaceous nanoparticles (CNP, Printex90, Degussa, Frankfurt, Germany) were used. Printex90 do have a primary diameter of 14 nm that can form bigger agglomerates in solution. The surface area measured by Brunauer-Emmett-Teller analysis is 272 m^2/g [111]. To prepare a dispersion, 2 – 3 mg particles were weighted and dissolved in pyrogen-free water to a final concentration of 1 mg/ml. After sonification for 5 minutes in a sonication

ice bath, the dispersion was sonicated with a sonication lance for 30 seconds at 30% power on ice, followed by a sonification in the bath for 5 minutes.

Dynamic light scatter measurements were performed to determine the size distribution of particles. For that, 80 µl of the dispersed particles were measured at room temperature.

2.2. *In vivo* mouse experiments

Mice were treated humanely and with consideration to reduce suffering, according to the German law of protection of animal life. All animal experiments followed approved protocols by the local Animal Care and Use Committee (District Government of Upper Bavaria; permit number: ROB - 55.2 - 2532.Vet _ 02 – 22 - 76). C57BL/6J mice were purchased from Charles River Laboratories (Sulzfeld, Germany) and housed in individual ventilated cages (IVC) in groups of 3 or 4 mice. 178 female mice in total were divided into 22 groups. Mouse samples were collected at 7 different endpoints: 6 days after infection, 24 hours and 7 days after the first instillation, after the second instillation and after the fifth instillation.

In general, mice were either left uninfected or were infected with MHV-68 on the first day of experiments. Endpoint of the first group was 6 days after the infection to capture acute infection. 4 weeks after the infection and after establishment of latency, mice were instilled with either PBS or 50 µg CNP for the first time and endpoints were 24 hours and 7 days later. After another 4 weeks, mice were instilled a second time with PBS or CNP and accordingly, endpoints were set 24 hours and 7 days after the second instillation. To capture chronic-like exposure consequences, mice were instilled a third, fourth and fifth time with a time interval of 4 weeks between each instillation. The final endpoints were set 24 hours and 7 days after the fifth instillation. Untreated control animals were included. All mouse experiments were conducted with the help of David Kutschke.

2.2.1. Intranasal infection with MHV-68

Mice were anesthetized intraperitoneally (i.p.) with a mixture of Medetomidine (0.5 mg/kg body mass), Midazolam (5.0 mg/kg body mass) and Fentanyl (0.05 mg/kg body mass) (MMF). To protect the cornea, Bepanthen eye ointment was applied and after testing for loss of the hindlimb pedal withdrawal reflex, mice were infected intranasally (i.n.) with 5×10^4 PFU MHV-68 in 30 µl PBS. After

that, anesthesia was antagonized with a mixture of Atipamezole (2.5 mg/kg body mass), Flumazenil (0.5 mg/kg body mass) and Naloxone (1.2 mg/kg body mass) subcutaneously (s.c.) to reduce the time under anesthesia to a minimum.

2.2.2. Intratracheal instillation

After anesthetization with MMF, Bepanthen eye ointment was applied as corneal protection. Loss of hindlimb pedal withdrawal reflex confirmed a sufficient depth of anesthesia. For intubation with a small size button cannula, animals were fixed with their upper incisors in an elastic device in supine position. The cannula was inserted into the trachea, until it reached the bifurcation not yet. 50 µl CNP or PBS dispersion were instilled intratracheally with a 1 ml syringe. This was done with the help of David Kutschke. Mice were awakened by subcutaneous injection of the aforementioned antagonists and observed until fully awakened.

2.2.3. Organ removal for histology

Mice were anesthetized intraperitoneally with a lethal mixture of ketamine (150 mg/kg) and xylazine (10 mg/kg) and killed painlessly by blood withdrawal at the *vena cava caudalis* after loss of the hindlimb pedal withdrawal reflex. The lung was perfused with 10 ml PBS from the right ventricle to remove all remaining erythrocytes. Especially in immunofluorescence staining, the red blood cells can lead to a high background fluorescence. The trachea was intubated with a 20 G venous catheter and fixed with a thread. 1 ml of 4% paraformaldehyde (PFA) was injected into the endotracheal tube to retain the structure of the lung. The endotracheal tube was removed, and the trachea was sealed with the prepared threat. The lung was removed from the chest and incubated in a 50 ml falcon tube with 10 ml 4% PFA over night at 4°C.

2.2.3.1. Paraffin embedding

Lungs were prepared for dehydration by separating the lung into single lung lobes, the right lung consists of four lobes, the left lung has only one single lobe. Every lung lobe was cut into 2 – 3 mm thick slices. The lobes of left and right lung were put separately into two embedding cassettes. Dehydration and paraffinization of the tissue were done overnight for 16 hours in a spin tissue processor. To embed the tissue into paraffin blocks, an embedding station was used. Left and right lungs were embedded separately and stored at 4°C until cutting with the microtome.

2.2.3.2. Microtome cutting

Paraffin blocks were cut with a microtome into 3 µm thick slices and put on a Superfrost™ Plus microscopic slide. After drying at 40°C, slides were stored at 4°C until further use.

2.2.4. Bronchoalveolar lavage and cytospin preparation

Mice were anesthetized intraperitoneally with a lethal mixture of ketamine (150 mg/kg) and xylazine (10 mg/kg) and killed painlessly by blood withdrawal at the inferior vena cava after loss of the hindlimb pedal withdrawal reflex. For bronchoalveolar lavage (BAL), the trachea was cannulated with a 20 G venous catheter as endotracheal tube and the lung was infused with 1 ml PBS for six times. The first 2 ml lavage fluid were collected in a separate 5 ml round-bottom tube, the remaining 4 ml fluid were pooled in a 15 ml falcon tube. The lavage was done by David Kutschke. All tubes were centrifuged for 20 minutes at 4°C and 400 RCF. The supernatant of the first 2 ml bronchoalveolar lavage fluid (BALF) were collected and distributed between three 1.5 ml tubes. These were snap-frozen in liquid nitrogen and stored at -80°C for further analysis. The supernatant of the second tube was discarded and the cell pellet of both tubes was pooled in 1 ml RPMI 1640 medium containing 10% FBS. A Neubauer chamber and 0.2% trypan blue solution were used to determine total living cell numbers. 30,000 cells were needed for each cytospin slide in a maximum volume of 200 µl, and four slides were prepared from each lavage sample. To do that, the volume of 30,000 cells was pipetted into the matching slide holder and centrifuged for 6 minutes at 400 RCF. After letting the cytospins dry, half of them were stored at room temperature for May-Gruenwald-Giemsa staining and half of them at -20°C for immunofluorescent staining. After generating the cytospins, the residual cells were centrifuged at 10,000 RPM for 10 minutes. The cell pellets were snap-frozen in liquid nitrogen and stored at -80°C until further use.

2.2.5. Organ removal for RNA isolation

After painless killing as described above, the lung was taken out completely. We divided it into single lobes and snap-froze them in liquid nitrogen. These samples were stored in a -80°C freezer until homogenization.

2.2.5.1. Lung homogenization

Frozen lung lobes were kept cool with liquid nitrogen to prepare lung powder with a Mikro-Dismembrator U. Unused powder was stored at -80°C until further use.

2.2.6. Staining of tissue sections

2.2.6.1. Haematoxylin and Eosin staining (H&E)

To remove surrounding paraffin, the cut tissue samples were put at 60°C overnight, or at least for 1 - 2 hours. The slides were deparaffinized and rehydrated according to the following scheme. They were incubated for 5 minutes in xylene; this was repeated in a new tube of xylene for another 5 minutes. Then the slides were put in 100% ethanol for one minute and this was also repeated. After that, the slides were incubated for one minute each in 90%, 80% and 70% ethanol and rehydrated for one minute in distilled water. We used Mayer's Haemalaun for nuclear staining. For this, the solution was filtered before usage and the slides were incubated for 5 minutes, then dipped once into tap water, dipped into 0.1% HCl-Ethanol, and washed for 10 minutes with running tap water. Afterwards, the slides were dipped into distilled water once and the cell plasma was stained with 0.5% Eosin for 8 minutes after filtering the staining solution.

Dehydration of the tissue was done with an ascending ethanol series, dipping the slides first into 70% ethanol, then 80%, 90% and 96%. They were put into 100% ethanol for 2 minutes and this step was repeated in new ethanol. In the end, slides were incubated in xylene for 5 minutes twice. The slides were covered with Entellan and a coverslip and stored at room temperature for long-term.

2.2.6.2. Immunohistochemistry (IHC) staining – Vulcan fast red

The 3 µm tissue slides were deparaffinized and rehydrated as described before.

To block endogenous peroxidase activities, a 1.8% H_2O_2-Methanol-Solution was prepared freshly. The lung slides were incubated for 20 minutes at room temperature in this solution and rinsed in distilled water afterwards.

For heat induced epitope retrieval (HIER), either a Citrate or an EDTA buffer were prepared. For this, HIER Citrate Buffer pH 6.0 or HIER T-EDTA Buffer pH 9.0 were diluted 1:10 in distilled water. Slides were retrieved in a decloaking chamber following this program: 125°C for 30 seconds and afterwards 90°C for 10 seconds. Slides were gradually cooled down with TBS wash buffer for a slow cool down.

TBS wash buffer contained TRIS Wash Buffer (20x), diluted with distilled H_2O to get 1 x TBS buffer. Slides were washed three times with TBS for two minutes each. After the second washing step, an intact circle was drawn with a hydrophobic pen and dried. Slides were washed for a third time afterwards. The slides were placed into a staining chamber and incubated with one or two drops of Rodent Block M blocking solution for 30 minutes at room temperature. Then, they were washed three times for 5 minutes with TBS buffer. The desired primary antibody was diluted to working concentration in antibody diluent (AD), containing 1% bovine serum albumin (BSA) in PBS with 0.3% Triton X-100. 100 µl were added to each sample and incubated overnight at 4°C.

On the following day, slides were washed three times for 5 minutes with TBS buffer and incubated for 30 minutes with the desired AP polymer, binding to the primary antibody. They were washed afterwards three times for 5 minutes each. 2.5 ml of Vulcan Fast Red Buffer were mixed with one drop chromogen dye and one drop was added to each tissue slide. After enzymatic reaction, the protein of interest appears in a pink colour, the time of incubation depends on the primary antibody used, it can vary between 5 to 15 minutes. To stop the reaction, slides were dipped into distilled water once. The tissue was counterstained by dipping them for one to ten seconds in haematoxylin, depending on the strength of the antibody staining. After that, they were dipped in distilled water twice and in tap water for 5 minutes, to blue the sections.

The slides were dried for 15 to 30 minutes at 60°C, dehydrated twice in xylene for 5 minutes, mounted with Entellan and covered with 24 x 50 mm glass coverslips.

2.2.6.3. Immunofluorescence (IF) staining

Slides were deparaffinized and rehydrated in the same way as for H&E staining. For epitope retrieval, we used the decloaking chamber as described before with the IHC staining, with either citrate or EDTA solution.

Slides were washed once with PBS-T, containing 0.1% Tween-20 in PBS. After that, an intact circle was drawn with a hydrophobic pen and washed twice with PBS-T, two minutes each. The slides were put into a staining chamber and 100 µl of a blocking solution according to the secondary antibody that will be used were added, for example 5% goat serum in PBS containing 0.3% Triton X-100. Blocking solution was incubated for one hour at room temperature.

After incubation time was over, slides were washed three times for two minutes each with PBS-T and the primary antibody, diluted in AD, was added. Incubation was overnight at 4°C.

The next day, slides were washed three time for 5 minutes with PBS-T and 100 µl fluorescence labeled secondary antibody diluted in AD were added to each slide. Incubation was done for one hour at room temperature in the dark.

To be able to double label two different primary antibodies from the same host, slides needed to be washed again three times for 5 minutes with PBS-T and incubated for one hour at room temperature with 100 µl normal rabbit serum blocking solution. To block the surface of immunoglobulins, slides were washed with PBS-T three times and unconjugated Rabbit Fab fragment was diluted in blocking solution (1:45). Slides were incubated for 90 minutes at 37°C.

After washing with PBS-T, the second primary antibody was diluted in AD and added to the samples, followed by incubation at 4°C overnight.

After washing the slides three times in PBS-T, the second fluorescent secondary antibody diluted in AD with DAPI was added and incubated for one hour at room temperature. After that, the slides were washed three times in PBS-T, followed by one washing step in PBS, to get rid of the tween, mounted with DAKO fluorescence mounting medium and stored at 4°C.

2.2.6.4. TUNEL assay for DNA fragmentation detection

TUNEL (TdT-mediated dUTP-biotin nick end labelling) assay is a method to detect DNA fragmentation by labelling the 3′ - hydroxyl termini.

For TUNEL staining, tissue slides were deparaffinized and rehydrated as described before. Slides were incubated in 0.85% NaCl for 5 minutes and washed twice with PBS for 5 minutes each. An intact circle was drawn with a hydrophobic pen in between. 100 µl Proteinase K retrieval solution, containing 20 µg/ml Proteinase K and 50 mM EDTA in Tris-HCl pH 8.0 were added and incubated for 5 minutes at room temperature.

Tissue slides were washed with PBS for 5 minutes and 4% PFA solution was added to each slide to fix the tissue for 5 minutes at room temperature. After washing for 5 minutes with PBS, slides were covered twice for 5 minutes with wash buffer, supplied in the assay kit. 50 µl DNA label solution was added to each tissue,

prepared as follows for one test: 10 µl TdT Reaction Buffer, 0.75 µl TdT Enzyme, 8 µl Br-dUTP and 32,25 µl ddH_2O. A coverslip was placed gently on top to ensure even distribution and slides were incubated at 37°C for one hour.

After three times washing for 5 minutes with PBS, 100 µl antibody solution were added, containing 5 µl Anti-BrdU-Red antibody and 95 µl rinse buffer. Again, a coverslip was placed on top and incubation was done for half an hour at room temperature, protected from light.

Finally, slides were washed three times with PBS-T and once with PBS and mounted with DAKO fluorescence mounting medium.

2.2.7. Staining of BAL Cell Cytospins (May-Gruenwald-Giemsa)

Cytospin slides were incubated for 10 minutes in May-Gruenwald stain. They were rinsed for 2 minutes in tap water and incubated afterwards for 15 minutes in Giemsa stain, diluted 1:20 with tap water. After dipping into tap water once, the slides were left in fresh tap water for another 2 minutes. Dried slides were covered with Entellan and a coverslip for long-term storage at room temperature.

2.2.8. Imaging

2.2.8.1. Imaging of Histological Staining

Imaging of H&E, IHC and IF staining of lung tissue as well as BAL cell staining was performed on an Olympus BX-51 light microscope. Fluorescent images were taken with DAPI, AF-488, Cy-3 and Cy-5 filters included.

2.2.8.2. BAL Cell Differentiation

BAL differential cell counts were quantified on May-Gruenwald-Giemsa stained cytospins. For this, 200 cells were differentiated on two different slides per animal. Four different cell types were recognized, including macrophages, neutrophilic granulocytes, lymphocytes, and multinucleated macrophages. The total number of cells was calculated based on the known total cell number that was obtained in the lavage.

2.2.8.3. Quantification of mean linear intercept (MLI)

To quantify MLI in H&E-stained lung tissues, slides were scanned using an Axioscan 7. Random regions were extracted and analysed according to the protocol published by Salaets et al. [112].

2.2.8.4. Quantification of tissue inflammation

Quantification of tissue inflammation was performed using an Olympus BX-51 light microscope. Design-based stereology with computer-assisted stereological toolbox running Visopharm Integrator System (VIS) software (v6.0.0.1765) was used to analyse and quantify tissue inflammation. H&E-stained samples are used and scanned images are visualized at 20x objective magnification. A line grid with points was superimposed and at least 30 random fields per lung were analysed. Intersections of lines with airways ($I_{intercept\ A}$) and vessels ($I_{intercept\ V}$) as well as points falling into an area of inflammatory tissue ($P_{inflamed\ area}$) were counted. Tissue inflammation level was calculated using the following formula: $\frac{\sum P_{inflamed\ area} \times L_{(p)}}{\sum I_{intercept\ (A+V)}}$. $L_{(p)}$ is the line length per point.

2.2.8.5. Quantification of IF stainings

To quantify IF stained tissue slides, the Olympus BX-51 light microscope was used. Images of three random fields of each animal were saved, including 405 nm, 568 nm and 647 nm channels. Images were analysed using the Fiji plugin TrackMate [113]. Number of positively stained cells were normalised to numbers of DAPI-stained cells.

2.2.9. RNA isolation from tissue

For RNA isolation, lung powder was dissolved in 1 ml TRIzol and shredded for 30 seconds with a disperser at full speed. 0.2 ml chloroform was added and shaken vigorously for 15 seconds. After incubation for 5 minutes at room temperature, the samples were centrifuged at 4000 RCM for 20 minutes. After transfer of the colourless, upper phase, containing RNA, to a fresh gDNA Eliminator spin column, the RNA isolation was continued according to the manufacturer's protocol.

RNA concentration and purity were measured with a Spectrophotometer. RNA was stored at -80°C until further use.

2.2.10. Multiplex Chemokine Assay

To detect and quantify the chemokine release into the bronchoalveolar space, a Bio-Plex Pro Mouse Chemokine Panel 31-Plex Kit was used. The kit included the following chemokines for detection: CXCL13, CCL27, CXCL5, CCL11, CCL24, CX3CL1, GM-CSF, CCL1, IFN-γ, IL-1β, IL-2, IL-4, IL-6, IL-10, IL-16, CXCL10, CXCL11, CXCL1, CCL2, CCL7, CCL12, CCL22, CCL3, CCL4, CCL20, CCL5,

CCL19, CXCL16, CXCL12, CCL17 and TNF-α. Experiment and analysis were performed according to the manufacturer's instructions. Cytokine and chemokine expression was measured using the Luminex 200 System.

2.2.11. Pierce Bicinchoninic acid (BCA) Assay

Pierce BCA assay was performed to determine total protein concentrations in BAL fluids. A reference standard dilution was prepared using a 0.5 mg/ml BSA stock solution as follows:

Concentration µg/ml BSA	0.5 mg/ml BSA solution (µl)	PBS (µl)
0	0	250
0.025	12.5	237.5
0.05	25	225
0.1	50	200
0.2	100	150
0.3	150	100
0.4	200	50
0.5	250	0

The assay was done in 96-well plates with duplicates of each standard and sample. 20 µl of BAL fluid sample were incubated with 200 µl of working solution (Reagent A : Reagent B, 50:1) for 30 minutes at 37°C. Absorbance was read in a Tecan Reader at 562 nm. Protein concentration was calculated according to the standard curve.

2.2.12. Enzyme-linked immunosorbent assay (ELISA)

ELISA was used to determine the concentration of specific proteins in BAL fluid samples. If no pre-coated well-plates were supplied, coating was done with the specific capture antibody overnight. After washing three times with wash buffer, 250 µl blocking buffer were added to each well. A reference standard was prepared, covering the expected concentrations measured. BAL fluid samples were either used undiluted or diluted 1:10 in assay buffer. 50 to 100 µl were added to the respective wells and incubated for 2 hours at room temperature or 37°C. The plate was washed three times with wash buffer to get rid of unbound antigens and detection antibody was added to each well for 2 hours at room temperature or one hour at 37°C. A few washing steps later, wells were incubated with avidin horseradish peroxidase for 20 minutes at room temperature or one hour at 37°C. After washing again, 3,3′,5,5′-Tetramethylbenzidine substrate was added to each well for 15 to 30 minutes at 37°C, to start enzymatic colour change. The enzymatic

reaction was stopped by adding H_2SO_4. Optical density was determined at 450 nm using a Tecan Reader. Concentration of each sample was calculated using the standard curve equation.

2.3. Cell culture

2.3.1. Macrophage cell lines Ana-1 and Ana-1/MHV-68

The murine bone marrow derived macrophage cell line Ana-1 (RRID:CVCL_0142) [114] was cultured in RPMI-1640 medium supplemented with 15% FBS, 2 mM L-glutamine, 1% Non-essential amino acids, 100 U/ml Penicillin and 100 µg/ml Streptomycin. Persistently with MHV-68 infected Ana-1 cells, named Ana-1/MHV-68 [8], were cultured in RPMI-1640 medium with 10% FBS, 2 mM L-glutamine, 100 U/ml Penicillin, 100 µg/ml Streptomycin and 5 µg/ml Hygromycin B under maintenance conditions. Within experiments, Hygromycin B was not added to the growth medium.

2.3.2. CCL-206 fibroblasts

CCL-206, also named MLg 2908, is a fibroblast cell line from lungs of mice and was cultured in DMEM/F12 medium supplemented with 10% FBS, 100 U/ml Penicillin and 100 µg/ml Streptomycin.

2.3.3. BHK-21 kidney fibroblasts

BHK-21 (ATCC: CCL-10) is a fibroblast cell line from baby hamster kidney cells. These cells were cultured in Glasgow MEM medium, supplemented with 5% FBS, 5% Tryptose Phosphate Broth, 100 U/ml Penicillin, 100 µg/ml Streptomycin and 2 mM L-glutamine.

2.4. Organoid culture

2.4.1. Primary murine lung cell isolation

C57BL/6J wildtype mice or SPC H2B-GFP transgenic mice [115] were put to sleep intraperitoneally with a lethal anesthesia mixture of ketamine (150 mg/kg) and xylazine (10 mg/kg) and killed painlessly by blood withdrawal at the inferior vena cava after testing for loss of the hindlimb pedal withdrawal reflex. After exposing the trachea, we used a venous catheter as endotracheal tube and fixed it with thread. A pneumothorax was placed carefully, the diaphragm removed, and the thorax opened. We flushed out blood from the lung via the heart with PBS. We added

1.5 ml Dispase to the lung via the endotracheal tube, applied 0.3 ml agarose solution (1%) to the endotracheal tube and waited 2 minutes until it has solidified. The lung was taken out carefully and incubated in 2 ml of Dispase for 45 minutes at room temperature.

To isolate epithelial cells out of the lungs via magnetic bead sorting, each lung was separated into the lobes in a petri dish with 5 ml of DMEM medium supplemented with 3.6 mg/ml glucose, 2% GlutaMAX, 100 U/ml Penicillin, 100 µg/ml Streptomycin and 10 mM HEPES containing DNaseI. The cells were isolated carefully by mechanically dissecting the lungs with forceps. Then, we filtered the suspension through a 100 µm filter and washed it thoroughly and scraped the tissue that remains on the filter with a plunge from a 2 ml syringe. The cell suspension was filtered again, this time through a 40 µm filter. This process was repeated for every lung used. We centrifuged the cells for 10 min, 200 RCF, acceleration 5, deceleration 1 at 15°C. Red blood cells were lysed by adding 1 ml of red blood cell lysis buffer for 5 minutes. The supernatant was removed, and we resuspended the cells in 10 ml ice cold MACS buffer, prepared from PBS containing 0.5% FBS and 0.4% EDTA. After counting the cells from each lung by mixing 420 µl MACS buffer with 20 µl cell suspension, we calculated the cell number with a Neubauer chamber. Cells were spun down for 10 minutes at 200 RCF, acceleration 5 and deceleration 1 at 15°C. After removement of the supernatant, 90 µl of MACS buffer as well as 10 µl of murine CD31 and 10 µl of murine CD45 microbeads per 10^7 total cells were added to the cell pellet. Cells were mixed well and incubated for 15 min at 4°C. The tube was filled up to 15 ml with MACS buffer and centrifuged for 10 min, at 200 RCF, acceleration 9, deceleration 6, 15°C. The pellet was resuspended in 1 ml MACS buffer per column used. 2 LS columns per lung were placed into a MACS separator and rinsed with 3 ml MACS buffer prior to collecting the cells in a 15 ml falcon tube. Before the buffer ran out in the column, we added 1 ml cell suspension on each column. We washed two to three times with 3 ml MACS buffer and collected the flow-through. The cell suspension was centrifuged for 10 minutes at 200 RCF, acceleration 9, deceleration 6 at 15°C. We resuspended the cell pellets of two lungs in 5 ml MACS buffer and counted the cells. After centrifugation, the cells were resuspended in 90 µl MACS buffer and 10 µl of murine CD326 (EpCAM) microbeads per 10^7 total cells. Cells were mixed well and incubated for 15 min at 4°C. Then the tube was filled up to 15 ml with MACS buffer

and centrifuged for 10 minutes at 200 RCF, acceleration 9, deceleration 6 at 15°C. After removal of the supernatant, the pellet was resuspended in 1 ml MACS buffer per lung. One LS column per lung was prepared in the MACS separator and the flow-through was collected in a 15 ml falcon tube. As before, the columns were rinsed with 3 ml of MACS buffer before adding 1 ml cell suspension to each column. Columns were washed two to three times with 3 ml MACS buffer and finally filled up with 3 ml MACS buffer to collect the column cells with the provided plunge in a new 15 ml falcon tube. The collected EpCAM positive cells were centrifuged for 10 minutes at 200 RCF, acceleration 9, deceleration 6 at 15°C. Finally, the cell pellet was resuspended in 1 ml of organoid media, consisting of DMEM/F12 media supplemented with 1% GlutaMAX, 100 U/ml Penicillin, 100 µg/ml Streptomycin, 1% amphotericin B, 1% insulin-transferrin-selenium-sodium pyruvate, 0.1 µg/ml cholera toxin, 0.025 µg/ml epidermal growth factor, 30 µg/ml bovine pituitary extract and 5% FBS and the cells were counted.

2.4.2. Organoid seeding

CCL-206 fibroblasts were inhibited in cell proliferation with 10 µg/ml Mitomycin C (MMC). For that, cells were incubated for 2 hours with MMC, washed 3 times afterwards with PBS and recovered for at least one hour in culture media. Macrophages (Ana-1/MHV-68 or Ana-1) were treated accordingly with 4 µg/ml MMC.

Freshly isolated primary lung epithelial cells were mixed with the same number of fibroblasts (Co-Culture; 1:1) or fibroblasts and macrophages (Triple-Culture; 1:1:1) in 25 µl organoid medium per well. We diluted them with the same amount of Matrigel and seeded the cell mixture in 50 µl drops with 10,000 cells of each cell type, either in 96 well plates or 8 well chambers. The cultures were maintained in organoid media with 0.01 µM freshly added all-trans retinoic acid. 10 µM Y-27632, a Rho-associated kinase inhibitor, was added for the first 48 h of culture. Media was refreshed every 2-3 days.

2.4.3. Treatment of organoids

For different treatment conditions, organoids were cultured for five days in normal growth media and treatment was started at day six. For CNP, 100 µg/ml, for LPS, 1 µg/ml were diluted in culture media. Endpoint was 48 hours later.

2.4.4. Immunofluorescence staining of organoids

After growing organoids for several days, wells were fixed in 8-well chambers using acetone and methanol. For that, wells were washed with PBS once. 200 µl of a 1:1 acetone/methanol mixture were added, the lid was secured with tape and placed into the freezer at -20°C for 5 minutes. It was washed twice with PBS and stored at 4°C until staining, sealed with parafilm.

For immunofluorescence staining, the requested primary antibody was added, diluted in 200 µl PBS with 0.1% BSA and 0.1% Triton X-100 per well. Organoids were incubated with the primary antibody at 4°C overnight. Wells were washed three times with PBS for at least 30 minutes each time. The secondary antibody (e.g., Goat anti-Rabbit Alexa Fluor 568, 1:500) and DAPI (1:1000) were diluted in PBS with 0.1% BSA and 0.1% Triton X-100. 200 µl were added to each well and incubated overnight at 4°C in the dark. The secondary antibody was removed, and wells washed once with PBS for at least 15 minutes. After removal of the PBS, the plastic chamber was removed with the supplied device. Drops of DAKO fluorescence mounting medium were added to each organoid drop and a coverslip was gently placed on top, prepared with modelling clay on the edges, to avoid demolition of the three-dimensional structures. Slides were left to dry overnight at 4°C face up in the dark. Images were taken with a Zeiss LSM 880 confocal microscope.

2.4.5. RNA isolation from organoids

For isolation of RNA from the organoids, four to five wells were pooled in 1 ml TRIzol in a 2 ml Eppendorf tube. The cells were shredded for 30 seconds with a disperser at full speed and the lysate was incubated for 5 minutes at room temperature. 0.2 ml chloroform were added and shaken vigorously for 15 seconds. Again, samples were incubated at room temperature for 5 minutes and centrifuged for 20 minutes at 4000 RCM. The colourless, upper phase containing RNA was transferred to a fresh gDNA eliminator spin column and RNA isolation was continued according to the manufacturers protocol. RNA concentration and purity were measured with a NanoDrop. RNA was stored at -80°C until further use.

2.4.6. cDNA synthesis

A maximum of 1 µg total RNA was added to a PCR-clean tube and filled up to 10 µl with RNase free water, if required. 1 µl 0.1 mM Random Nonamers were

added and incubated for 5 minutes at 70°C in the Thermo Cycler machine. Samples were cooled down for 5 minutes on ice and incubated for 5 to 10 minutes at room temperature.

A master mix was prepared as follows:

Master Mix for 1 sample:

5x First Strand Buffer	4 µl
10 x DTT (0.1M)	2 µl
Superscript II RT (200 U/µl)	1 µl
RNase Inhibitor (40 U/µl)	1 µl
20 x 4dNTP mix (10 mM)	1 µl

I added 9 µl Master Mix to each sample and mixed thoroughly. The samples were incubated at 42°C for 1 hour for cDNA synthesis and at 70°C for 15 minutes to inactivate Superscript in a Thermo Cycler. The samples were centrifuged and diluted 1:5 or 1:2 with RNAse free water. cDNA was stored at -20°C.

2.4.7. Quantitative polymerase chain reaction (qPCR)

The required primer mix was prepared by diluting the forward and reverse primer with RNase free water to a final concentration of 10 µM.

A master mix was prepared as followed for each gene and for one well:

qPCR Master Mix:

RNase free water	2.4 µl
SybrGreen Master Mix	5 µl
Primer Mix	0.6 µl

Technical duplicates were pipetted for each gene. To do so, 8 µl Master Mix were added to each well of a 96 well plate and 2 µl of cDNA were added on top. Non template controls with water instead of cDNA were always included. The plate was covered with transparent sealing and centrifuged at 1500 RPM for 1.5 minutes.

The plate was put into a Light Cycler 480 and the PCR was run for initial enzyme activation (one cycle at 50°C for 2 minutes and 95°C for 15 minutes) and 40 cycles amplification (95°C for 15 seconds, 60°C for 1 minute).

To calculate the fold change in gene expression, each target gene was compared to the expression of the housekeeper gene Actb (β-Actin). Calculations were based on

the cycle threshold (Ct) value and shown as $2^{-\Delta Ct}$, whereas $\Delta Ct = Ct_{\text{target gene}} - Ct_{\text{housekeeping gene}}$.

2.4.8. Plaque assay for viral titre determination

To determine the amount of infectious viral particles in a supernatant sample of organoid culture after CNP or LPS treatment, plaque assay was performed. For that, BHK-21 cells were detached from a confluent 75 cm^2 cell culture flask and resuspended in 10 ml medium. 0.5 ml cell suspension was diluted in 9.5 ml fresh medium and 1 ml of this dilution was added per well in a 24 well plate. The cells were incubated for 24 hours at 37°C and 5% CO_2.

For a 1:10 serial dilution, six 5 ml tubes per supernatant sample were prepared and 900 µl BHK-21 medium was added to each tube. The desired samples were thawed from -80°C and vortexed thoroughly. 100 µl of the solution was titrated into the first tube, while being careful not to touch the liquid inside and vortexed thoroughly. 100 µl of the first tube were taken out and transferred to the second one with a new pipette tip. This was continued until the sixth tube was reached, to get a dilution series from 10^{-1} to 10^{-6}.

We removed the medium from the prepared BHK-21 cells in the 24 well plate and pipetted 900 µl of the dilution series in each well, starting with 10^{-6} and continuing to 10^{-1} with the same pipette tip. The plate was then incubated for 90 minutes at 37°C and 5% CO_2. After this, supernatant was removed, and 1.5 ml Methylcellulose overlay medium was added to each well. This was incubated for 5 days at 37°C and 5% CO_2.

After the 5 days, the overlay medium was removed and 300 µl Crystal Violet staining solution was added to each well and left for 10 to 15 minutes at room temperature for fixation and staining. After careful washing with tap water, the plates were left to dry for at least one day.

To count plaques and determine the titre, the dilution wells, where between 10 and 100 plaques can be clearly separated were examined and counted with a 5x magnification. Virus titre was calculated with the following equation:

$$Number\ of\ Plaques \times 1.1\ (input\ factor) \times dilution = number\ pfu/ml$$

Input factor: $\frac{1}{ml\ inoculum/plate} = \frac{1}{0.9} = 1.1$; Inoculum per plate: $\frac{900\ \mu L}{1000\ \mu L} = 0{,}9$

III. RESULTS

1. Chronic-like particle exposure of latently with herpesvirus infected mouse lungs

A previous study on latent herpesvirus infection and additional particle exposures could show changes in lung structure and inflammation after a second particle hit [9]. This project was conducted as a follow up study. To mimic occupational or urban exposure to ambient particles during repeated episodes of high burden levels, a chronic-like exposure pattern was performed in this project. The impact of repeated exposure in latently with herpesvirus infected mice on lung health and the immune system was the primary focus of this investigation.

Briefly, C57/BL6J mice were infected with MHV-68, a murine gamma herpesvirus, or left uninfected as control. After establishment of latency 4 weeks later, mice were instilled with either CNP (50 µg) or PBS as control. 4 more instillations at intervals of 28 days followed, which results in a total number of 5 instillations of particles in a chronic-like pattern. Samples were collected 24 hours and seven days after the first, second and fifth instillation to account for acute and chronic effects on the mouse lungs (**Figure 2**). Groups that were compared at the aforementioned timepoints include untreated control, acute infection, latently MHV-68 infected mice with PBS instillation, latently infected mice with CNP instillation and mice with only CNP instillation. Particles used were Printex90, CNPs with a primary diameter of 14 nm, forming bigger agglomerates in solution. The surface area measured by Brunauer-Emmett-Teller analysis is 272 m^2/g [111].

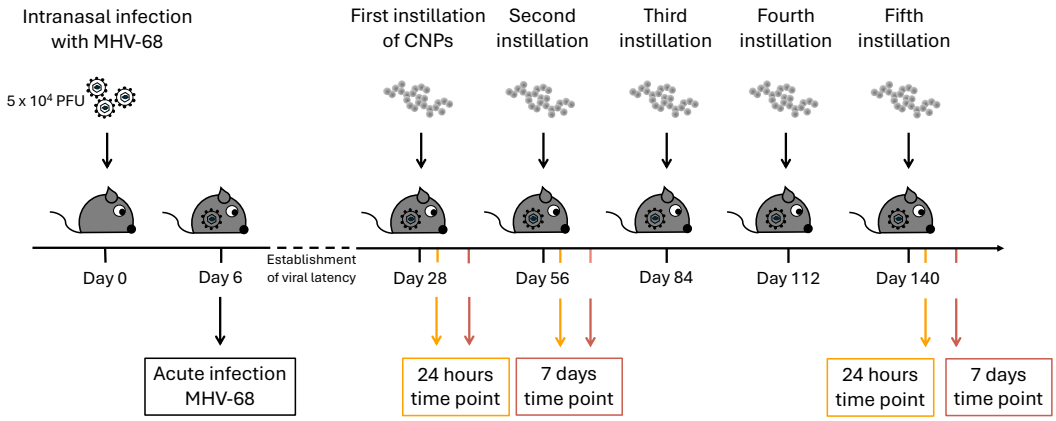

Figure 2 *Schematic illustration of the experimental setup.*

C57/BL6J mice were intranasally infected with 5×10^4 PFU of MHV-68. After establishment of latency 28 days later, mice were instilled intratracheally with 50 µg CNP or PBS as control. The same instillation was repeated at days 56, 84, 112 and 140. Samples were collected 6 days after infection and 24 hours and 7 days after the first, second and fifth instillation. 3 to 6 mice per group were used for histological and additional 3 to 6 for molecular examinations.

All mice, regardless of treatment, gained the same amount of weight during the experiment. Mice from the untreated control group reached a bodyweight of 23.3 ± 1.4 g at day 140 of the experiment. Latently infected animals with sham instillations weighed 24.7 ± 1.8 g, infected mice with CNP exposure 25.1 ± 1.5 g. Mice with only CNP instillations had a bodyweight of 25.3 ± 1.8 g at the end of the experiment. Thus, there was no detectable difference in bodyweight changes between all groups and no evidence for systemic effects or stress to the animals during experiments (**Figure 3**).

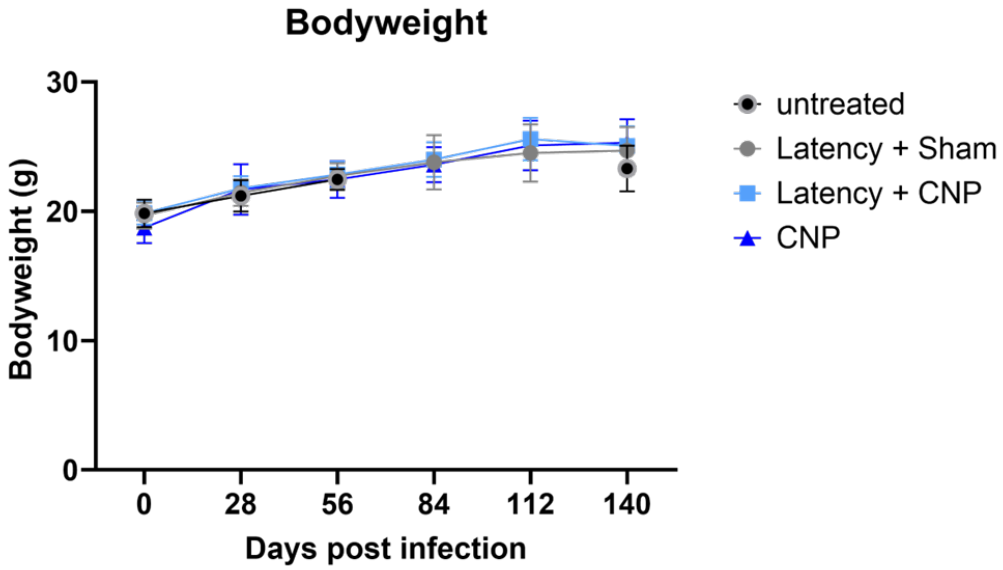

Figure 3 *Bodyweight of mice during the experiment.*

Representation of changes in bodyweight in gram (g) during the experiment. Black dots show untreated control mice, grey circles infected mice with sham instillation, light blue triangles infected mice with particle instillation and dark blue squares mice with only particle instillation. Each group includes between 3 and 27 measurements.

2. Chronic inflammation in the airspace

2.1. Inflammatory cell influx into the airspace

Bronchoalveolar lavage (BAL) was performed to assess the number of cells being recruited to the airspace. The total number of BAL cells increased in mice infected with the virus and exposed to particles, with an increase in the number of

instillations. Numbers were significantly higher 24 hours after repeated and five-time particle exposure in infected as well as uninfected mice compared to untreated control mice. Interestingly, 7 days after the second instillation of CNP, only infected mice showed significant changes, after the fifth instillation all CNP treated mice did (**Figure 4 a**). BAL cell differentiation of Giemsa stained cytospins helped to distinguish the cell types responsible for this increase. Rising neutrophil numbers in the airspace can be used as indicator for inflammation. As expected, CNP exposure led to a significant increase in neutrophils already 24 hours after the first instillation. This acute inflammation was resolved within 7 days. On the contrary, repeated CNP instillation induced not only a significant acute increase in neutrophil numbers but showed unresolved neutrophils remaining in the airspace after one week, rising with the number of instillations (**Figure 4 b**). This observed chronic inflammatory pattern was also reflected in the changes in macrophage numbers, the second representative of innate immune cells besides neutrophils. Macrophages are in healthy control mice the main cell type recovered by BAL with a median level of 93% in this experiment. Here we could see a progressive increase in macrophage numbers with the number of CNP instillations with significant changes only 7 days after five-time CNP exposure (**Figure 4 c**). Notably, cells with more than one nucleus were found more frequently in these samples. These multinucleated macrophages were significantly increased 24 hours and 7 days after the fifth CNP instillation in MHV-68 infected mice and one week after the last CNP instillation in non-infected mice (**Figure 4 d**). One cell type that could mainly be detected in latently infected mice with exposure to CNP were lymphocytes, important cells of the adaptive immunity. A significant increase in cell numbers was identified from the second particle trigger onwards, rising with the number of particle instillations and one week after the last exposure (**Figure 4 e**). Significance could also be detected when comparing the *Latency + CNP* group with *Latency + Sham* and *only CNP* groups. Two-time CNP exposure one week after the last exposure showed a significantly higher number of lymphocytes in BAL in infected compared to uninfected mice (p-value = 0.0095). A significant increase in lymphocyte numbers was also detected 7 days after the fifth instillation in infected mice compared to uninfected animals (p-value = <0.0001) and sham instilled mice (p-value = <0.0001). **Figure 4 f** demonstrates the massive increase in lymphocytes in the *Latency + CNP* group one week after the fifth particle exposure as parts of a whole. Around 46% of recovered BAL cells did account as lymphocytes in this

group, in contrast, the *only CNP* group contained around 23% lymphocytes and *Latency + Sham* also contained approximately 23%. From *Untreated Control* animals, only 5% of recovered BAL cells were lymphocytes. This means the proportion of lymphocytes in the airspace doubled in latently infected and particle treated mice compared to all the other groups.

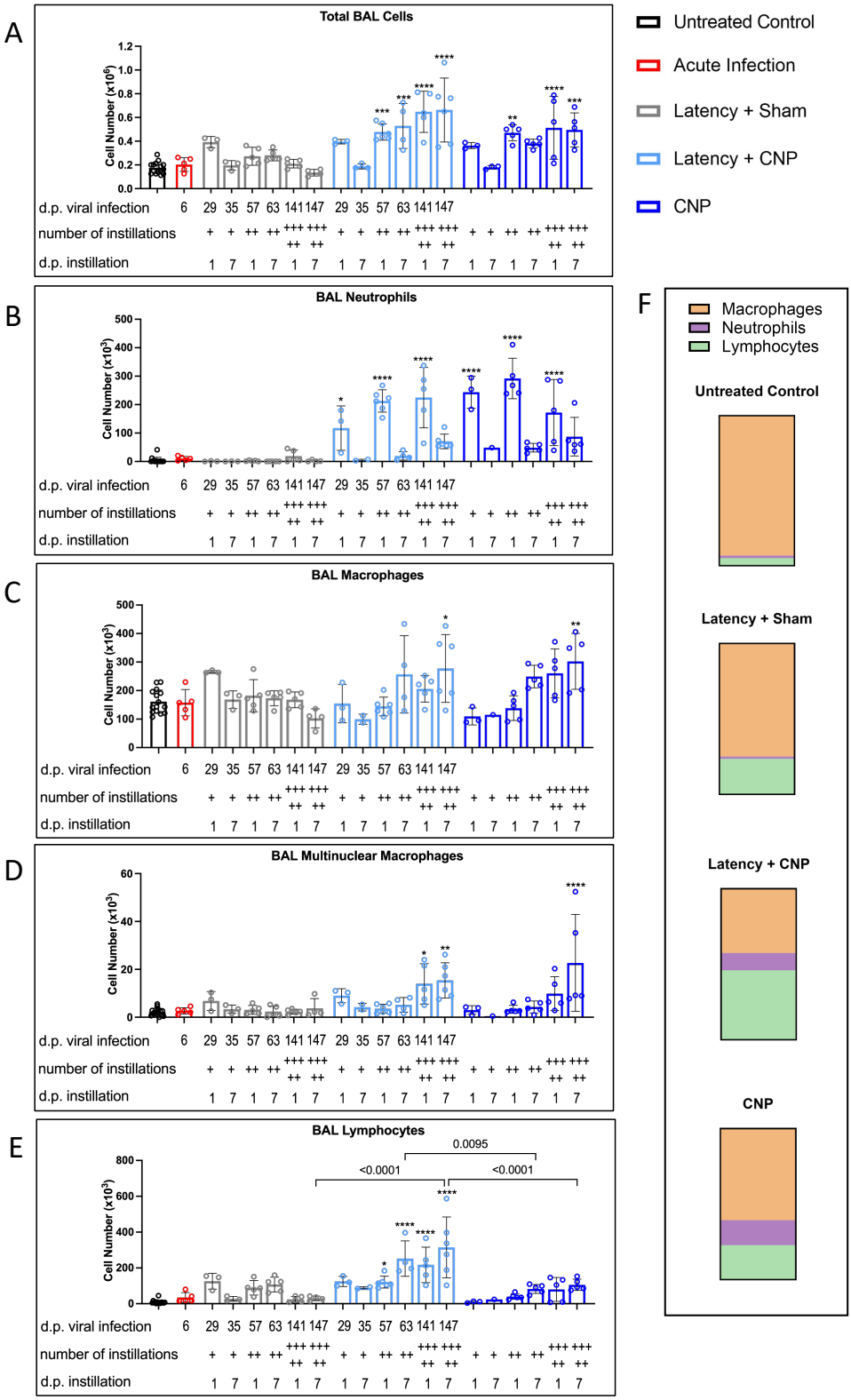

Figure 4 *Accumulation of inflammatory cells in the pulmonary airspace.*

(A) Quantification of total cells recovered by BAL. Differentiation of BAL cells was done by cytospin preparation and Giemsa staining. (B) Neutrophils, (C) macrophages, (D) multinucleated macrophages and (E) lymphocytes were distinguished and quantified. (F) Percentage of macrophages (orange), neutrophils (purple) and lymphocytes (green) recovered by BAL from mice, 7 days after five-time CNP or Sham instillation and untreated control mice. 15 mice from the untreated control and 3 – 6 mice from each group were included. Data are presented as mean ± SD. Ordinary one-way ANOVA followed by

Tukey's multiple comparison test, compared to *Untreated Control*. * p-value < 0.05, ** p-value < 0.01, *** p-value < 0.001, **** p-value < 0.0001.

Images of BAL cell cytospins illustrate clearly the differences determined in differential cell counts. BAL samples of *Untreated Control* mice contained more than 90% macrophages. The *Latency + CNP* group 24 hours after the fifth instillation revealed a much more heterogenous picture. Neutrophils and lymphocytes appeared more abundantly. Due to the repeated CNP instillations, numerous macrophages were laden with black particles and some even fused to bigger macrophages with more than one nucleus (**Figure 5**). These giant cells evolve in an environment of chronic inflammation and are often found in granulomatous infections or due to frustrated phagocytosis of foreign bodies.

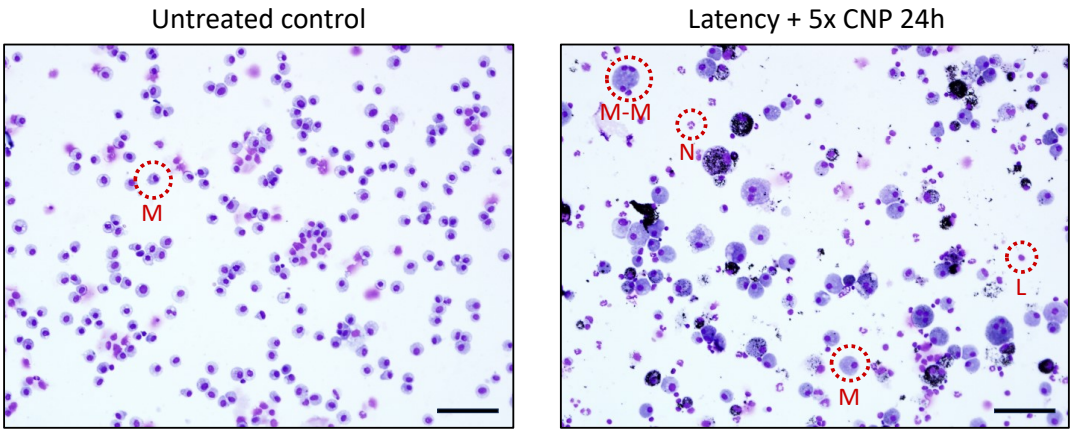

Figure 5 *Lymphocytes, neutrophils, and multinuclear macrophages in BALF.*

Representative brightfield images of Giemsa stained cytospins from BAL cells. The left image shows an untreated control sample with mainly macrophages (M) appearing. The right image shows neutrophils (N), lymphocytes (L), macrophages (M) and multinucleated macrophages (M-M) in an infected and five-time CNP exposed sample, 24 hours after the last exposure. Scale bar = 50 µm.

2.2. Inflammatory cytokine release into the airspace

The differentiation of BAL cells demonstrated the recruitment of numerous inflammatory cells to the airspace in response to particle exposure during viral latency. In order to get an overview about what is attracting these cells, I performed a multiplex assay to screen for 31 different chemokines in BAL fluids. **Figure 6** shows a heatmap summarizing the changes happening in the airspace upon infection and particle exposure. An acute reaction to the MHV-68 infection led to an increase in interferon gamma (IFN-γ) and interleukin 2 (IL-2), typical cytokines known to be secreted during viral infection and promoting adaptive immune responses. Sham instilled mice after viral infection did show a similar pattern as *Untreated Control*

mice, pointing towards a latent infection without further disturbance. In the *Latency + CNP* and *CNP only* groups, different pro-inflammatory cytokines got released into the airspace showing a broader increase in cytokine levels. Early responses after the first particle instillation resulted in secretion of typical pro-inflammatory cytokines, such as IL-6, IL-1β and TNF-α. Interestingly, five-time repeated CNP exposures showed a different panel of chemokines being released, including CCL3, CCL4, CCL7, CCL12, CCL19, CCL20, CCL22, CXCL5 and CXCL13, chemokines that are known for recruitment of neutrophils, macrophages and lymphocytes to the site of inflammation.

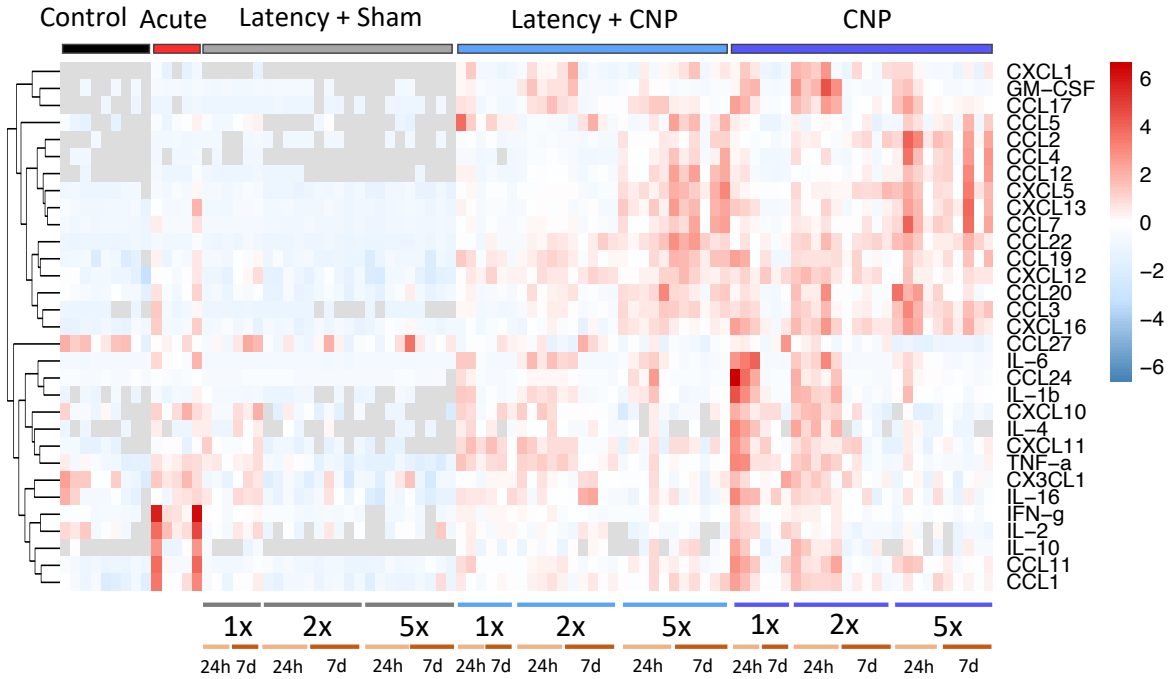

Figure 6 *Chemokine screening in BALF.*

Heatmap of 31 chemokines measured in BALF samples by multiplex analysis of untreated mice, acute infection, latency followed by PBS instillation (Latency + Sham), latency followed by CNP (50 µg) instillation (Latency + CNP) and CNP (50 µg) exposure only (CNP). Values of each animal are mapped individually.

When we had a closer look into neutrophil chemoattractants, we could observe significantly higher levels for CXCL1 compared to control samples, mainly as an acute response 24 hours after CNP exposure. For latently infected mice with subsequent particle exposure, CXCL1 was also significantly increased 7 days after the fifth instillation, for only particle exposed mice we could observe a significant change already one week after the second instillation (**Figure 7 a**). This fits nicely to the number of neutrophils getting recruited to the airspace as described above.

CXCL5 got significantly increased in the airspace in both CNP exposed groups with increasing levels with number of instillations, starting after the second instillation for uninfected CNP exposure and after the fifth instillation for latently infected mice (**Figure 7 b**). The most intriguing finding for both, CXCL1 and CXCL5, was the increase in cytokine levels within one week after the last CNP exposure in the *Latency + CNP* group. This accumulation was not seen in *only CNP* without infection.

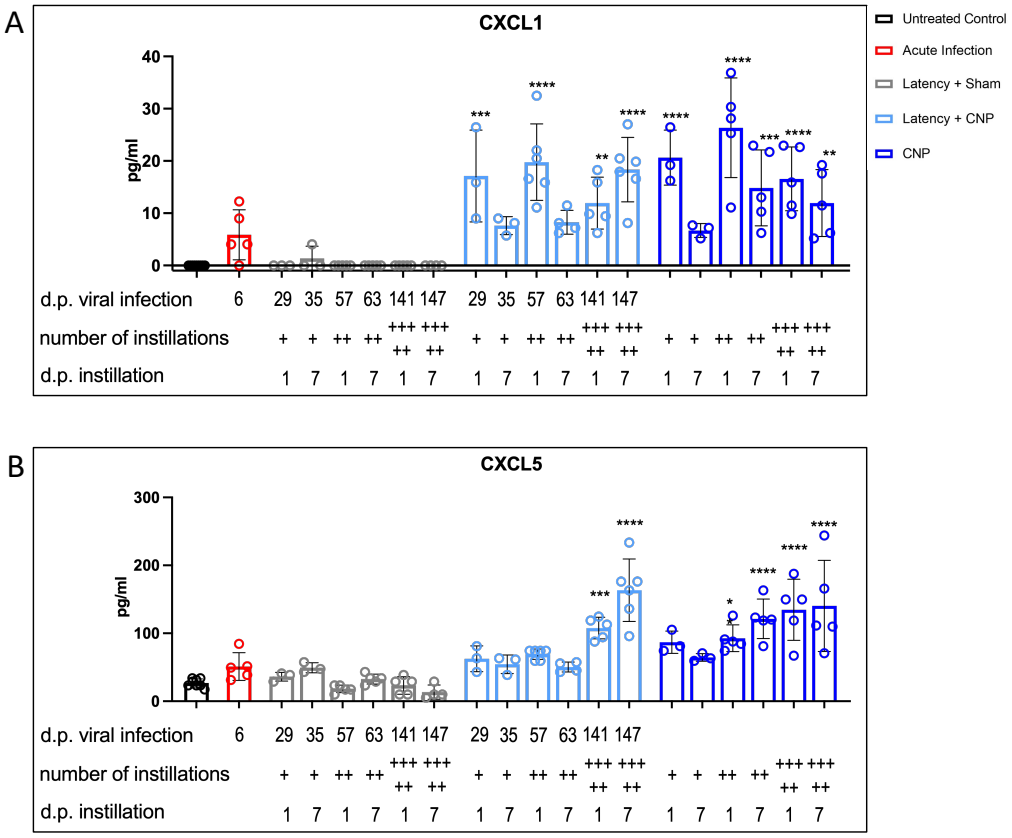

Figure 7 *Release of neutrophil-attracting cytokines into the airspace of particle-exposed lungs.*

Concentrations of CXCL1 and CXCL5 were measured in BALF samples by a Bio-Plex assay. Data are presented as mean ± SD. Ordinary one-way ANOVA followed by Tukey's multiple comparison test, compared to *Untreated Control*. ** p-value < 0.01, *** p-value < 0.001, **** p-value < 0.0001.

CCL2, CCL3, CCL4 and CCL7 are amongst the cytokines relevant for leukocyte recruitment and often found in acute and chronic inflammation. Accordingly, we could see significantly increased secretion of these cytokines mainly in the five-time particle exposed mice. CCL2 and CCL7 can act trough the CCR2 receptor, leading to neutrophil and monocyte recruitment to the site of secretion. Here, CCL2 in the BAL fluid was significantly elevated 24 hours and one week

after the fifth CNP exposure in the latently with MHV-68 infected mice. Within the *only CNP* exposed group, there was a significant increase already after the second particle instillation (**Figure 8 a**). A slightly different picture could be observed for CCL7. Significance is only found 7 days after the fifth particle instillation in infected mice and one and 7 days in the CNP treated group (**Figure 8 b**). CCL3 and CCL4 play an important role in neutrophil, macrophage, natural killer cell (NK-cell) and T-cell attraction. In this experiment, CCL3 showed significant changes only in both particles treated groups, besides the acute infection. Latency followed by CNP exposure led to a significant increase in CCL3 in the BAL fluid 24 hours after the second and at both time points after the fifth particle instillation. CNP exposure alone increased the CCL3 level significantly in all groups except for one week after the first instillation (**Figure 8 c**). CCL4 was secreted to the airspace in particle exposed lungs. Significance could only be observed after the fifth CNP instillation in latently infected mice. Particle exposure alone had a bigger effect on CCL4 release, showing significance acutely 24 hours after the first, second and fifth instillation as well as one week after the last (**Figure 8 d**). For all four cytokines shown here, we could observe the same differences one week after the last particle exposure as we did for CXCL1 and CXCL5. Cytokine levels did increase within one week after the fifth particle exposure only with latent viral infection, not in the *CNP only* group. This consistent finding supports the hypothesis of an aggravation of lung inflammation and health in the *Latency + CNP* group after chronic particle exposure.

Overall, secretion and release of leukocyte attracting cytokines seemed to be CNP related, irrespective of viral infection, which is in accord with the quantified numbers of neutrophils and macrophages getting recruited to the airspace in both CNP instilled groups. Nevertheless, recruitment of lymphocytes was observed exclusively in mice infected with MHV-68 following particle exposure. However, no matching cytokine release to the airspace was identified among the 31 chemokines that were screened here.

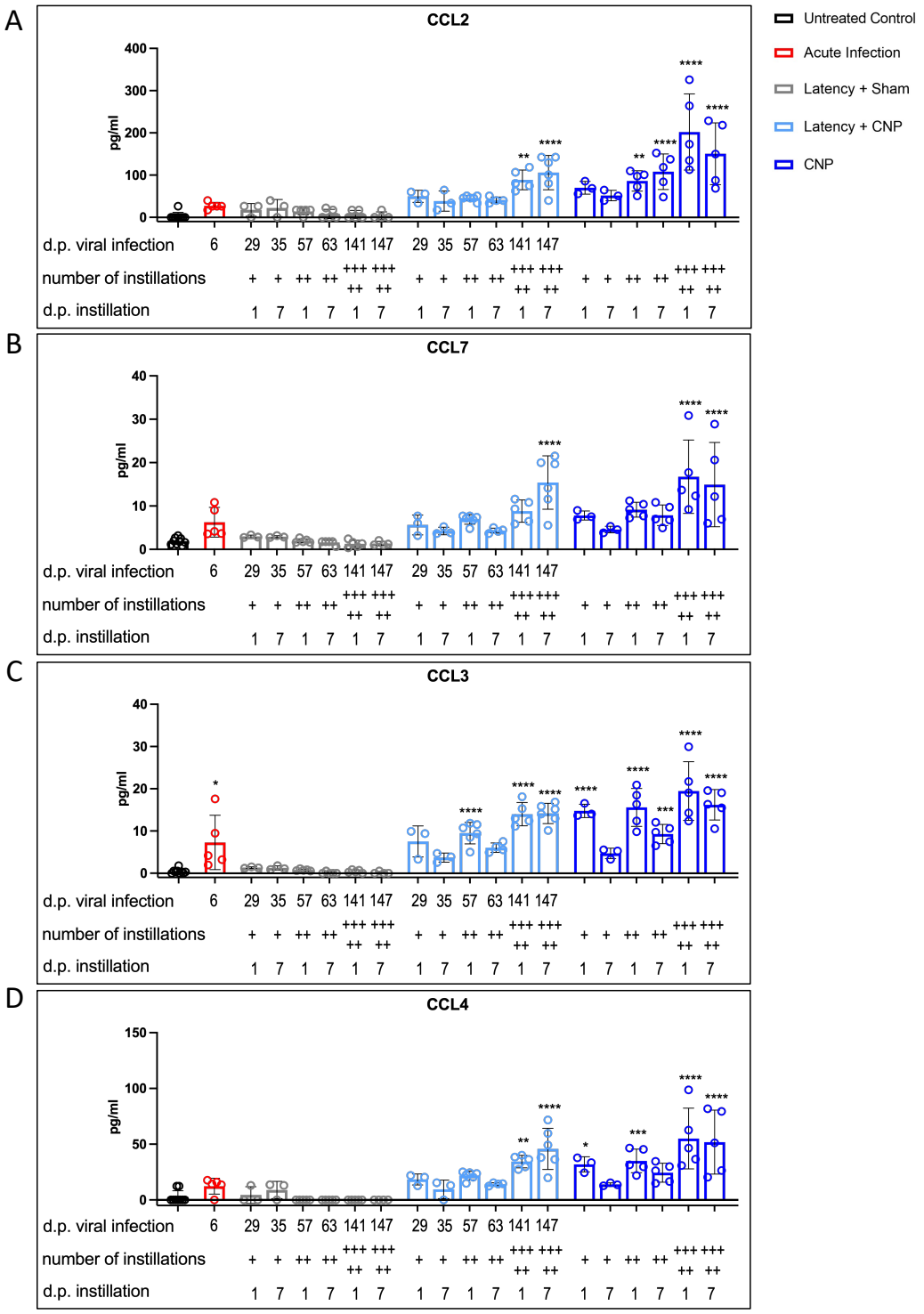

Figure 8 *Leukocyte recruiting cytokines in the airspace increase with number of particle instillations.*

Concentrations of (A) CCL2, (B) CCL7, (C) CCL3 and (D) CCL4 were measured in BALF samples by a Bio-Plex assay. Data are presented as mean ± SD. Ordinary one-way ANOVA followed by Tukey's multiple comparison test, compared to *Untreated Control*. * p-value < 0.05, ** p-value < 0.01, *** p-value < 0.001, **** p-value < 0.0001.

3. Chronic inflammation in lung tissue

Given the massive recruitment of inflammatory cells into the airspace, I was interested in corresponding changes in lung tissue. Analysis of H&E-stained lungs revealed massive, mainly peribronchiolar and perivascular, infiltrations of mononuclear cells into the tissue of infected mice with five-time repeated particle exposure (**Figure 9 a**). Quantification of infiltrating cells showed a significant increase in tissue inflammation only in the *Latency + 5-time CNP* group after 7 days (**Figure 9 b**). This finding aligned with lymphocyte accumulations in the airspace of the same group, suggesting a lymphocytic component in these infiltrations.

And indeed, by staining for T- and B-cell markers, we could see that a major component of infiltrating cells was $CD45R^+$ B-cells. $CD8^+$ as well as few $CD4^+$ T-cells were also part of those peribronchiolar and perivascular infiltrations. In most infiltrations, but especially in focal infiltrations in the *Latency + CNP* group, B-cells did form a dense core, surrounded by $CD8^+$ T-cells and very few $CD4^+$ T-helper cells (**Figure 10**). $CD8^+$ T-cells are also known as cytotoxic T-cells and usually involved in recognizing and destroying infected cells. The distinct arrangement of B- and T-cells we could find here hints towards the formation of inducible bronchial associated lymphoid tissue (iBALT).

Further characterization of the infiltrates was done using specific markers for lymphocytes and NK-cells in immunofluorescence staining. As stated before, many perivascular and peribronchiolar infiltrating cells could be identified as $CD8^+$ T-lymphocytes (**Figure 11 a, b**). Natural-killer receptor group 2, member D (NKG2D) is a receptor found mainly on the surface of NK-cells that is able to recognize several ligands which are upregulated in cells upon stressful stimuli. Not only NK-cells, but also T-cells can get stimulated to express NKG2D under certain circumstances. Notably, cells expressing NKG2D were identified as being recruited to the lung tissue after five-time particle exposure, independent of infection with MHV-68 (**Figure 11 a**). Granzyme B is a serine protease granzyme that is stored in the lytic granules of NK-cells and cytotoxic T-cells. Upon secretion into the cytoplasm of target cells, it induces a programmed cell death, a process known as apoptosis. Granzyme B positive cells also belong to the infiltrating cells found here (**Figure 11 b**). These cells are most likely NK-cells, as nearly no co-localization with the cytotoxic T-cell marker CD8 was found. These perivascular and

peribronchiolar infiltrations, especially $CD8^+$ T-cells, could be found in all particle-instilled mouse lungs, but were still more prominent in the latently with MHV-68 infected mice.

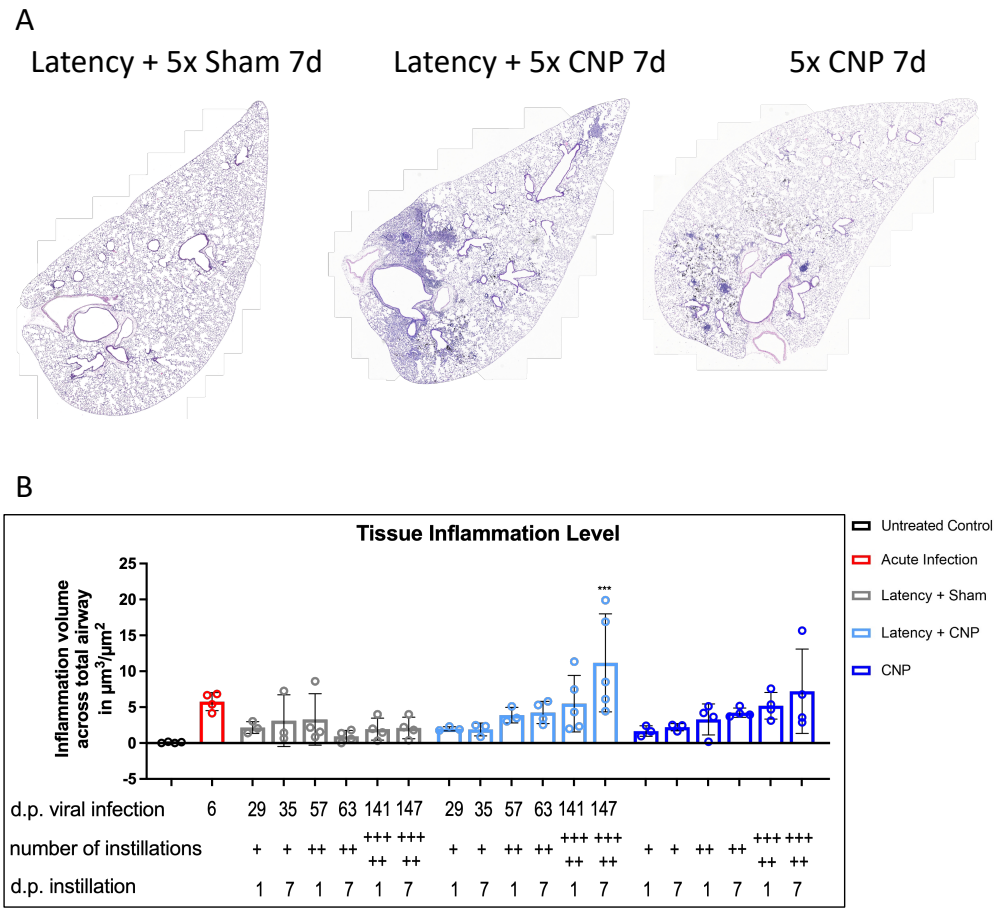

Figure 9 *Cellular infiltrations in latently infected lungs with repetitive particle triggers.*

(A) Representative H&E-stained lung lobe scans of latently infected mice exposed to sham or CNP five times, 7 days after the last instillation, and mice only exposed to CNP 7 days after the fifth exposure. (B) Quantification of cellular infiltrations, termed tissue inflammation level, using a computer assisted stereological quantification method. Data are presented as mean ± SD. Ordinary one-way ANOVA followed by Tukey's multiple comparison test, compared to *Untreated Control*. *** p-value < 0.001.

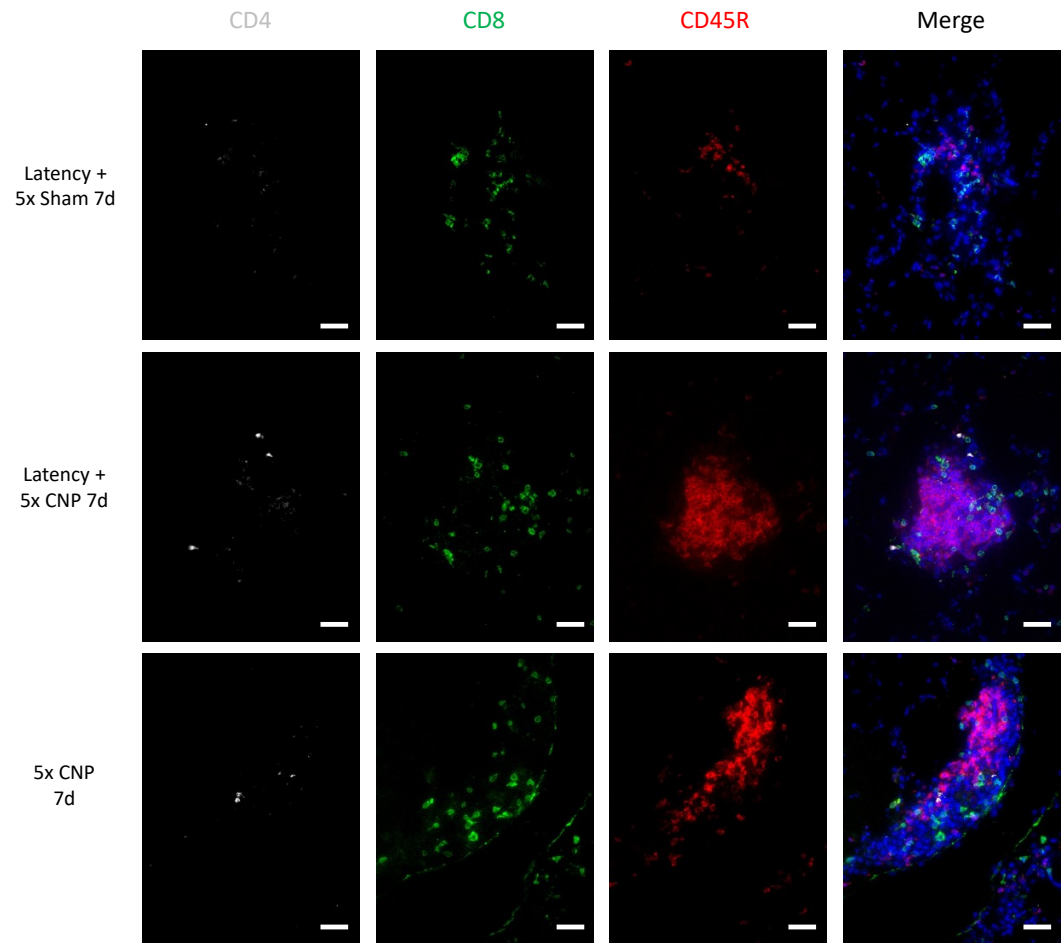

Figure 10 *Recruitment of mainly CD8$^+$ T-cells and B-cells to the lung tissue.*

Representative immunofluorescent staining of lung tissue. Slides were stained for CD4 (white), CD8 (green), CD45R (red) and DAPI (blue). Scale bar = 20 µm.

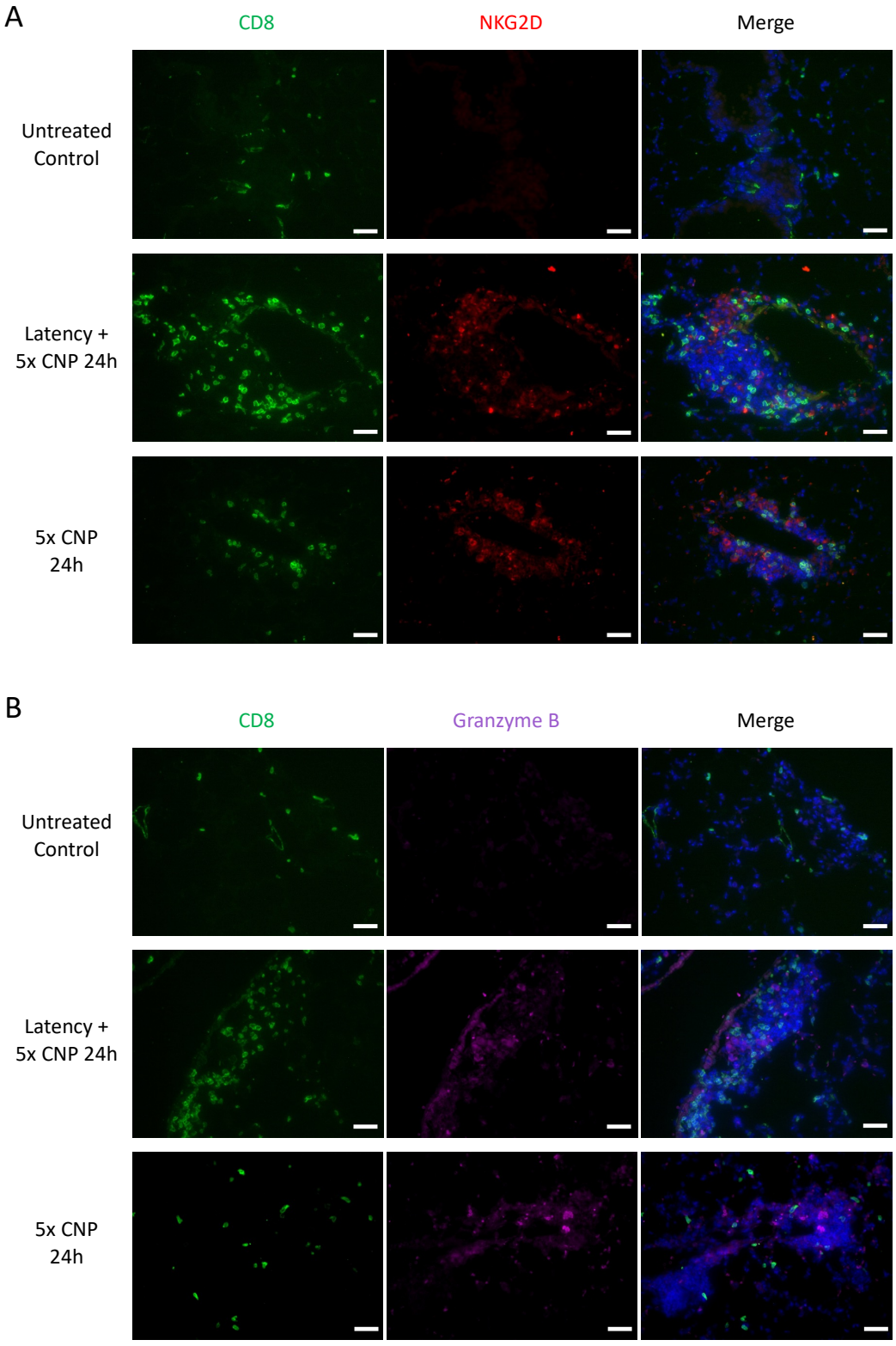

Figure 11 *Recruitment of CD8$^+$ T-cells and NK-cells to the lung tissue.*

Representative immunofluorescent staining of lung tissue. (A) Slides were stained for CD8 (green), NKG2D (red) and DAPI (blue). (B) Slides were stained for CD8 (green), Granzyme B (purple) and DAPI (blue). Scale bar = 20 µm.

4. Epithelial cell damage and loss of alveolar type 1 cells

Another conspicuous feature when looking at the lung sections was an enlargement of the alveoli in the infected mice with repeated particle instillation (**Figure 12 a**). The lung of one mouse from this group showed prominent alterations, displaying enlargements throughout the entire organ. Significant enlargement of the mean linear intercept (MLI) was detected one week after the fifth CNP exposure in latently infected mice only (**Figure 12 b**). This was a first hint towards damage and loss of alveolar structure in the infected and particle exposed mice.

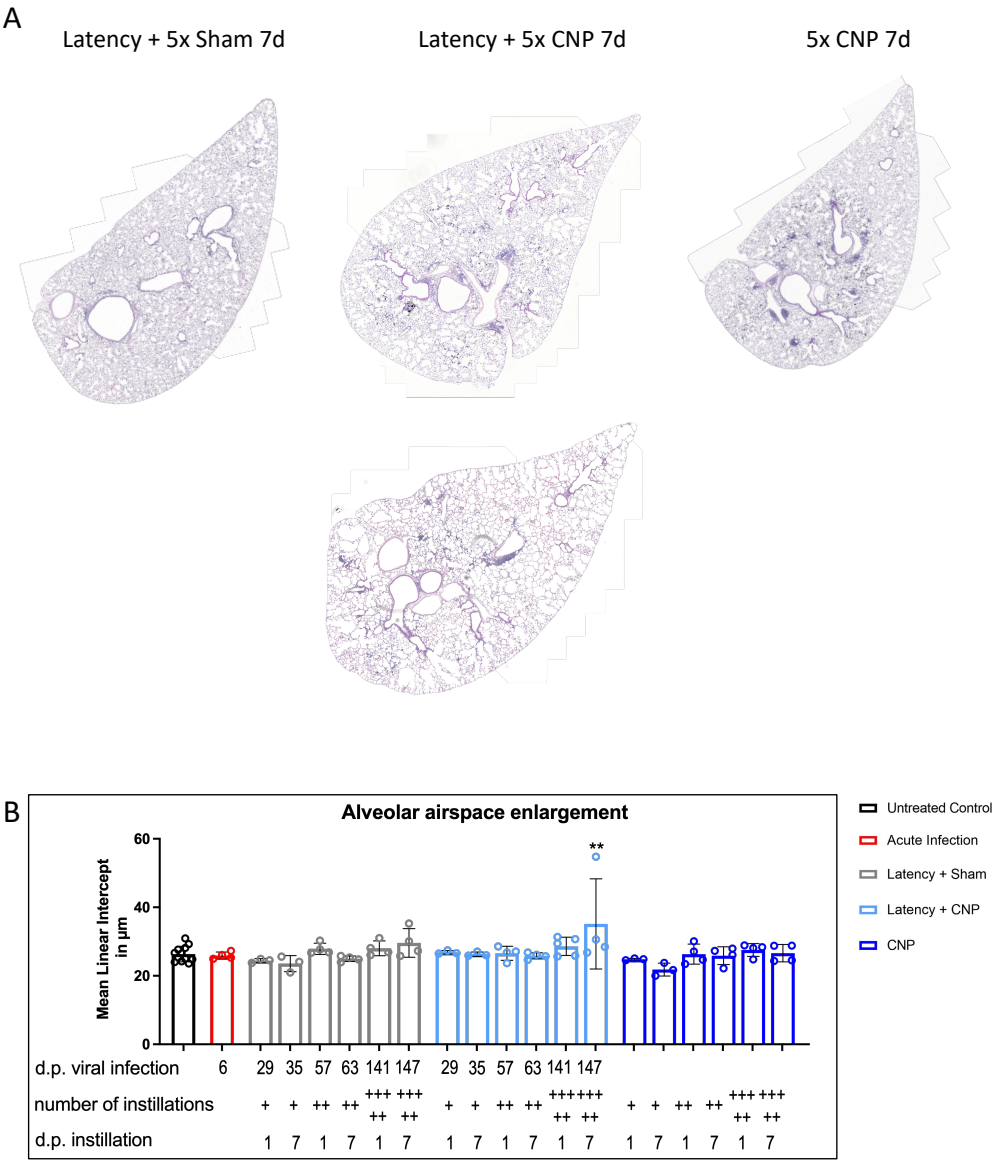

Figure 12 *Alveolar airspace enlargement in infected and particle exposed lungs.*

(A) Representative scans of H&E-stained lung lobes. The left lobe represents an infected mouse one week after the fifth instillation with PBS as sham control. Both lobes in the middle show latently infected mice followed by five-time CNP exposure and the lobe on the right is a representative image of a lobe from an *only CNP* exposed mouse. (B)

Stereological quantification of the mean linear intercept of alveoli in µm. Data are presented as mean ± SD. Ordinary one-way ANOVA followed by Tukey's multiple comparison test, compared to *Untreated Control*. ** p-value < 0.01.

The alveolar epithelium consists of two cell types, alveolar type 1 (AT1) and alveolar type 2 (AT2) cells. AT1 cells cover more than 95% of the alveolar surface and it is known that they are more vulnerable to injury than AT2 cells. Interestingly, AT2 cells can act as stem cells in this niche. Consequently, they can differentiate into AT1 cells and replenish the damaged alveoli. Assessing the number of AT2 and AT1 cells in my samples was a way to determine the state of alveolar injury and replenishment. Surfactant protein C (SPC) is one of the proteins contained in pulmonary surfactant. It is exclusively produced in AT2 cells as precursor protein before being processed and secreted. Pro-SPC is therefore the optimal target to identify AT2 cells in lung tissue. Homeodomain only protein homeobox (HOPX) is a protein involved in the formation of the distal lung. It was shown that adult murine lungs show HOPX expression in AT1 cells, although it has to be mentioned that it was also found on AT2 cells to a smaller extend. Other known markers for AT1 cells are aquaporin 5 (AQP5) or podoplanin. Both of them are membrane-bound and were therefore excluded for quantification. **Figure 13 a** provides an overview of the pattern of pro-SPC as well as HOPX IF staining in lung tissue. No changes could be detected regarding AT2 cell numbers in five-time exposed mice in comparison to control mice (**Figure 13 b**). Interestingly, we could detect a significant decrease in type 1 epithelial cells one week after the fifth particle instillation in infected mice (**Figure 13 c**). If one considers that the majority of the epithelial surface is constituted by AT1 cells, this reduction could explain the aforementioned enlargement of alveoli observed in this specific group.

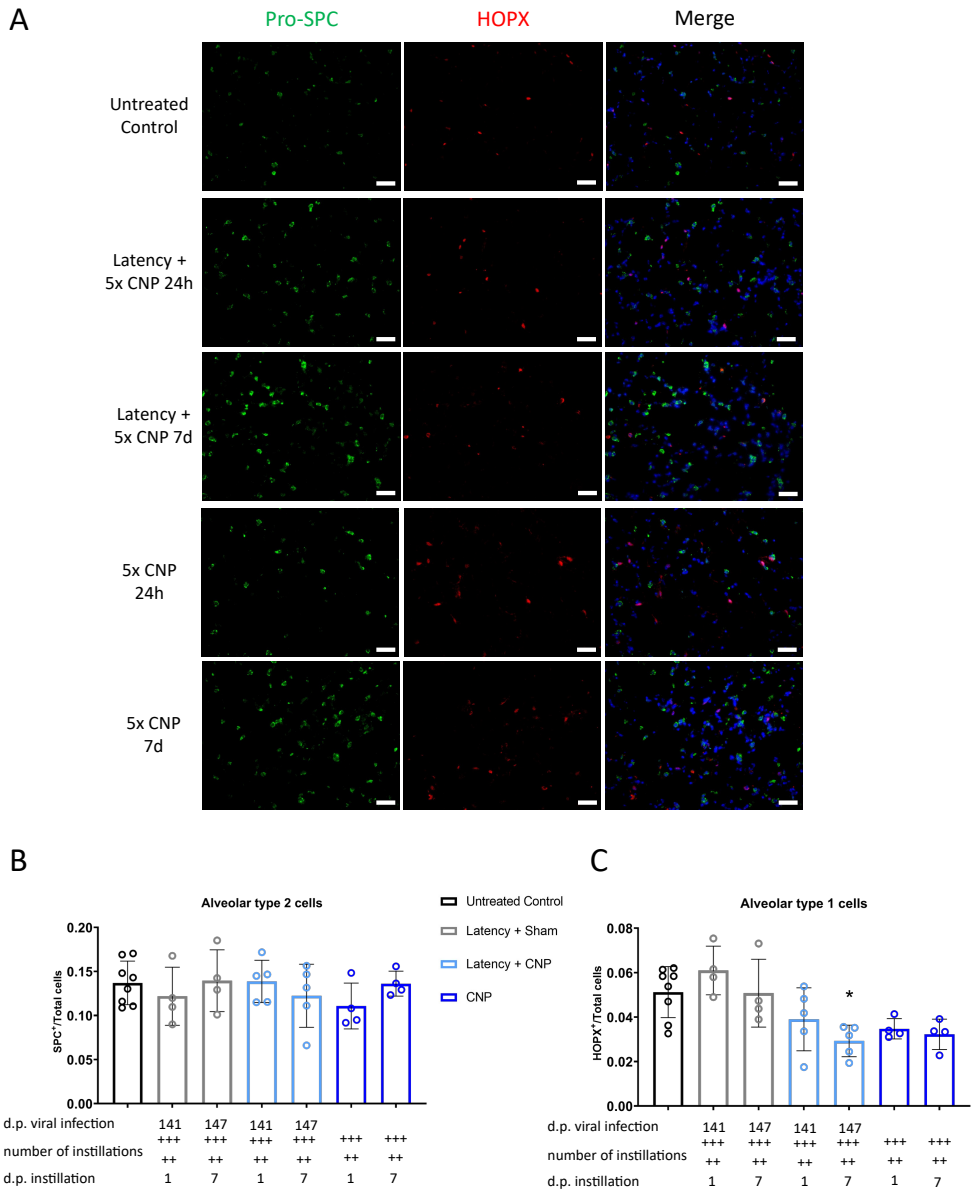

Figure 13 *Loss of alveolar type 1 epithelial cells in infected mice exposed to CNP.*

Pro-SPC as well as HOPX were stained as markers for AT2 and AT1 cells, respectively. (A) Representative images of IF stained lung sections. Slides were stained for pro-SPC (green), HOPX (red) and DAPI (blue). Scale bar = 20 µm. (B) Quantification of pro-SPC positive cells in relation to total DAPI stained cells. (C) Quantification of HOPX positive cells in relation to total DAPI stained cells. Data are presented as mean ± SD. Ordinary one-way ANOVA followed by Tukey's multiple comparison test, compared to *Untreated Control*. * p-value < 0.05.

A frequently used method to measure alveolar-capillary barrier disruption is the determination of proteins in the lavage fluid. Especially increased immunoglobulin M (IgM) levels in BAL fluids indicate an increased leakage of vascular proteins into the airspace. Total protein was significantly increased compared to untreated control mice only in particle exposed groups. A significant increase was observed to manifest as an acute reaction to particle exposure 24 hours

after the first and second instillations. After the fifth instillation of CNP, a statistically significant increase appeared one week after the exposure, exhibiting a delayed reaction pattern (**Figure 14 a**). This observation was not specific to viral latency, but rather to the particle instillation. To get more specific information about an alveolar-capillary barrier disruption, IgM levels were measured in BAL fluids. Here we could also see significant changes only in both particle instilled groups. Nevertheless, a significant elevation in BAL IgM was only observed after five-time CNP exposure in both experimental groups, with the exception of the 24 hours timepoint after the first instillation in the *Latency + CNP* group. Nevertheless, no discernible distinction in barrier disruption could be identified between the *CNP only* and *Latency + CNP* groups (**Figure 14 b**).

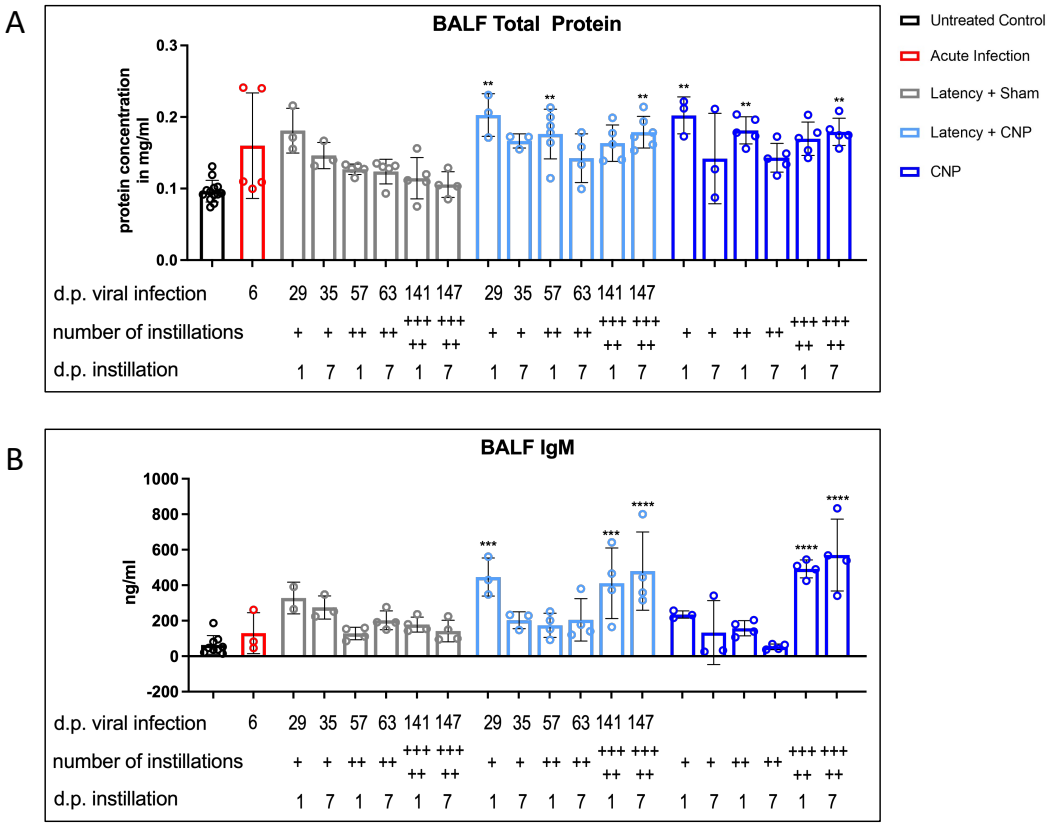

Figure 14 *Increased protein and IgM concentrations after five-time repeated CNP exposure.*

(A) Total protein concentration in mg/ml of BAL fluid samples measured by bicinchoninic acid assay. (B) IgM content in ng/ml of BAL fluid samples measured by ELISA. Data are presented as mean ± SD. Ordinary one-way ANOVA followed by Tukey's multiple comparison test, compared to *Untreated Control*. ** p-value < 0.01, *** p-value < 0.001, **** p-value < 0.0001.

Cytokeratin 18 (CK18) is a protein found in lung epithelial cells of the lung and is their major intermediate filament. It is released in its full-length (M65) following

necrosis and cleaved by caspases (M30) during apoptosis of these cells. Hence, CK18 can be a sensible marker to detect epithelial cell death in the lung. The ratio of caspase cleaved and full-length CK18 revealed a significant alteration 24 hours after the first sham instillation as well as one week after the fifth particle instillation in infected mice only (**Figure 15**). A higher ratio of cleaved to full-length CK18 indicates that the cell death mode occurring here is apoptosis, rather than necrosis.

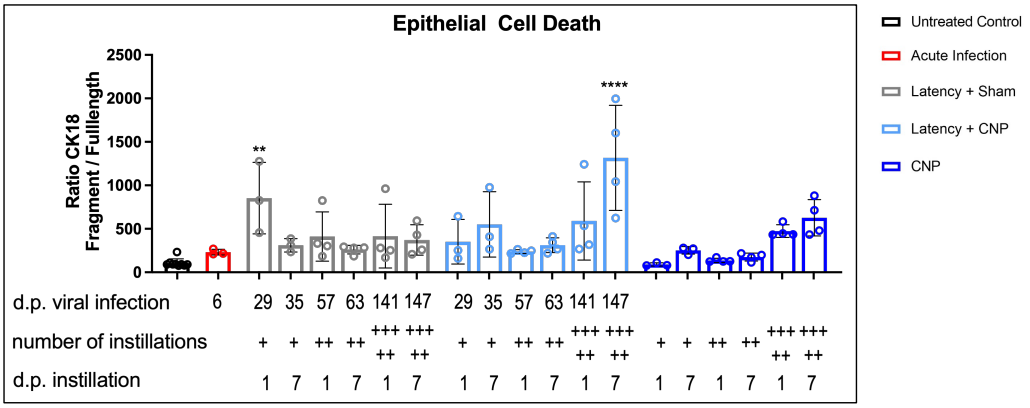

Figure 15 *Ratio of fragmented to full length cytokeratin 18 increased in latency one week after five-time particle exposure.*

Ratio of measurements of M65, a marker for the intact cytokeratin 18 and M30, a marker for the caspase cleaved cytokeratin 18 in BAL fluid samples by ELISA. Data are presented as mean ± SD. Ordinary one-way ANOVA followed by Tukey's multiple comparison test, compared to *Untreated Control*. ** p-value < 0.01, **** p-value < 0.0001.

Unrepaired DNA double-strand breaks can result in apoptosis of the affected cell [116]. Terminal deoxynucleotidyl transferase dUTP nick end labelling (TUNEL) is a method to label the 3'-hydroxyl ending in double-strand DNA breaks. The DNA fragmentation gives information about the apoptotic process behind. In this study we can observe an increase in TUNEL signal in particle exposed mouse lungs throughout the whole lobe. In infected and particle exposed mice, these signals were co-localized with epithelial-like cells (**Figure 16**). That's another result giving a hint towards apoptosis happening in alveolar epithelial cells.

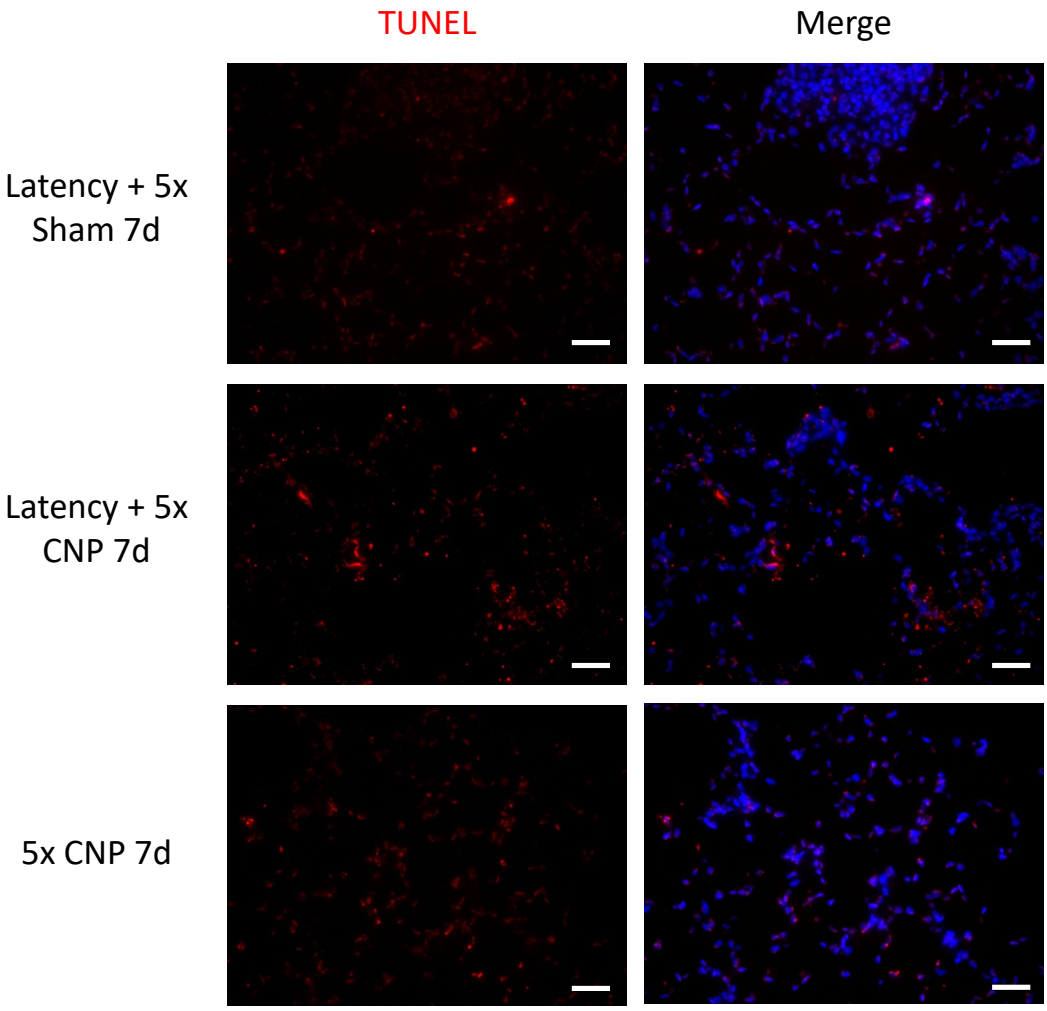

Figure 16 *Elevated DNA fragmentation after five-time particle exposure in infected lungs.*

Representative immunofluorescent staining of lung tissue. Double stranded DNA fragmentation stained in red with TUNEL and DAPI in blue. Scale bar = 20 µm.

Taken together, an overall pathological description of mouse lungs with viral infection after five-time particle exposure revealed the presence of pronounced focal increases in infiltrating lymphocytes and diffuse macrophage infiltrations. The macrophages were observed to contain a substantial quantity of black material. A slight thickening of the interalveolar walls was found, and one mouse in the group exhibited prominent emphysema in the lung. The patterns observed in the lymphocytes, macrophages and alveolar wall thickening of five-time CNP exposed mice without infection were similar, although to a lesser extent. No evidence for emphysema was detected in these mice. Infected animals with sham instillation did not differ from untreated control mice.

5. Acute infection but no reactivation detectable in lung tissue

Six days after intranasal infection with 5×10^4 PFUs MHV-68, strong expression of lytic viral proteins could be detected using a polyclonal rabbit serum containing antibodies against lytic proteins of MHV-68. **Figure 17** shows a distinct pink staining for lytic MHV-68 proteins in epithelial cells during the acute infection phase. 24 hours after the fifth particle instillation, pink staining was also observed in infiltrating cells, exhibiting a distinct pattern that differed from that observed in acute infection. This could hint towards a reactivation happening upon the particle stimulus. Unexpectedly, some cells that got labelled with the polyclonal rabbit serum could be found in particle exposed mice without viral infection. Notably, the localization of stained cells is different in the *only CNP* group compared to the *Latency + CNP* group. In only particle exposed mice, staining is detected mostly in the alveolar region in cells resembling alveolar macrophages. Most likely, this reflects a cross-reaction with non-viral antigens in particle exposed mice. Nevertheless, infection of the mice could be proven by the distinct pattern during acute infection, that was not found in any other treatment group.

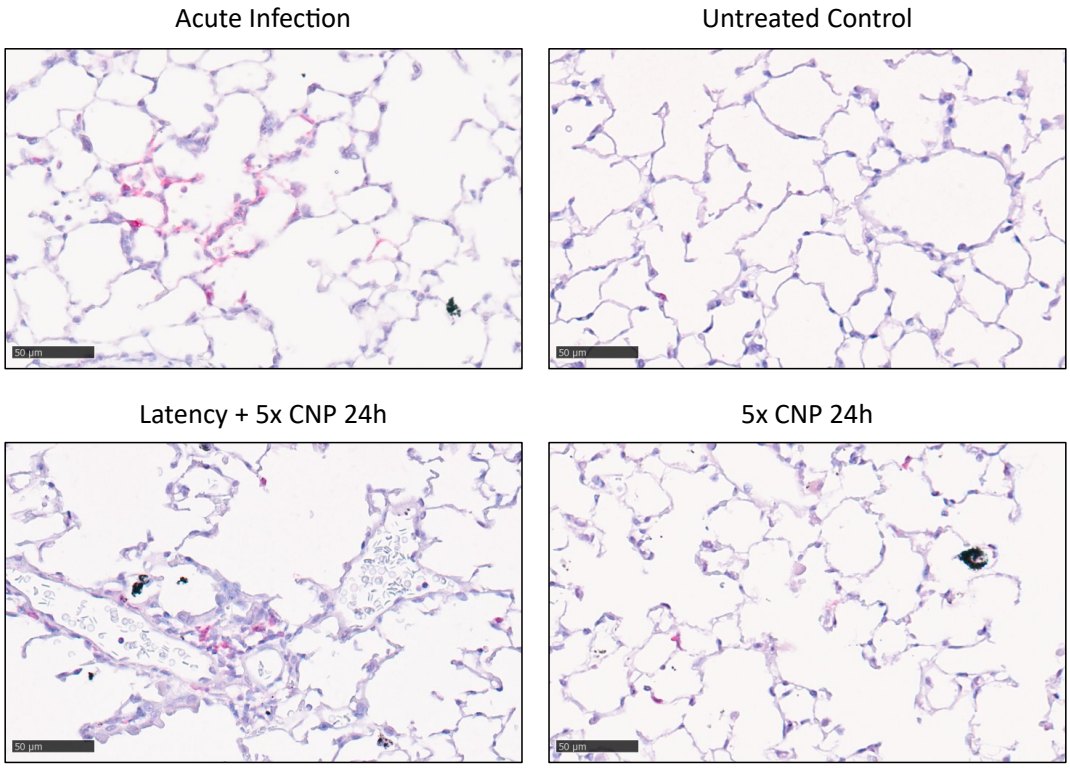

Figure 17 *Acute infection detectable in lung tissue.*

Representative images of IHC stained lung tissue showing MHV-68 lytic viral proteins in pink. Purple counterstaining was done using haematoxylin. Scale bar = 50 µm.

6. *In vitro* immunocompetent lung organoids to model the *in vivo* scenario of CNP triggered virus reactivation and tissue injury

The use of animal models is an invaluable tool for the identification of general alterations and correlations within an experimental setup. Nevertheless, exploiting simplified models to answer specific scientific questions opens up new possibilities. Previous studies in the research field of herpesvirus reactivation upon particle exposure did use submerged culture conditions with a single macrophage cell line persistently infected with MHV-68 [8,9]. However, submerged culture conditions with a single immortalized cell line do not adequately recapitulate what happens in the organ under investigation. One approach to create a more realistic model is the use of three-dimensional lung organoids generated from primary cells. Lung organoids are increasingly being used to recreate organ-like conditions *in vitro* and this tool is particularly useful when epithelial cell responses and recovery are in focus of investigation [117]. Thus, in this project we decided to use such a well-established three-dimensional lung organoid model and extend it to generate immunocompetent organoids. In addition to organoids derived from primary epithelial cells and fibroblasts, we also included macrophages persistently infected with MHV-68.

To create lung organoids, $CD31^-$ $CD45^-$ $EpCAM^+$ epithelial cells were isolated from mouse lungs and co-cultured with fibroblasts within an extracellular matrix (Matrigel). In a matter of days, single epithelial cells could form spherical lung organoids with the support of surrounding fibroblasts. Immunocompetent organoids were generated in the same way, with addition of a macrophage cell line, either uninfected or persistently infected with MHV-68 (**Figure 18**). Han and Haefner could already observe epithelial cell injury in latently with MHV-68 infected mice upon exposure to CNP [9]. In addition, the animal experiments described in this thesis did reveal a similar finding, with increased damage correlated with increased numbers of particle exposure. The aim of this study was to create an advanced *in vitro* model to recapitulate the observed *in vivo* situation. Within the defined setting of immunocompetent, persistently infected organoids, cellular crosstalk and mechanisms behind epithelial cell death might be studied.

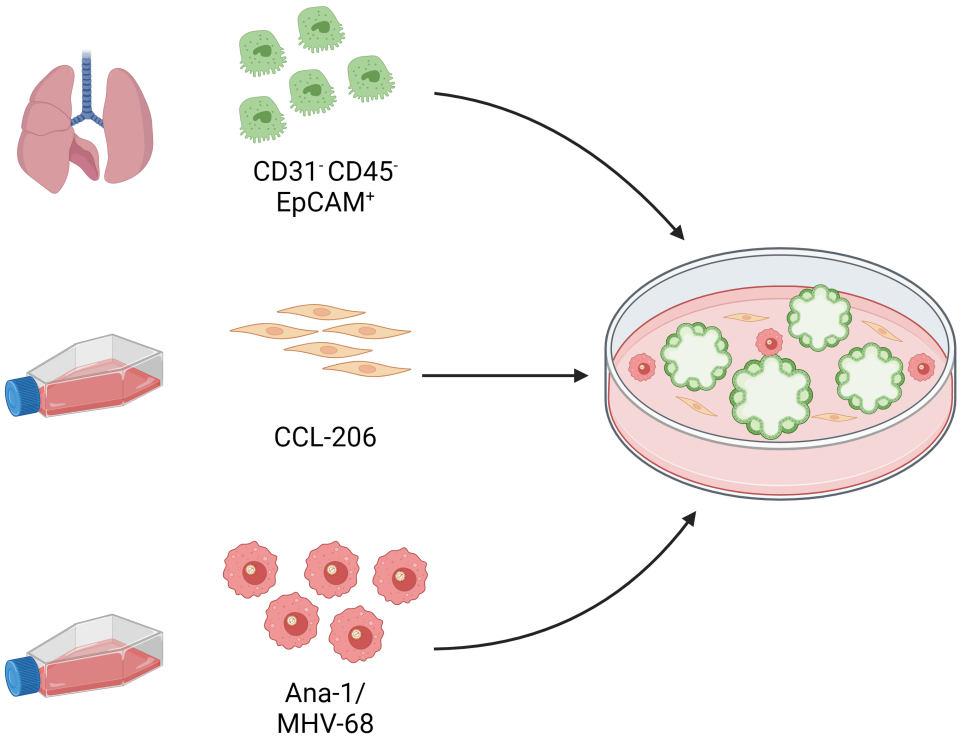

Figure 18 *Schematic illustration of the lung organoid setup.*

CD31$^-$ CD45$^-$ EpCAM$^+$ primary mouse lung epithelial cells were cultured together with a fibroblast cell line (CCL-206) in a 1:1 ratio within Matrigel. To create an immunocompetent organoid culture, a bone-marrow derive macrophage cell line (Ana-1) was added in a 1:1:1 ratio. To model reactivation upon different stimuli, macrophages persistently infected with MHV-68 were used instead of the uninfected cell line (Ana-1/MHV-68). Created in BioRender.com.

6.1. Macrophages support lung organoid growth

Comparing the behaviour regarding growth in organoids cultured either in co-culture with fibroblasts only or in triple-culture with uninfected macrophages or MHV-68 infected macrophages revealed a significant increase in number of organoids in triple-culture conditions (**Figure 19 a, b**). The increase in organoid formation was observed to be stable for the uninfected macrophage culture, the mean number of organoids increased from 27.42 (SD 17.11) in co-culture to 48 (SD 27.6) in triple-culture. The mean number of organoids formed in triple-cultures with persistently MHV-68 infected macrophages was found to be similar to that observed in uninfected cultures (45.95). However, the standard deviation was significantly higher (46.55) in the infected organoids, indicating a greater degree of variability. The variations between biological and even technical replicates may be attributed to the spontaneous reactivation of MHV-68 in certain instances. Fibroblasts in all culture conditions spread within the matrix and supported organoid growth also via direct contact with epithelial cells (**Figure 19 c**). **Figure**

19 d shows the close interaction that happened between macrophages in red and grown organoids. Macrophages actively moved towards lung organoids and got into close contact with them. These findings demonstrate that communication and interaction happened within immunocompetent organoids with a favourable influence of macrophages on organoid formation.

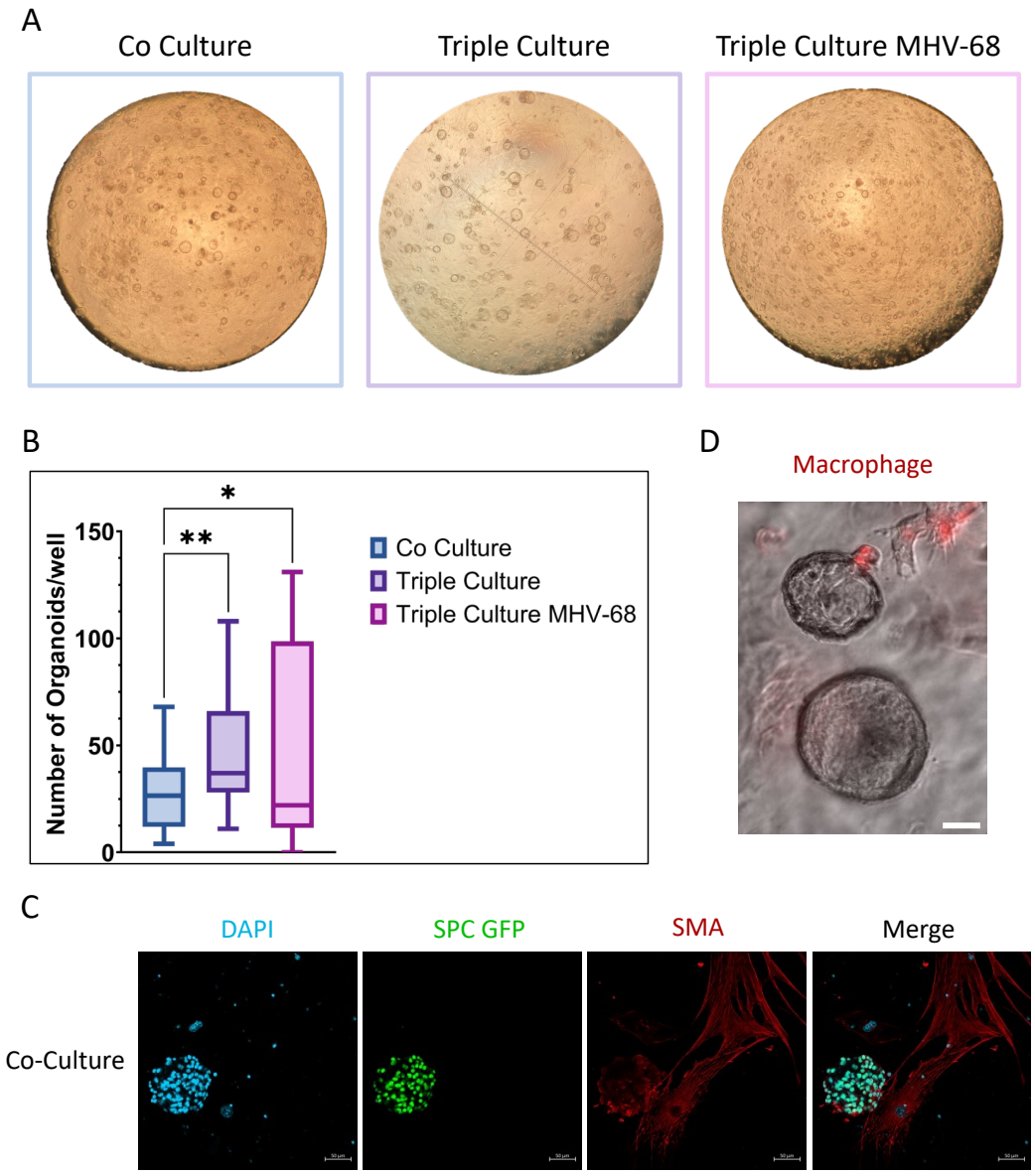

Figure 19 *Macrophages support lung organoid growth.*

(A) Representative brightfield images of lung organoids grown for one week. "Co Culture" includes primary lung epithelial cells and fibroblasts, "Triple Culture" epithelial cells, fibroblasts and macrophages and "Triple Culture MHV-68" includes epithelial cells, fibroblasts and persistently with MHV-68 infected macrophages. "Co Culture" and "Triple Culture MHV-68" images were taken with a 4x objective, "Triple Culture" with a 5x objective. (B) Quantification of number of organoids per well. 48 wells in "Co Culture", 37 wells in "Triple Culture" and 21 wells in "Triple Culture MHV-68" were included. Data are presented as min to max box plots with the box marking lower and upper quartiles and

the median value marked with a line. Ordinary one-way ANOVA followed by Tukey's multiple comparison test. * p-value < 0.05, ** p-value < 0.01. (C) Representative images of immunofluorescent staining showing DAPI (blue), SPC-GFP (green) and alpha smooth muscle actin (SMA) (red) in co-culture conditions. Scale bar = 50 µm. (D) Representative brightfield image of „Triple Culture" organoids including macrophages stained in red with a live-cell dye. Scale bar = 50 µm.

6.1.1. Alterations in epithelial cell composition of immunocompetent organoids

As we could observe an influence on epithelial cell formation, organization and growth by adding macrophages to the organoid culture, we wanted to investigate potential changes in these epithelial cells. Markers in gene expression for AT2 cells, namely surfactant protein C (*Sftpc)* and B (*Sftpb*), showed a trend to increase in immunocompetent organoids, especially with MHV-68 infected macrophages included. A similar pattern could be observed regarding *Aqp5* expression, a common marker for AT1 cells. On the contrary, keratin 8 (*Krt8*) expression showed a slight decrease in organoids including MHV-68 infected macrophages in comparison to both uninfected groups. *Krt8* is known to be expressed in alveolar epithelial cells during differentiation from AT2 to AT1 cells. Considered that *Krt8* expression was quite low in all of the groups, the greater increase in *Aqp5* expression still points to an enhanced differentiation of initial AT2 cells to AT1 cells in the presence of MHV-68 infected macrophages. Alpha Tubulin (*Tuba1a*) can be used as a marker of ciliated cells and was less expressed in infected triple-culture conditions than in co-culture and uninfected triple-culture groups (**Figure 20 a**). To verify not only upregulation in gene expression but also on the translational level, IF staining was conducted for some of the markers mentioned above. Indeed, markers for surfactant production in AT2 cells (pro-SPC), AT1 cells (AQP5), differentiating alveolar cells (KRT8) and ciliated cells (ACTUB) could be detected in triple-culture conditions (**Figure 20 b**). Taken together, MHV-68 infected immunocompetent organoids did have a slightly different epithelial cell pattern than co-cultured organoids, with more alveolar epithelial cells and a reduction in bronchial cells.

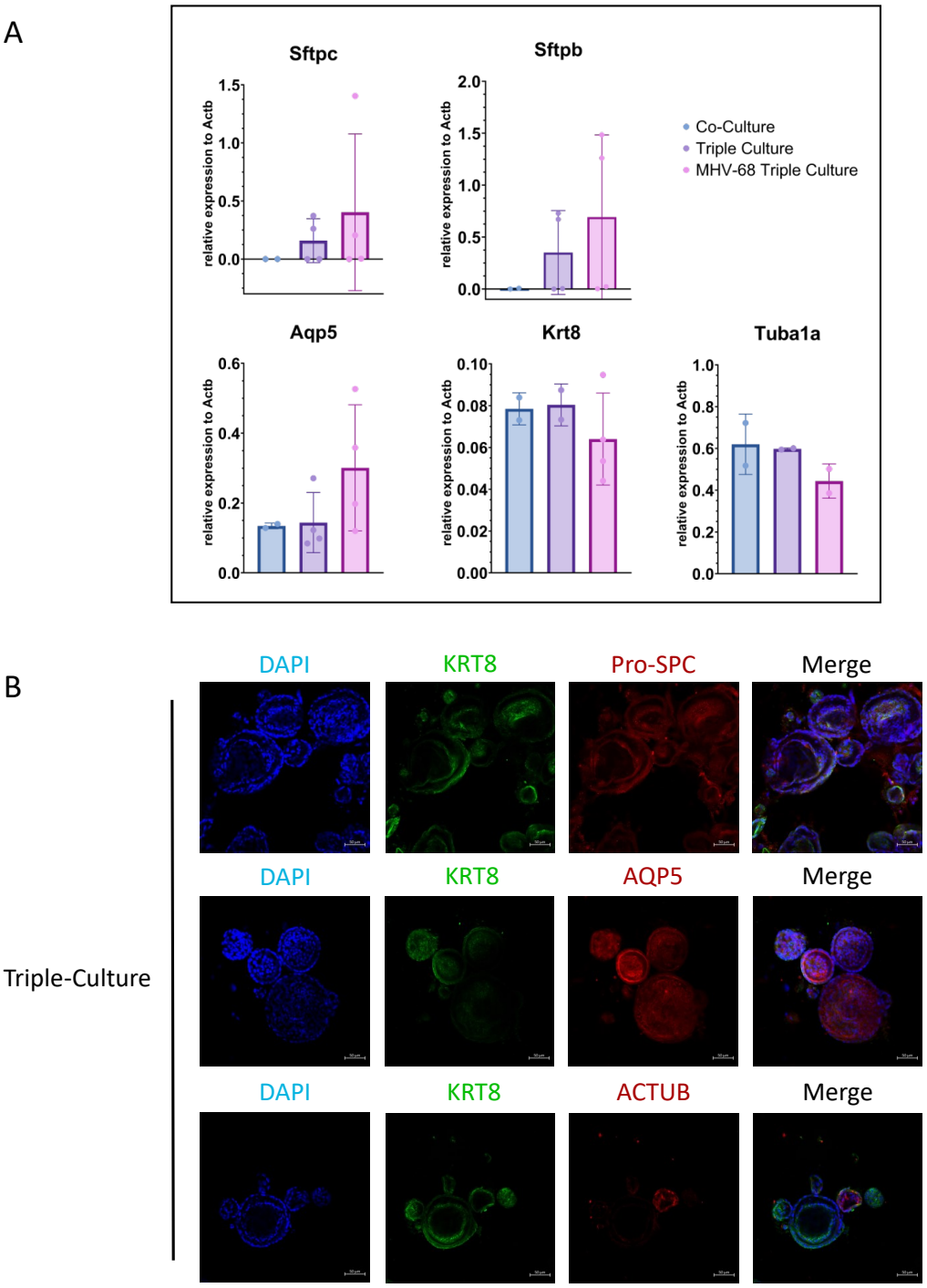

Figure 20 *Characterization of different epithelial cell markers.*

(A) Relative gene expression of epithelial cell markers at day 14 measured in organoid co-cultures with only fibroblasts (Co-Culture), fibroblasts and macrophages (Triple Culture) or fibroblasts and MHV-68 infected macrophages (MHV-68 Triple Culture) compared to β-Actin. 2 – 4 experiments were included. Data are presented as mean ± SD. Ordinary one-way ANOVA followed by Tukey's multiple comparison test did not show significant changes. (B) Representative images of immunofluorescent stainings with DAPI (blue), Keratin 8 (KRT8) (green) and pro-SPC (red) in triple-culture conditions are shown in the upper panel. Stainings with DAPI (blue), KRT8 (green) and AQP5 (red) are shown in -culture in the center panel and DAPI (blue), KRT8 (green) and acetylated alpha Tubulin (ACTUB) (red) in the lower panel. Scale bar = 50 µm.

6.2. Reactivation of MHV-68 in immunocompetent organoids

Persistently with MHV-68 infected macrophages have been shown to reactivate lytic viral replication upon particle and LPS exposure in submerged conditions [8,9]. In immunocompetent organoids including epithelial cells, fibroblasts and persistently infected macrophages, viral titers did increase nearly 2-fold after LPS treatment (mean 1.898, SD 0.9014), but did decrease significantly upon exposure to CNP (**Figure 21 a**). The ratio of open reading frame 50 (*Orf50*) to open reading frame 73 (*Orf73*), an indicator for viral reactivation, did increase after CNP exposure and even stronger upon a LPS trigger (**Figure 21 b**). Persistently with MHV-68 infected macrophages carry a recombinant MHV-68 containing a GFP expression cassette, enabling the detection of lytic infected cells by fluorescence imaging. Staining with a polyclonal rabbit serum for lytic viral proteins showed clear co-staining of both virus-related markers, mostly in fibroblast-like shaped cells. Viral proteins are present in each condition, including untreated control organoids, although to a lower extend. Due to a great variation between experiments, MHV-68 reactivation upon different triggers was not significantly increased, but a trend for a gradual increase upon particle and especially LPS exposure could be observed.

Taken together, immunocompetent organoids showed optimal conditions for cellular crosstalk between the included cell types. Unfortunately, reactivation of MHV-68 was not only inducible by particle or LPS stimulation of cells but did also happen in untreated organoid cultures to some extent. This was most likely due to spontaneous reactivation of MHV-68 under these culture conditions.

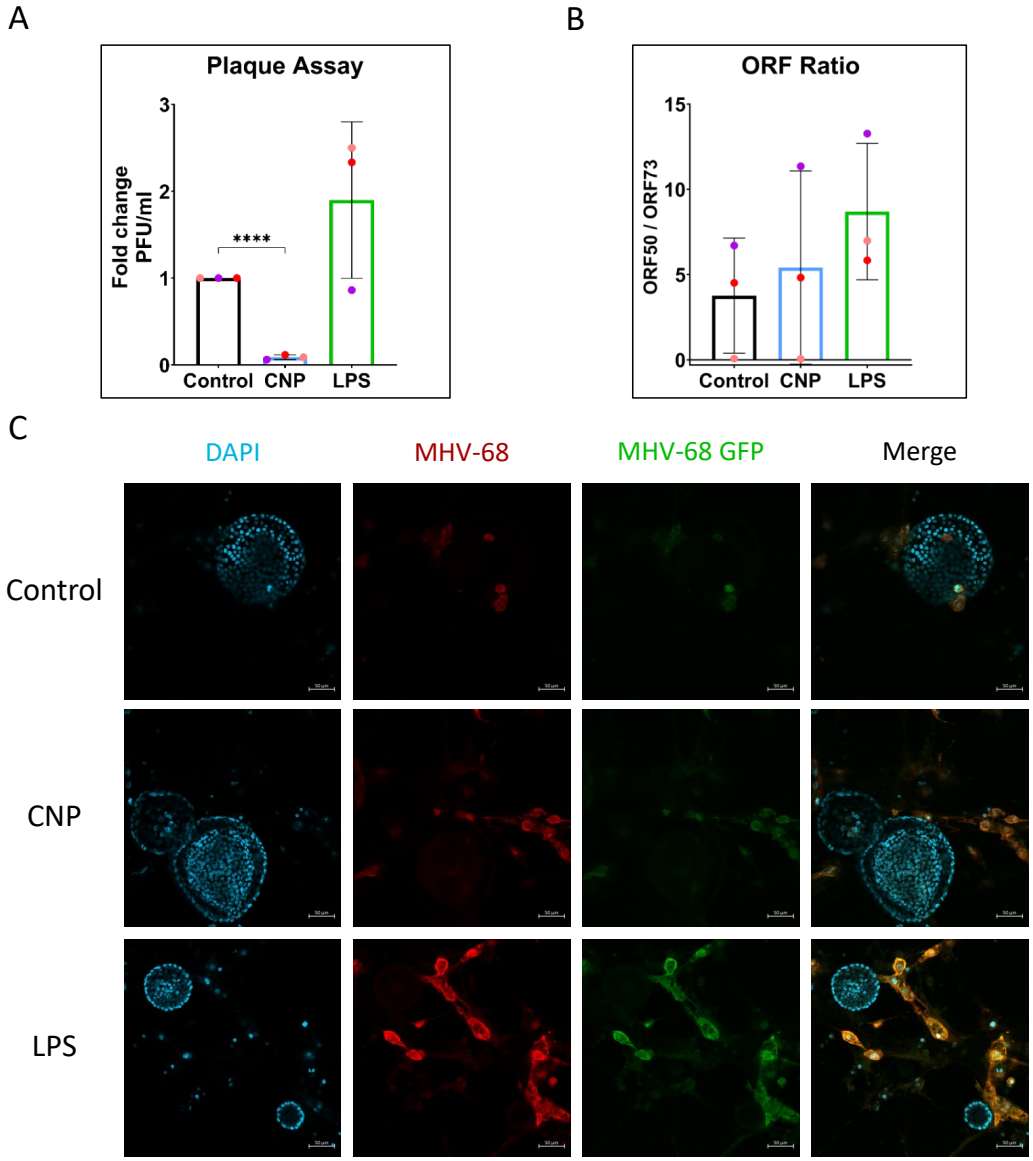

Figure 21 *MHV-68 reactivation upon CNP and LPS trigger.*

Organoids including MHV-68 infected macrophages were cultured for one week before they were exposed to 100 µg/ml CNP or 1 µg/ml LPS. (A) Viral titers as PFU/ml were measured 48 h after treatment in the supernatant. Values are presented as fold change of PFU/ml from untreated control cultures. Data are presented as mean ± SD. Each coloured dot represents one experiment. Repeated measures one-way ANOVA followed by Tukey's multiple comparison test. **** p-value < 0.0001. (B) Ratio of gene expression of ORF 50, a gene only expressed during lytic replication in MHV-68 and ORF 73, a gene expressed both during lytic and latent infection as measurement of viral reactivation on transcriptional level. Data are presented as mean ± SD. Each coloured dot represents one experiment. Repeated measures one-way ANOVA followed by Tukey's multiple comparison test did not show significance. (C) Representative IF staining of triple culture organoids including MHV-68 infected macrophages after CNP or LPS treatment with DAPI (blue), lytic MHV-68 protein (red) and MHV-68 GFP expression (green). Scale bar = 50 µm.

IV. DISCUSSION

In this study we could observe that repeated and chronic-like carbon nanoparticle instillation to mouse lungs can induce chronic inflammation in the airspace as well as in lung tissue. Following a pattern of transient, acute inflammation after the first particle exposure, five-time repeated exposure to CNP did result in an inflammatory environment including not only acute innate immune responses but also engaging long-lasting adaptive immunity, especially in mice latently infected with MHV-68. This inflammation was accompanied by damage of the alveolar walls with loss of alveolar type 1 cells. Apoptosis was shown to be involved in this process.

As an *in vitro* model, immunocompetent organoids were developed and to be used to investigate particle-induced herpesvirus reactivation and cellular communication.

1. Choice of an appropriate model

It is essential to choose an appropriate model that adequately addresses the research question asked. In our case, we decided on using a murine model to capture alterations in lung morphology and immunity upon nanoparticle exposure in latently with MHV-68 infected lungs.

The lung of mammals with its division in bronchiolar and alveolar regions is unique among vertebrates. Reptiles for example use an aspiration ventilation system. They alter their body cavity pressure by buccal pumping and costal aspiration to facilitate inhalation and exhalation. Avians developed a highly efficient lung-air sac system with pneumatized bones. During inhalation, fresh air gets into the posterior air sacs and gets pressed into the lungs and parabronchi for gas exchange during the following exhalation [118]. Mammals make use of a broncho-alveolar system. The lungs are filled with air with the help of the diaphragm and intercostal muscles. Pulmonary pleurae and surfactant in the alveoli ensure tension and prevent collapsing of the lung. Gas exchange, the main function our lungs do fulfil, is conducted in the alveoli, whereas the bronchiolar airway system transports inhaled and exhaled air. Due to these tremendous differences within the subphylum of vertebrates, it is necessary to choose an appropriate model within the mammalian class when studying pathophysiological changes in the lung related to human

beings.

In addition to gas exchange, lungs do have several additional physiological functions. For instance, the lung is involved in the renin-angiotensin-aldosterone system. Pulmonary vascular endothelial cells release the angiotensin converting enzyme and cleave angiotensin 1 to the active angiotensin 2. This influences vasoconstriction, aldosterone secretion and sodium reabsorption resulting in alterations in blood pressure and extracellular volume [119]. Besides involvement in vocalization [120] or heat regulations [121], lungs play a crucial role in the immune system as first line of defence to inhaled harms. Taken into consideration that environmental air needs to get into the lungs for gas exchange within the thin barriers in the alveoli, a well-orchestrated defence strategy against pathogens evolved. Physical barriers, cellular as well as humoral immunity defend the lungs against infections and harmful agents. This means, that changes in lung function, morphology and immunity will not only have an impact on the lung itself, but also influence other parts of the organism and vice-versa. In order to obtain reliable data on effects of unknown dimensions in the lung and body, as in our study, it is essential to conduct investigations on a whole organism with functioning immune responses and crosstalk between organs.

As described in the introduction, gamma herpesvirus infection is associated with a viremia and spreading within the whole host body. Several cell types are involved in the relocation of viral DNA, including epithelial cells, macrophages, dendritic cells, and B-cells. The most important site of MHV-68 infection besides the lung is the spleen, a reservoir of latently infected cells [28]. Proper infection and establishment of latency can thus only occur in a fully working organism, transporting the virus from the initial infection site in the lungs to the spleen. In addition, reactivation of virus does not depend on a single signalling pathway but is influenced by several triggers, including stress, hormonal imbalance, cell differentiation or fever [7]. These are all factors that highlight the necessity of using an animal model to generate robust and informative results.

Rodents, especially mice, are in our case the most promising and useful model. Gamma herpesviruses do have a strict host tropism, making it nearly impossible to study human herpesvirus infections and latency in a non-human environment. In addition, it is challenging to study mechanisms and immune alterations within the human host. Thus, MHV-68 is a great opportunity to study gamma herpesviruses,

as the murine herpesvirus does share a large proportion of the genome with the human EBV and KSHV [26]. Although we do have solid data on how infection, spreading and reactivation is occurring in laboratory mice [27-30], it must be mentioned that *Mus musculus* is not the natural host of MHV-68, natural host is the wood mouse (*Apodemus sylvaticus*). The effects of MHV-68 in wood mice in comparison to BALB/c mice were assessed in a study by Hughes and colleagues in 2010. The study did reveal less replication in the lungs after primary inoculation, more focal granulomatous infiltrations, viral latency in inducible bronchus-associated tissues (iBALT), more abundant follicle generation in latently infected spleens as well as higher production of neutralizing antibodies in wood mice compared to BALB/c laboratory mice [122]. Despite those differences, the majority of features and mechanisms regarding infection and pathogenesis are displayed within laboratory mice. Especially long-term effects after 40 days observed in this study do show comparable phenotypes. In view of the availability of animals and knowledge that was already gathered about the pathogenesis of MHV-68 in laboratory mice, this model is at the time the preferred one to make use of. The availability of numerous gene knockouts enables us to study the host inflammatory response in more detail and elucidate mechanistic insights in the future.

2. Innate immune response to chronic CNP exposure

The first reaction to pulmonary deposited nanoparticles we could observe in this study was the activation of the innate immune system. Neutrophils were being recruited to the alveolar airspace within 24 hours after each particle instillation (**Figure 4**). This acute and transient inflammation, which was resolved within one week after the first instillation, is well described. A single instillation of 20 µg CNP led to an acute neutrophilic inflammation in the lung with a peak 24 hours after the exposure in one study conducted in our lab a few years ago [48]. Several other studies in mice show comparable results [123-126]. Interestingly, a substantial number of neutrophils did remain in the airspace for at least one week after the particle instillation if it was repeated five times (**Figure 4**). Although not significant, detection of a 15- to 19-fold increase compared to control mice until one week after CNP exposure indicates, that the resolution, that was successful after the first and second instillation, was not finished after five-time repeated exposure. This prolonged neutrophilic inflammation can also be observed in different chronic

lung diseases, perpetuating pulmonary damage. In COPD for example, a pathological condition with repeated injury, pulmonary neutrophilia is associated with lower lung function [127,128]. Persistent neutrophilic inflammation can also be detected in cases of chronic and severe Asthma [129,130]. Remaining neutrophils as measurement for the level of airspace inflammation suggest a chronic, non-resolving inflammation after chronic-like CNP instillation in our study, independent of viral latency in this case.

Besides neutrophils, macrophage numbers also increased in BAL fluid in both CNP instilled groups, with or without prior MHV-68 infection, rising with number of instillations (**Figure 4**). One week after the fifth instillation, the number of macrophages had nearly doubled compared to untreated control samples. This delayed influx of macrophages into the alveolar airspace can be linked to the remaining neutrophils. Cytokines like CCL2, CCL3, CCL4 and CCL7 are known to be released by activated neutrophils to attract monocytes and recruit them to the airspace [131]. Interestingly, these chemokines were increasingly found one week after the last exposure in latently infected mice with subsequent particle exposure, but decreased within this week in uninfected mice (**Figure 8**). This points towards a prolonged and persistent immune response in infected mice. In addition to an increase in number of macrophages, multinucleation was also increasing with the number of particle instillations (**Figure 4**). These multinucleated giant cells are formed by fusion of several macrophages under inflammatory conditions and usually found in granulomatous disease or during frustrated phagocytosis of foreign bodies [132]. In our case, a foreign body response due to the carbonaceous nanoparticles in the airspace probably leads to a chronic inflammation and the formation of giant cells [133]. This fusion does not happen as an acute response, but is rather a long-term reaction to particle exposure [134]. Furthermore, five-time repeated instillation of 50 µg CNP in our study results in accumulation of a high dose of CNP remaining in the lungs and thus might cause overload of the macrophages and subsequent multinucleation. This formation of multinucleated macrophages is rarely observed for small and spherical NPs like CNP at a lower dose.

The innate immune system is the first line of defense after exposure of the lungs to carbon nanoparticles. In an acute exposure scenario with a single nanoparticle instillation, prior infection with herpesvirus did not impact the appropriate cellular

response and clearance of the foreign bodies. But we can see that a five-time repeated chronic particle exposure does change the response of neutrophils and macrophages, even promoting formation of multinucleated giant cells. On the one hand, cellular inflammation and activation is prolonged and not resolved within one week after the fifth CNP exposure in both particle exposed groups, on the other hand, infection with MHV-68 does lead to a progressive increase in cytokine production and release within one week after the last particle exposure. This is not the case in particle instilled mice without prior infection, here the cytokines involved in innate immune cell recruitment do show a decline after one week.

3. Adaptive immune response, iBALT formation and bystander T-cell activation

Five-time repeated exposure to carbon nanoparticles did not only increase the recruitment of innate immune cells into the airspace, but did also result in the attraction of lymphocytes after viral infection. Lymphocyte accumulation in the airspace was only found in the *Virus + Particle* group after repeated particle exposure (**Figure 4**). Notably, we could not observe any major differences in lymphocyte attracting cytokine release to the airspace between the *Latency + CNP* and the *only CNP* group (**Figure 6** and **Figure 8**). Eventually, the specific responsible cytokines or chemokines for adaptive immune cell recruitment into the airspace were not within the scope of the utilized screening kit, thus not detected in our case.

The accumulation of lymphocytes was not restricted to the airspace, but also found in diffuse as well as focal mononuclear cell infiltrations in lung tissues, mainly located peribronchiolar and perivascular (**Figure 9**). Activation of the adaptive immune system with recruitment of mononuclear cells into the lung tissue was observed in both particle-exposed groups, although more abundantly after viral infection. Further characterization of these infiltrating cells revealed numerous B-cells as well as $CD8^+$ T-cells and NK-cells being involved (**Figure 10** and **Figure 11**).

In the lungs, lymphocyte accumulations can be arranged in different patterns. Nodular inflammatory foci include $CD8^+$ T-cells and cluster of myeloid cells [135,136]. Organized and compact accumulation of macrophages, sometimes also including giant cells and lymphocytes or associated with necrosis, can be defined

as granulomas [137]. The distinct pattern of separated B- and T-cell domains we found in this project is likewise described in tertiary lymphoid tissues in the lung called inducible bronchus-associated tissue (iBALT). As the name already states, iBALT is usually located peribronchiolar and perivascular in lung tissue and develops following infection or chronic inflammation. This is also the location where we can find most lymphocytic infiltrations in our samples. iBALT formation is described to play a crucial role in several chronic pulmonary challenges and disorders, like COPD [135,136], cigarette smoke exposure [135], asthma [138], and several viral infections, including MHV-68 in wood mice [122,139,140]. Just like within conventional lymphoid tissue, naïve lymphocytes get recruited from the circulation to get in contact with antigen-presenting cells near the airways. The pulmonary immune response is then formed by the active participation of iBALT. This influence can either be beneficial or harmful for the lungs, depending on the trigger and environment leading to iBALT formation [141]. For example, in response to influenza virus infection, iBALT formation was associated with increased survival, less pulmonary pathologies and better clearance of virus. Apart from that, iBALT can contribute to chronic inflammatory conditions and exacerbation of disease, as described in COPD for instance [142].

Due to the similarities that we can find regarding pulmonary pathologies in this study with COPD studies, such as the described iBALT formation, emphysema development and chronic inflammation, a detrimental influence of iBALT on lung health is probable. In COPD, lymphoid follicles are associable with disease progression and severity [143]. Colleagues from our institute could show, that cigarette smoke induced COPD in mice is associated with less emphysema formation in B-cell deficient mice without iBALT formation. It is suggested, that B-cells are not only involved in iBALT formation, but also contribute to macrophage recruitment and subsequent AT2 cell damage and emphysema formation [144]. As we can observe most detrimental effects on lung morphology after five-time repeated particle exposure in infected mice here, and this is also the group with most inflammatory cell infiltrations organized in iBALT-like structures, I propose a more harmful than beneficial effect of those within lung immunity.

We can observe a stronger cellular inflammatory response in mice, that were infected with MHV-68 prior to repeated carbon nanoparticle exposure than in *only CNP* exposed mice (**Figure 9**), hence, viral infection seems to alter the immune

response to a subsequent insult in the lungs. It is known that latent herpesvirus infections do change the microenvironment and have an impact on innate and adaptive immune responses to different pathogens. Latent herpesvirus infection in mice shows for example a protection against bacterial infections [145] and enhances the antibody response to influenza vaccination in young and healthy mice as well as humans [146]. Especially herpesvirus-primed memory T-cells do play a crucial role in shaping this distinct immunological environment, as they are regularly found in the latently infected host [147-149]. There is a growing body of evidence, that infections with unrelated pathogens can lead to the activation of herpesvirus-specific T-cells through an unspecific bystander mechanism [150-153]. In this case, T-cell activation is not dependent on the usual T-cell receptor interaction with MHC presentation of foreign antigens, but on recognition of distinct cytokines or activation of Toll-like receptors (TLR). TLRs on T-cells can recognize pathogen associated molecular patterns (PAMPs) and when detected, T-cells can produce interferon gamma (IFN-γ) through this so-called bystander activation. It has been shown, that EBV and MHV-68 are capable of activating TLR2 [154-156]. Repetitive reactivation of MHV-68 in our study could lead to a recognition of released PAMPs via TLR2 on memory T-cells and subsequent activation and release of IFN-γ. Another plausible scenario is that pro-inflammatory cytokines such as IL-12, IL-15 and IL-18 induce memory $CD8^+$ T-cells to differentiate into effector cells [153,157,158]. These activated cells are either stimulated to produce IFN-γ, mainly after IL-18 recognition, or increase cytotoxicity via upregulation of NKG2D expression and Granzyme B release in response to IL-15, as nicely summarized by Kim and Shin [159]. Hence, bystander activation of T-cells can be either beneficial or detrimental for lung health. It could be possible that MHV-68 specific memory T-cells may be activated by recurrent CNP exposure to the lungs and subsequent lung inflammation in a bystander-dependent manner. This activation then leads to increased cytotoxic activity against epithelial cells, resulting in epithelial cell death and emphysema formation. The formation of NKG2D expressing T-cells would need to be investigated further, as in the immunofluorescent staining of infiltrating mononuclear cells in **Figure 11**, NKG2D rarely colocalizes with $CD8^+$ cells. This suggests rather an accumulation of NK-cells and cytotoxic effects of these, than a bystander activation of T-cells at the current state of analysis.

4. Symbiotic herpesvirus infection shapes immune system

It must be highlighted, that the investigation of immune responses in mice infected with herpesvirus prior to any other challenge may be the most relevant to display and understand human and animal immunology. Usually, for the sake of simplicity and to generate robust and reliable data, animals that are specifically pathogen free are used for studies regarding environmental challenges. Like this, it is easier to annotate alterations observed to the examined challenge and to draw the appropriate conclusions. Nevertheless, herpesviruses co-evolved as symbionts with all species and shape the immune system in dimensions, that are not yet fully understood. This study shows nicely that latent herpesvirus infections should be considered as an important modifier of the immune system, which is blocked out in uninfected models. In addition to that, nearly every human being carries at least one herpesvirus, which means that disease patterns and pathologies mostly include immune responses within herpesvirus-primed immune systems.

5. Alveolar epithelial cell damage and barrier disintegration

Analysing the overall morphology of lung tissue in the different groups in our study revealed a significant enlargement of the alveolar airspace one week after the fifth nanoparticle exposure. This was observed only in latently with MHV-68 infected mice (**Figure 12**). These findings were aligned with a significant reduction in the number of AT1 epithelial cells (**Figure 13**) and the identification of apoptosis-related markers in this specific group (**Figure 15**, **Figure 16**). This AT1 cell loss in combination with the described accumulation of inflammatory cells in BAL fluid and lung tissue are only described in MHV-68 infected mice with five-time repeated particle exposure. Hence, chronic lung injury and emphysema formation can be associated with herpesvirus infection in particle exposed mouse lungs. In addition to that we could measure a significantly increased concentration of protein and especially IgM in BAL fluid samples after five-time particle exposure in both, MHV-68 infected and uninfected mice (**Figure 14**).

Elevated protein levels, in particular large proteins like IgM, in the alveolar airspace point towards a disintegration of the alveolar-capillary barrier. IgM is a pentameric antibody that is usually circulating in the blood stream and lymph fluid and is too big to move across the thin gas exchanging barrier between capillaries and alveoli in healthy conditions [160]. If this fragile barrier gets damaged by chronic

inflammation or oxidative stress for example, a leakage of plasma proteins into the airspace is possible, leading to an increase in IgM and other proteins in the BAL fluid. The resulting damage to alveolar walls gets also detectable in the enlargement of alveolar airspace and reduction in AT1 cell number that we can observe in our study. Importantly, the retention of inflammatory cells in the airspace as well as in tissue infiltrations and a further increase in several inflammation related cytokines one week after a fifth CNP exposure in latently with MHV-68 infected mice match with the emphysema-like changes found.

It is described that emphysema can emerge due to alveolar cell senescence [161], oxidative stress [162] or an imbalance between apoptosis and proliferation in epithelial and endothelial cells [163,164]. Nanoparticles can induce oxidative stress in the lung [111,165,166]. It was shown that even the MHV-68 infection itself can induce oxidative stress in mouse lungs [167]. In a previous study in our lab, subsequent phosphorylation of p38 and activation of mitogen-activated protein kinase (MAPK) was linked with reactivation of MHV-68 in mouse lungs. This reactivation could even be attenuated by specific inhibition of the p38 phosphorylation and the MAPK signalling pathway [9].

Transcription factors p53 and activator protein 1 (AP-1) are known to be able to create a pro-apoptotic response and can be activated downstream of the p38 MAPK signalling pathway. Activation of caspases and phosphorylation of different proteins by p38 can also be connected to apoptosis, although it depends on the quality and quantity of extracellular and intracellular stimuli, if activation of diverse MAPKs leads to the induction of apoptosis or its prevention [168]. As we do create and observe a chronic and persistent inflammatory environment in this study, especially in latently infected and particle exposed lungs, this sustained activation of signalling cascades may be one factor in favour of an apoptotic cell fate. Single and two-time repeated particle exposure to herpesvirus infected lungs might result in transient inflammation and activation of p38 MAPK, leading to a repair and rescue of cells. In contrast, five-time and chronic triggering of the lung seems to exceed a threshold of cell fate leading to an increase in induction of apoptosis in epithelial cells and consequently enlargement of alveolar airspace.

Another or additional possible explanation for the observed epithelial cell damage and loss could be a direct link to the MHV-68 infection and reactivation. Lytic replication of herpesviruses in lung cells can lead to a direct killing of these, as the

release of virions usually ends with lysis of the infected cell. Not only the virus itself, but also immune cells recognizing infected cells can induce cell death mechanisms to prevent the virus to spread to other cells. Rex et al. have summarised the interplay of innate and adaptive immune responses to infection with gamma herpesvirus [169]. After primary recognition of viral infection through pattern recognition receptors like TLRs or cellular and nuclear DNA sensors, signalling pathways are activated to secrete pro-inflammatory cytokines and type I interferons (type I IFN). These are important to directly control viral replication in acute MHV-68 infection and reactivation. We could also confirm this increase in pro-inflammatory cytokines like IFN-γ or IL-2 in reaction to the acute infection with MHV-68 in our BAL cytokine profile shown in **Figure 6**. NK-cells are recruited through cytokines and can either attract more immune cells to the infection site or act on the infected cells by inducing apoptosis, at least in human EBV infection. Regarding the murine MHV-68 infection and reactivation, NK-cells seem to be less important in containing viral spreading. Type I IFN is also essential to shape the adaptive immune response by influencing T-cell activation on different levels. Cytotoxic $CD8^+$ T-cells contribute significantly to fight against MHV-68 and EBV during primary infection, latency, and reactivation, mainly through secretion of granzymes, perforin and IFN-γ and initiation of apoptosis in the recognized infected cells. In our study, we could also find Granzyme B secretion in lymphocytic infiltrations in mouse lungs, although not only in infected mice but also in reaction to chronic CNP exposure (**Figure 11**).

Following hundreds of millions of years of co-evolution with their respective hosts, gamma herpesviruses have developed a plethora of immune evasion strategies to prevent viral clearance and to establish lifelong latency. Innate immune responses are dampened for example by inhibition of type I IFN responses on several levels [170]. In addition, MHV-68 for example evades NK-cell cytotoxicity by upregulation of inhibitory surface receptors on infected cells [171]. Despite the effective cellular immune response of T-cells towards herpesvirus infection, MHV-68 and EBV are nevertheless able to establish lifelong latency. One strategy of MHV-68 to escape T-cell recognition is for example the downregulation of MHC class I on the surface of infected cells [5]. In addition to that, when already infected B-cells enter the thymus, they influence primary T-cell development in favour of viral epitopes [169]. The latent infection and constant expression of virus-related

antigens can also lead to T-cell exhaustion, a state of T-cell dysfunction [172]. This is no issue in most individuals, but in immunocompromised people or patients with lymphoproliferative disorders and high EBV load, T-cells can show signs of exhaustion [169].

Interestingly, besides gamma herpesviruses evasion from recognition and elimination by the hosts immune system, they can also escape and inhibit apoptosis of the infected cell. Several viral genes and proteins do target the cellular apoptotic pathway at different steps. For example, the viral FLICE-like inhibitory protein does inhibit the caspase 8 and 10 dependent cellular death. All representatives of gamma herpesviruses do encode for a Bcl-2 homolog. Cellular Bcl-2 proteins regulate anti-apoptotic pathways in the mammalian cell, and the viral homolog exploits this mechanism. In addition, the pro-apoptotic tumour suppressor p53 is a target of viral apoptosis manipulation. Even NF-κB is modulated by viral genes to prevent apoptosis and anti-viral cytokine production [173].

These anti-apoptotic features of MHV-68 and other gamma herpesviruses could be one possible explanation for the often rather slight differences between the *Latency + CNP* and *CNP only* groups. The rather dormant latency in the *Latency + Sham* group did have nearly no influence on lung immunity or morphology, resembling *Untreated Control* mice. Lymphocyte recruitment to the airspace (**Figure 4**) and progressive secretion of leukocyte attracting cytokines (**Figure 8**) did differentiate latent viral infection with chronic particle exposure from *only CNP* exposure. Considering that soluble CK18 in BALF was mainly found in latently infected mice (**Figure 15**), epithelial cells still seem to be targeted by immune cells and undergo apoptosis, despite the various immune evasion and anti-apoptotic strategies of MHV-68.

6. Heterogenous distribution of injury patterns in the lung

Inflammation as well as emphysema-like changes in mouse lungs in our study were not evenly distributed across the whole lung but showed a rather heterogenous pattern with several foci distributed randomly throughout the lung tissue (**Figure 9** and **Figure 12**). Heterogenous distribution of pathologies in lungs is a common phenomenon observed in various lung diseases, including acute respiratory distress syndrome [174], COPD emphysema [175] and IPF [176], hence also a plausible explanation for the inhomogeneity in disease distribution we could observe. In

addition to that, intratracheal nanoparticle instillation does not distribute the particles completely evenly in the lungs. Yang and colleagues in our institute illustrated vividly, that nanoparticles administered intratracheally to the lungs did aggregate and deposit in the bronchial compartment and also reached pulmonary acini, although not to the same extend and homogenous distribution as different inhalation methods did. A redistribution of particles within the acini occurred within a 14-day period, resulting in a more uniform dispersion [177]. In order to evaluate whether the method of particle administration influences the pathological pattern or severity in this study, it is planned that parts of the experiment will be repeated using inhalation of nanoparticles. In consideration of the frequent and natural occurrence of inhomogeneity in pathologies, the focal and patchy cellular infiltrations, as well as the enlargements of alveolar airspaces observed in this study are likely indicative of the actual response of latently infected lungs to recurrent particle exposures.

7. Reactivation of MHV-68 under detection limit

As described earlier, previous studies in our lab could show that single and repeated intratracheal exposure to carbon nanoparticles can lead to reactivation of MHV-68 in latently infected mice. This reactivation was mainly located in $CD11b^+$ infiltrating macrophages [8,9]. CD11b, the integrin alpha M, was found to be expressed in eosinophils, neutrophils, interstitial macrophages, dendritic cells as well as monocyte derived macrophages and monocytes [178]. Reactivation seems not to be directly linked to particle exposure, as alveolar macrophages, and not $CD11b^+$ cells, are predominantly engulfing particles.

In my follow-up experiments I was able to visualize acute viral replication in alveolar epithelial cells six days after intranasal infection with MHV-68. Clear and abundant staining of lytic viral proteins was detectable in clusters of epithelial cells in this acute infection phase, confirming accurate and sufficient infection. Minimal to no lytic viral proteins were visible in latently infected mouse lungs instilled with sham solution. This confirms silent and latent MHV-68 infection without uncontrolled disturbance. In line with the previous studies, repeated CNP exposure to latently infected mice revealed lytic viral protein staining in peribronchiolar and perivascular infiltrating cells as well as some individual cells in the lung. Surprisingly, we could detect single positive stained cells also in mouse lungs after

CNP exposure without viral infection, questioning the MHV-68 specificity of the antiserum used (**Figure 17**). For the detection of lytic viral proteins, we did make use of a polyclonal serum collected from immunized rabbits. It is likely, that a cross-reaction of the polyclonal serum with an MHV-68 unrelated, but apparently CNP exposure related protein might cause the unexpected signal in staining. The same pattern in slight colouring was found in all particle treated groups. In addition to the polyclonal rabbit serum, I also tested several monoclonal antibodies recognizing for example ORF4, coding for regulators of complement system proteins in lytic replication [110] and viral uracil DNA glycosylase (vUNG), also involved in viral replication [179]. The ORF4 antibody did stain similar areas in epithelial cells 6 days after the acute infection as the polyclonal rabbit serum did, but to a smaller extent. Reactivation after CNP exposure was below detection limit of this antibody. Initial testing of a recombinant antibody for tracking vUNG [180] did fail to show clear signals within the staining protocols we use in our laboratory. In addition, detection of viral gene expression in BAL cells was also not successful.

Reactivation of MHV-68 in latently infected cells in the lung is not a phenomenon occurring abundantly throughout the whole pulmonary system but is restricted to just a few recruited, activated, and triggered cells. This makes it difficult to detect reactivating cells for example on gene expression level in whole lung samples or BAL cells. Staining for distinct proteins expressed in lytic replication is an appropriate method to identify single cells within the tissue. In addition to the high sensitivity, antibody staining on lung tissue also provides information about location and abundance of the targeted protein. In this project, reactivation of MHV-68 upon repeated and chronic CNP exposure unfortunately stayed below detection limit, if one disregards unspecific cross-reactional signals in all particle exposed groups. Nevertheless, my colleagues Lianyong Han and Verena Häfner could already show, that reactivation is triggerable through single and repeated CNP exposure and even attenuated by inhibition of p38 MAPK signalling [9].

8. Lung organoids - an *in vitro* model to investigate reactivation.

In vitro models are a great opportunity to investigate mechanisms and particularly dynamic cell communication networks from complex experimental setups in a simplified, defined, and manipulable setting. The lung confronts us with particular

challenges, taking into account that epithelial cells and several immune cells get in contact with the airflow and are at the same time embedded in tissue. This unique condition hampers accurate modelling of the conditions in the lung. Together with a colleague I already summarized how one might overcome these challenges in the field of nanomaterial toxicity assessment and how to choose an appropriate *in vitro* model, spanning from submerged and air-liquid interface cultures of cell lines to primary and induced pluripotent stem-cell derived organoids [117].

In this project, we are combining two challenges to lung cells, nanoparticle exposure as well as latent infection with herpesvirus. In mouse lungs we could observe epithelial cells in contact to the instilled CNP and particle uptake in alveolar macrophages. In addition, reactivation of MHV-68 was predominantly detectable in $CD11b^{+}$ infiltrating macrophages, but structural changes leading to lung emphysema or even fibrosis require injury in the epithelial cell compartment. With regard to these findings in the previous study [9], which we could also reproduce in the described *in vivo* experiments in this study, the goal was to investigate the communication between latently infected macrophages with epithelial cells in response to carbon nanoparticles *in vitro*. That is why we wanted to make use of an experimental setup to study cellular crosstalk, by including latently infected monocyte derived macrophages and primary lung epithelial cells. Immunocompetent organoids represent an advanced and still defined model for this purpose, recapitulating specific aspects of lung tissue *in vitro*. Lung organoids are more and more used in toxicity studies taking advantage of the stem cell character and behavior of primary epithelial cells in comparison to immortalized cell lines [181,182]. Yu et al. demonstrated nicely, how to use lung organoids to decipher mechanisms happening in the epithelial niche. They found AT2 to AT1 cell transition being heavily involved in epithelial damage upon PM2.5 exposure and, amongst others, MAPK signalling to be involved [183]. Even interactions of viral infections with ambient particle exposures are already in focus of research, exploiting lung organoids [184].

In my project, combining persistently infected macrophages with primary murine epithelial organoids and mesenchymal cells, I created immunocompetent organoids to study communication and interaction between the different cell types (**Figure 19**). Grown lung organoids did depict several epithelial cell markers found in the alveolar and bronchial compartment in the lungs (**Figure 20**). In response to carbon

nanoparticles or LPS, lung organoid cocultured with persistently MHV-68 infected macrophages did show enhanced virus reactivation (**Figure 21**).

One limitation in this setup was the fact, that uniting the three cell types posed already enough stress to the infected Ana-1 macrophages to trigger reactivation of the dormant virus in some cases. The high variability and elevated baseline of reactivation hampered the detection of further reaction to the triggers to be studied, like CNP or LPS. In addition, detecting infectious virus in the supernatant using plaque assay did for some reason fail in the CNP treated samples. Hence it was already shown to work in submerged conditions in single Ana-1/MHV-68 cultures [9], there might be a problem specific to the setup of 3D organoid cultures. Lung organoids require an extracellular matrix (Matrigel in my case) in order to grow. It seems like the viral particles do interact with CNP within this matrix and therefore hinder release of infectious viral particles into the supernatant. This difficulty did not affect LPS triggered virus detection. Nevertheless, virus reactivation was detectable on gene expression level as well as in lytic viral protein staining in both exposed groups. Interestingly, lytic viral proteins were not only found in latently infected macrophages, but also in elongated cells, resembling fibroblasts. Considering that MHV-68 is known to rapidly infect fibroblasts, and these cells are even exploited to reproduce infectious virus, it is no surprise that the mesenchymal support cells in this organoid culture are also target cells for virus infection. They even served as indicator cells for lytic infection.

Exposure to particles was conducted in a submerged manner in this experiment for reasons of practicality, what may be another reason for unstable results. Organoids grow into three dimensional spheres, facing their apical cell surface towards the lumen. For pulmonary epithelial cells this means that the cell surface getting in contact to the airflow in the lung is in organoids under submerged conditions within the lumen of the sphere. Particles that were administered in the surrounding medium thus hardly reach the lumen and apical cell surface as it would be the case *in vivo* for pulmonary delivered particles. To overcome this difficulty, one method could be to microinject harmful substances of investigation into the lumen of each organoid [185]. Although particles get in contact to the apical and surfactant producing surface of epithelial cells like this, it is very laborious and time-consuming to treat each individual organoid in one culture like this and to adapt the quantity of particles to organoid sizes. Nevertheless, several studies could

already confirm that organoids can recapitulate responses to harmful agents more accurately than two-dimensional immortalized cell cultures can do, even under submerged exposure conditions. This is especially true for soluble substances, like LPS in our case, as they can easily transfer through the medium and extracellular matrix to reach the target cells. On the contrary, insoluble, uncoated particles, like the spherical CNP used here, have difficulties to diffuse and move within extracellular matrix towards the cells, due to their distinct physicochemical properties.

Although lung organoids represent an advanced yet defined *in vitro* culture system recapitulating the lung more accurately than submerged cell cultures of cell lines, for pulmonary delivery of insoluble particles the 3D architecture of organoids requires particular considerations. In this project, immunocompetent organoids including macrophages persistently infected with MHV-68 in addition to primary epithelial cells and mesenchymal support cells were successfully cultured and described. Communication between the three niches was observed, as the addition of macrophages increased organoid growth significantly and a direct interaction was noticed (**Figure 19**). A challenge and open problem that would need more advancement is the induction and detection of MHV-68 reactivation upon CNP trigger. Future work should focus on the development of reliable readouts for virus reactivation, for example the use of a fluorescent reporter virus construct could allow the detection of viral gene and protein expression in real time. Once the trigger provokes a constant and reliable response in the lung organoid culture, this model is ready to be used for further examinations like cellular crosstalk, mechanisms and pathways following particle exposure and subsequent virus reactivation.

9. Outlook

Chronic lung diseases are a major health concern in our modern society. They still account for 4 million of deaths per year worldwide and are the third leading cause of death [49]. Thus, studying the underlying causes and factors leading to and worsening different lung diseases is crucial to improve this situation. An underlying latent infection with herpesvirus does shape the immune system of people affected in a way, which is not yet understood and rarely taken into account in studies regarding lung health. Long-term exposure to air pollution on the other hand is

increasingly studied. One cohort study from 2019 for example could show increasing emphysema in the lung of participants significantly associated to long-term ambient air pollutants in the US [70].

In this preclinical study, long-term exposure to soot-like carbon nanoparticles resulted in a chronic pulmonary inflammation with emphysematous changes, especially in mice with a latent herpesvirus infection. In view of the ubiquitous challenges for the human lung like herpesvirus infection as well as ambient air pollution, we must get a deeper insight into the interplay of the aforementioned. Differences in pulmonary responses between repeated CNP challenges in uninfected and latent MHV-68 infected mice arise the question, if the viral infection alters the immune response to subsequent pulmonary challenges in a way, that chronic lung diseases like emphysema develop faster or more severe. In addition to that, viral reactivation could also play a crucial role in cellular remodeling. As shown by colleagues in our group, medical intervention reduced reactivation of MHV-68 in a mouse model and might even reduce pulmonary pathologies [9].

These first achievements in fundamental research can likewise be applied in the field of veterinary medicine. Animals are exposed to ambient particles to the same extend as human beings and may benefit from further research in this relevant topic, including latent herpesvirus infections.

V. SUMMARY

Nearly every human being is infected with herpesviruses for a lifetime, a fact that in my opinion obligates to study the influence of this latent infection on shaping the host immune response to other challenges. This latent state can be disturbed by stress-induced reactivation, resulting in the production of lytic virus and viral spreading. In addition to this lifelong infection, the lungs are constantly exposed to environmental particles like fine dust. In previous investigations including both ubiquitous challenges to the lungs, latent herpesvirus infection and exposure to environmental particles, our group could show that pulmonary exposure to carbon nanoparticles (CNP) can trigger reactivation in latently with murine gamma herpesvirus 68 (MHV-68) infected mouse lungs. The reactivation was found to be mainly localized to $CD11b^+$ infiltrating macrophages and dependent on p38 MAPK signaling. A two-time repeated CNP instillation of latently with MHV-68 infected mice resulted in elevated alveolar damage and progressive emphysema-like changes [9]. In view of these findings, this project aimed to unravel the effects of a five-time repeated, chronic particle exposure to latently with MHV-68 infected mouse lungs. The emphasis was placed on investigations regarding lung inflammation and alveolar injury.

Five-time repeated CNP instillation to mouse lungs did result in an increase in recovered BAL inflammatory cells including innate immune cells like macrophages, multinucleated macrophages, and neutrophils, progressively rising with number of instillations. In response to an underlying latent MHV-68 infection, chronic CNP exposure was observed to increase the proportion of lymphocytes in BAL cells, thus engaging the adaptive immune system more than without viral infection. Cytokines and chemokines known to be involved in leukocyte recruitment were detected in BALF following repeated CNP exposure. A prolonged and increased cytokine detection after the fifth CNP instillation was only found in CNP exposed BALF samples after MHV-68 infection. Accumulations of mononuclear inflammatory cells in peribronchiolar and perivascular areas in the lung did contain B-cell cores surrounded by $CD8^+$ T-cells and NK-cells. Thus, chronic CNP exposure of latently with MHV-68 infected mouse lungs results in a chronic inflammatory environment with engagement of innate and adaptive immune cells.

In addition to that, five-time repeated CNP instillation in MHV-68 infected mice resulted in an enlargement of alveolar airspace one week after the last exposure, accompanied by a significantly reduced number of AT1 cells and enhanced signatures of apoptosis in these epithelial cells. Emphysema-like changes did worsen progressively with number of CNP instillations in MHV-68 infected mouse lungs and can be connected to epithelial cell apoptosis.

An *in vitro* model system to recapitulate cellular crosstalk and mechanisms leading to MHV-68 reactivation upon CNP trigger was developed. 3-dimensional immunocompetent lung organoids containing primary murine epithelial cells in combination with persistently with MHV-68 infected macrophages and fibroblastic support cells were used. Infected macrophages did enhance organoid formation significantly, and the organoids retained epithelial cell markers and structures within two weeks of culture. Reactivation was triggerable and detectable upon LPS stimulation as well as for most readouts for CNP exposure. However, the system was not yet robust enough to proceed with mechanistical investigations.

Taken together, my findings suggest that a chronic particle exposure to latently with herpesvirus infected lungs causes a progressive and chronic inflammation with damage and loss of alveolar epithelial cells, worsening with number of particle instillations and time.

VI. ZUSAMMENFASSUNG

Fast jeder Mensch ist ein Leben lang mit Herpesviren infiziert, eine Tatsache, die es meiner Meinung nach erforderlich macht, den Einfluss dieser latenten Infektion auf die Immunantwort des Wirts im Hinblick auf weitere externe Faktoren zu untersuchen. Die latente Infektion kann durch Stress unterbrochen werden, eine Reaktivierung wird ausgelöst und die Produktion von lytischen Viren sowie die Ausbreitung des Virus im Wirt wird aktiviert. Zusätzlich zu solchen lebenslangen Infektionen ist die Lunge ständig Umweltpartikeln wie Feinstaub ausgesetzt. In früheren Untersuchungen, die sowohl eine latente Herpesvirusinfektion als auch die Exposition gegenüber Umweltpartikeln umfassten, konnte unsere Gruppe zeigen, dass die pulmonale Exposition mit Kohlenstoff-Nanopartikeln (CNP) eine Reaktivierung in latent mit dem murinen Gamma-Herpesvirus 68 (MHV-68) infizierten Mäuselungen auslösen kann. Es wurde festgestellt, dass die Reaktivierung hauptsächlich in $CD11b^+$, infiltrierenden Makrophagen lokalisiert ist und vom p38 MAPK-Signalweg abhängig ist. Eine zweimalig wiederholte CNP-Instillation von latent mit MHV-68 infizierten Mäusen führte zu einer erhöhten alveolären Schädigung und zu progressiven emphysemartigen Veränderungen [9]. Angesichts dieser Befunde sollten in dem aktuellen Projekt mit dem Titel „Auswirkungen einer wiederholten Partikelexposition und einer latenten Virusinfektion auf die Lungenimmunität und Lungenerkrankungen“ die Auswirkungen einer fünfmal wiederholten, chronischen Partikelexposition auf latent mit MHV-68 infizierte Lungen untersucht werden. Der Schwerpunkt lag dabei auf Untersuchungen zu entzündlichen Prozessen in der Lunge und alveolären Schädigungen.

Die fünfmalig wiederholte Instillation von CNP in die Lunge von Mäusen führte zu einem Anstieg der Entzündungszellen in Bronchoalveolären Lavage (BAL)-Proben. Diese beinhalteten auch Zellen des angeborenen Immunsystems wie Makrophagen, mehrkernige Makrophagen und neutrophile Granulozyten. Deren Anteil stieg mit der Anzahl der Instillationen an. Als Reaktion auf eine zugrundeliegende latente MHV-68 Infektion konnte beobachtet werden, dass eine chronische CNP-Exposition den Anteil der Lymphozyten in den BAL-Zellen erhöht und damit das adaptive Immunsystem stärker aktiviert als ohne gleichzeitig vorliegende latente virale Infektion. Zytokine und Chemokine, von denen bekannt

ist, dass sie an der Leukozyten-Rekrutierung beteiligt sind, wurden nach wiederholter CNP-Exposition in der BAL Flüssigkeit nachgewiesen. Ein eine Woche anhaltender und erhöhter Nachweis nach der fünften CNP-Instillation wurde nur in CNP exponierten BAL-Proben nach MHV-68 Infektion gefunden. Anhäufungen von mononukleären Entzündungszellen in peribronchiolären und perivaskulären Bereichen der Lunge enthielten B-Zellen, die von $CD8^+$ T-Zellen und NK-Zellen umgeben waren. Die chronische CNP-Exposition von latent mit MHV-68 infizierten Mäuselungen führt somit zu einem chronischen Entzündungsmilieu mit Beteiligung von angeborenen und adaptiven Immunzellen.

Darüber hinaus zeigte sich bei fünfmaliger wiederholter CNP-Instillation in MHV-68 infizierten Mäusen eine Woche nach der letzten Exposition eine Vergrößerung des alveolären Luftraums, begleitet von einer signifikant reduzierten Anzahl von Typ 1 Alveolar Epithelzellen und verstärkten Zeichen der Apoptose in diesen Epithelzellen. Emphysemartige Veränderungen verschlimmerten sich demnach progressiv mit der Anzahl der CNP-Instillationen in MHV-68 infizierten Mäuselungen und können mit der Apoptose von Epithelzellen in Verbindung gebracht werden.

Außerdern entwickelte ich ein *in vitro* Modellsystem, um die zelluläre Kommunikation und Mechanismen zu erforschen, die zur MHV-68 Reaktivierung nach CNP-Exposition führen. Als Modell dienten dreidimensionale immunkompetente Lungenorganoide. Diese enthielten primäre murine Epithelzellen in Kombination mit persistent mit MHV-68 infizierten Makrophagen und fibroblastischen Unterstützungszellen. Die infizierten Makrophagen verbesserten die Bildung und das Wachstum der Organoide erheblich, und die Organoide behielten Epithelzellmarker und -strukturen bei. Die Reaktivierung war nach LPS-Stimulation auslösbar und nachweisbar. Nach einer Exposition mit CNP wurde eine Reaktivierung mit den meisten Endpunkten messbar, wenn auch noch nicht robust genug, um mit mechanistischen Untersuchungen fortzufahren.

Insgesamt deuten die Ergebnisse meiner Arbeit darauf hin, dass eine chronische Partikelexposition in latent mit Herpesviren infizierten Lungen eine fortschreitende und chronische Entzündung mit Schädigung und Verlust von alveolären Epithelzellen verursacht, die sich mit der Anzahl der Partikelexpositionen und fortschreitender Zeit verschlimmert.

VII. REFERENCES

1. Fröhlich, E.; Mercuri, A.; Wu, S.; Salar-Behzadi, S. Measurements of Deposition, Lung Surface Area and Lung Fluid for Simulation of Inhaled Compounds. *Front Pharmacol* **2016**, *7*, 181, doi:10.3389/fphar.2016.00181.

2. Pleil, J.D.; Ariel Geer Wallace, M.; Davis, M.D.; Matty, C.M. The physics of human breathing: flow, timing, volume, and pressure parameters for normal, on-demand, and ventilator respiration. *J Breath Res* **2021**, *15*, doi:10.1088/1752-7163/ac2589.

3. Gehr, P.; Bachofen, M.; Weibel, E.R. The normal human lung: ultrastructure and morphometric estimation of diffusion capacity. *Respiration Physiology* **1978**, *32*, 121-140, doi:https://doi.org/10.1016/0034-5687(78)90104-4.

4. Hudnall, S.D.; Chen, T.; Allison, P.; Tyring, S.K.; Heath, A. Herpesvirus prevalence and viral load in healthy blood donors by quantitative real-time polymerase chain reaction. *Transfusion* **2008**, *48*, 1180-1187, doi:10.1111/j.1537-2995.2008.01685.x.

5. Griffin, B.D.; Verweij, M.C.; Wiertz, E.J.H.J. Herpesviruses and immunity: The art of evasion. *Veterinary Microbiology* **2010**, *143*, 89-100, doi:https://doi.org/10.1016/j.vetmic.2010.02.017.

6. Adler, B.; Sattler, C.; Adler, H. Herpesviruses and Their Host Cells: A Successful Liaison. *Trends in Microbiology* **2017**, *25*, 229-241, doi:https://doi.org/10.1016/j.tim.2016.11.009.

7. Stoeger, T.; Adler, H. "Novel" Triggers of Herpesvirus Reactivation and Their Potential Health Relevance. *Front Microbiol* **2018**, *9*, 3207, doi:10.3389/fmicb.2018.03207.

8. Sattler, C.; Moritz, F.; Chen, S.; Steer, B.; Kutschke, D.; Irmler, M.; Beckers, J.; Eickelberg, O.; Schmitt-Kopplin, P.; Adler, H.; et al. Nanoparticle exposure reactivates latent herpesvirus and restores a signature of acute infection. *Part Fibre Toxicol* **2017**, *14*, 2, doi:10.1186/s12989-016-0181-1.

9. Han, L.; Haefner, V.; Yu, Y.; Han, B.; Ren, H.; Irmler, M.; Beckers, J.; Liu, Q.; Feuchtinger, A.; Yildirim, A.O.; et al. Nanoparticle-Exposure-Triggered Virus Reactivation Induces Lung Emphysema in Mice. *ACS Nano* **2023**, doi:10.1021/acsnano.3c04111.

10. Gatherer, D.; Depledge, D.P.; Hartley, C.A.; Szpara, M.L.; Vaz, P.K.; Benkő, M.; Brandt, C.R.; Bryant, N.A.; Dastjerdi, A.; Doszpoly, A.; et al. ICTV Virus Taxonomy Profile: Herpesviridae 2021. *Journal of General Virology* **2021**, *102*, doi:https://doi.org/10.1099/jgv.0.001673.

11. Selbitz, H.J.; Valentin-Weigand, P.; Truyen, U.; KG, G.T.V. *Tiermedizinische Mikrobiologie, Infektions- und Seuchenlehre*; Georg Thieme Verlag: 2023.

12. Davison, A.J. Herpesvirus systematics. *Veterinary Microbiology* **2010**, *143*, 52-69, doi:https://doi.org/10.1016/j.vetmic.2010.02.014.

13. Fields, B.N.; Knipe, D.M.; Howley, P.M.; Griffin, D.E. *Fields' Virology*; Wolters Kluwer Health/Lippincott Williams & Wilkins: 2007.

14. Buschle, A.; Hammerschmidt, W. Epigenetic lifestyle of Epstein-Barr virus. *Semin Immunopathol* **2020**, *42*, 131-142, doi:10.1007/s00281-020-00792-2.

15. Laichalk, L.L.; Thorley-Lawson, D.A. Terminal Differentiation into Plasma Cells Initiates the Replicative Cycle of Epstein-Barr Virus In Vivo. *Journal of Virology* **2005**, *79*, 1296-1307, doi:doi:10.1128/jvi.79.2.1296-1307.2005.

16. Fu, Z.; Cannon, M.J. Functional analysis of the CD4(+) T-cell response to Epstein-Barr virus: T-cell-mediated activation of resting B cells and induction of viral BZLF1 expression. *J Virol* **2000**, *74*, 6675-6679, doi:10.1128/jvi.74.14.6675-6679.2000.

17. Fahmi, H.; Cochet, C.; Hmama, Z.; Opolon, P.; Joab, I. Transforming growth factor beta 1 stimulates expression of the Epstein-Barr virus BZLF1 immediate-early gene product ZEBRA by an indirect mechanism which requires the MAPK kinase pathway. *J Virol* **2000**, *74*, 5810-5818, doi:10.1128/jvi.74.13.5810-5818.2000.

18. Smatti, M.K.; Yassine, H.M.; AbuOdeh, R.; AlMarawani, A.; Taleb, S.A.; Althani, A.A.; Nasrallah, G.K. Prevalence and molecular profiling of Epstein Barr virus (EBV) among healthy blood donors from different nationalities in Qatar. *PLoS One* **2017**, *12*, e0189033, doi:10.1371/journal.pone.0189033.

19. de-Thé, G. Epstein-Barr Virus Behavior in Different Populations and Implications for Control of Epstein-Barr Virus-associated Tumors1. *Cancer Research* **1976**, *36*, 692-695.

20. Venkitaraman, A.R.; Lenoir, G.M.; John, T.J. The seroepidemiology of infection due to Epstein-Barr virus in southern India. *Journal of Medical Virology* **1985**, *15*, 11-16, doi:https://doi.org/10.1002/jmv.1890150103.

21. Virgin, H.W.; Wherry, E.J.; Ahmed, R. Redefining Chronic Viral Infection. *Cell* **2009**, *138*, 30-50, doi:10.1016/j.cell.2009.06.036.

22. Brock, J.; Lange, M.; Guelbenzu-Gonzalo, M.; Meunier, N.; Vaz, A.M.; Tratalos, J.A.; Dittrich, P.; Gunn, M.; More, S.J.; Graham, D.; et al. Epidemiology of age-dependent prevalence of Bovine Herpes Virus Type 1 (BoHV-1) in dairy herds with and without vaccination. *Veterinary Research* **2020**, *51*, 124, doi:10.1186/s13567-020-00842-5.

23. Nordengrahn, A.; Merza, M.; Ros, C.; Lindholmc, A.; Palfl, V.; Hannant, D.; Belák, S. Prevalence of equine herpesvirus types 2 and 5 in horse populations by using type-specific PCR assays. *Vet Res* **2002**, *33*, 251-259, doi:10.1051/vetres:2002013.

24. Ronsse, V.; Verstegen, J.; Onclin, K.; Guiot, A.; Aeberlé, C.; Nauwynck, H.; Poulet, H. Seroprevalence of Canine Herpesvirus-1 in the Belgian Dog Population in 2000. *Reproduction in Domestic Animals* **2002**, *37*, 299-304, doi:https://doi.org/10.1046/j.1439-0531.2002.00363.x.

25. Ertl, R.; Korb, M.; Langbein-Detsch, I.; Klein, D. Prevalence and risk factors of gammaherpesvirus infection in domestic cats in Central Europe. *Virology Journal* **2015**, *12*, 146, doi:10.1186/s12985-015-0381-6.

26. Virgin, H.W.t.; Latreille, P.; Wamsley, P.; Hallsworth, K.; Weck, K.E.; Dal Canto, A.J.; Speck, S.H. Complete sequence and genomic analysis of murine gammaherpesvirus 68. *J Virol* **1997**, *71*, 5894-5904, doi:10.1128/JVI.71.8.5894-5904.1997.

27. Barton, E.; Mandal, P.; Speck, S.H. Pathogenesis and host control of gammaherpesviruses: lessons from the mouse. *Annu Rev Immunol* **2011**, *29*, 351-397, doi:10.1146/annurev-immunol-072710-081639.

28. Sunil-Chandra, N.P.; Efstathiou, S.; Arno, J.; Nash, A.A. Virological and pathological features of mice infected with murine gamma-herpesvirus 68. *J Gen Virol* **1992**, *73 (Pt 9)*, 2347-2356, doi:10.1099/0022-1317-73-9-2347.

29. Stewart, J.P.; Usherwood, E.J.; Ross, A.; Dyson, H.; Nash, T. Lung epithelial cells are a major site of murine gammaherpesvirus persistence. *J Exp Med* **1998**, *187*, 1941-1951, doi:10.1084/jem.187.12.1941.

30. Weck, K.E.; Kim, S.S.; Virgin, H.I.; Speck, S.H. Macrophages are the major reservoir of latent murine gammaherpesvirus 68 in peritoneal cells. *J Virol* **1999**, *73*, 3273-3283, doi:10.1128/JVI.73.4.3273-3283.1999.

31. Fuller, R.; Landrigan, P.J.; Balakrishnan, K.; Bathan, G.; Bose-O'Reilly, S.; Brauer, M.; Caravanos, J.; Chiles, T.; Cohen, A.; Corra, L.; et al. Pollution and health: a progress update. *The Lancet Planetary Health* **2022**, *6*, e535-e547, doi:10.1016/S2542-5196(22)00090-0.

32. Calderón-Garcidueñas, L.; Mora-Tiscareño, A.; Fordham, L.A.; Chung, C.J.; García, R.; Osnaya, N.; Hernández, J.; Acuña, H.; Gambling, T.M.; Villarreal-Calderón, A.; et al. Canines as Sentinel Species for Assessing Chronic Exposures to Air Pollutants: Part 1. Respiratory Pathology. *Toxicological Sciences* **2001**, *61*, 342-355, doi:10.1093/toxsci/61.2.342.

33. Mohamed, R.A.; Georges, K.; Rajh, S.; Suepaul, R.B. A pilot study on the lung morphology of shelter dogs in relation to air pollution in Trinidad. *Am J Vet Res* **2022**, *83*, doi:10.2460/ajvr.22.05.0077.

34. Lin, C.-H.; Lo, P.-Y.; Wu, H.-D. An observational study of the role of indoor air pollution in pets with naturally acquired bronchial/lung disease. *Veterinary Medicine and Science* **2020**, *6*, 314-320, doi:https://doi.org/10.1002/vms3.231.

35. Bettini, G.; Morini, M.; Marconato, L.; Marcato, P.S.; Zini, E. Association between environmental dust exposure and lung cancer in dogs. *The Veterinary Journal* **2010**, *186*, 364-369, doi:https://doi.org/10.1016/j.tvjl.2009.09.004.

36. Kim, L.D.; Kreitner, K.; Scott, D.M.; Seabaugh, K.; Duncan, C.G.; Magzamen, S. The effects of ambient air pollution exposure on Thoroughbred racehorse performance. *Equine Veterinary Journal* **2024**, *n/a*, doi:https://doi.org/10.1111/evj.14415.

37. Brankston, G.; Greer, A.L.; Marshall, Q.; Lang, B.; Moore, K.; Hodgins, D.; Hennessey, J.T.G.; Beeler-Marfisi, J. Increased Weekly Mean PM2.5, and NO2 Are Associated With Increased Proportions of Lower Airway Granulocytes in Ontario Horses. *Frontiers in Veterinary Science* **2020**, *7*, doi:10.3389/fvets.2020.00185.

38. Organization, W.H. *WHO global air quality guidelines. Particulate matter (PM2.5 and PM10), ozone, nitrogen dioxide, sulfur dioxide and carbon monoxide*; Geneva, 2021.

39. Guarnieri, M.; Balmes, J.R. Outdoor air pollution and asthma. *The Lancet* **2014**, *383*, 1581-1592, doi:https://doi.org/10.1016/S0140-6736(14)60617-6.

40. Schmid, O.; Stoeger, T. Surface area is the biologically most effective dose metric for acute nanoparticle toxicity in the lung. *Journal of Aerosol Science* **2016**, *99*, 133-143, doi:https://doi.org/10.1016/j.jaerosci.2015.12.006.

41. Pryor, J.T.; Cowley, L.O.; Simonds, S.E. The Physiological Effects of Air Pollution: Particulate Matter, Physiology and Disease. *Front Public Health* **2022**, *10*, 882569, doi:10.3389/fpubh.2022.882569.

42. Oberdörster, G.; Oberdörster, E.; Oberdörster, J. Nanotoxicology: An Emerging Discipline Evolving from Studies of Ultrafine Particles. *Environmental Health Perspectives* **2005**, *113*, 823-839, doi:doi:10.1289/ehp.7339.

43. Dames, E.; Rohani, V.; Fulcheri, L. Chapter Five - Plasma chemistry and plasma reactors for turquoise hydrogen and carbon nanomaterials production. In *Advances in Chemical Engineering*, Pelucchi, M., Maestri, M., Eds.; Academic Press: 2023; Volume 61, pp. 253-317.

44. Long, C.M.; Nascarella, M.A.; Valberg, P.A. Carbon black vs. black carbon and other airborne materials containing elemental carbon: Physical and chemical distinctions. *Environmental Pollution* **2013**, *181*, 271-286, doi:https://doi.org/10.1016/j.envpol.2013.06.009.

45. Carbon black, titanium dioxide, and talc. *IARC Monogr Eval Carcinog Risks*

Hum **2010**, *93*, 1-413.

46. Bourdon, J.A.; Saber, A.T.; Jacobsen, N.R.; Jensen, K.A.; Madsen, A.M.; Lamson, J.S.; Wallin, H.; Møller, P.; Loft, S.; Yauk, C.L.; et al. Carbon black nanoparticle instillation induces sustained inflammation and genotoxicity in mouse lung and liver. *Particle and Fibre Toxicology* **2012**, *9*, 5, doi:10.1186/1743-8977-9-5.

47. Ganguly, K.; Ettehadieh, D.; Upadhyay, S.; Takenaka, S.; Adler, T.; Karg, E.; Krombach, F.; Kreyling, W.G.; Schulz, H.; Schmid, O.; et al. Early pulmonary response is critical for extra-pulmonary carbon nanoparticle mediated effects: comparison of inhalation versus intra-arterial infusion exposures in mice. *Part Fibre Toxicol* **2017**, *14*, 19, doi:10.1186/s12989-017-0200-x.

48. Chen, S.; Yin, R.; Mutze, K.; Yu, Y.; Takenaka, S.; Konigshoff, M.; Stoeger, T. No involvement of alveolar macrophages in the initiation of carbon nanoparticle induced acute lung inflammation in mice. *Part Fibre Toxicol* **2016**, *13*, 33, doi:10.1186/s12989-016-0144-6.

49. Momtazmanesh, S.; Moghaddam, S.S.; Ghamari, S.-H.; Rad, E.M.; Rezaei, N.; Shobeiri, P.; Aali, A.; Abbasi-Kangevari, M.; Abbasi-Kangevari, Z.; Abdelmasseh, M.; et al. Global burden of chronic respiratory diseases and risk factors, 1990–2019: an update from the Global Burden of Disease Study 2019. *eClinicalMedicine* **2023**, *59*, doi:10.1016/j.eclinm.2023.101936.

50. Martinez, F.J.; Collard, H.R.; Pardo, A.; Raghu, G.; Richeldi, L.; Selman, M.; Swigris, J.J.; Taniguchi, H.; Wells, A.U. Idiopathic pulmonary fibrosis. *Nature Reviews Disease Primers* **2017**, *3*, 17074, doi:10.1038/nrdp.2017.74.

51. Raghu, G.; Remy-Jardin, M.; Richeldi, L.; Thomson, C.C.; Inoue, Y.; Johkoh, T.; Kreuter, M.; Lynch, D.A.; Maher, T.M.; Martinez, F.J.; et al. Idiopathic Pulmonary Fibrosis (an Update) and Progressive Pulmonary Fibrosis in Adults: An Official ATS/ERS/JRS/ALAT Clinical Practice Guideline. *Am J Respir Crit Care Med* **2022**, *205*, e18-e47, doi:10.1164/rccm.202202-0399ST.

52. Tang, Y.-W.; Johnson, J.; Cruz-Gervis, R.; Graham, B.; Brigham, K.; Oates, J.; Loyd, J.; Stecenko, A. Increased Detection of Herpesvirus DNA in Idiopathic Pulmonary Fibrosis. *Chest* **2001**, *120*, S74-S75, doi:https://doi.org/10.1016/S0012-3692(15)38729-8.

53. Lok, S.S.; Stewart, J.P.; Kelly, B.G.; Hasleton, P.S.; Egan, J.J. Epstein-Barr virus and wild p53 in idiopathic pulmonary fibrosis. *Respir Med* **2001**, *95*, 787-791, doi:10.1053/rmed.2001.1152.

54. Tang, Y.-W.; Johnson, J.E.; Browning, P.J.; Cruz-Gervis, R.A.; Davis, A.; Graham, B.S.; Brigham, K.L.; Oates, J.A., Jr.; Loyd, J.E.; Stecenko, A.A. Herpesvirus DNA is consistently detected in lungs of patients with idiopathic pulmonary fibrosis. *J Clin Microbiol* **2003**, *41*, 2633-2640, doi:10.1128/JCM.41.6.2633-2640.2003.

55. Lawson, W.E.; Crossno, P.F.; Polosukhin, V.V.; Roldan, J.; Cheng, D.-S.; Lane, K.B.; Blackwell, T.R.; Xu, C.; Markin, C.; Ware, L.B.; et al. Endoplasmic reticulum stress in alveolar epithelial cells is prominent in IPF: association with altered surfactant protein processing and herpesvirus infection. *American Journal of Physiology-Lung Cellular and Molecular Physiology* **2008**, *294*, L1119-L1126, doi:10.1152/ajplung.00382.2007.

56. Williams, K.J.; Maes, R.; Del Piero, F.; Lim, A.; Wise, A.; Bolin, D.C.; Caswell, J.; Jackson, C.; Robinson, N.E.; Derksen, F.; et al. Equine Multinodular Pulmonary Fibrosis: A Newly Recognized Herpesvirus-Associated Fibrotic Lung Disease. *Veterinary Pathology* **2007**, *44*, 849-862, doi:10.1354/vp.44-6-849.

57. Dunkel, B. Pulmonary fibrosis and gammaherpesvirus infection in horses. *Equine Veterinary Education* **2012**, *24*, 200-205, doi:https://doi.org/10.1111/j.2042-3292.2011.00340.x.

58. Williams, K.J.; Robinson, N.E.; Lim, A.; Brandenberger, C.; Maes, R.; Behan, A.; Bolin, S.R. Experimental Induction of Pulmonary Fibrosis in Horses with the Gammaherpesvirus Equine Herpesvirus 5. *PLOS ONE* **2013**, *8*, e77754, doi:10.1371/journal.pone.0077754.

59. Williams, K.J. Gammaherpesviruses and Pulmonary Fibrosis:Evidence From Humans, Horses, and Rodents. *Veterinary Pathology* **2014**, *51*, 372-384, doi:10.1177/0300985814521838.

60. Pusterla, N.; Magdesian, K.G.; Mapes, S.M.; Zavodovskaya, R.; Kass, P.H. Assessment of quantitative polymerase chain reaction for equine herpesvirus-5 in blood, nasal secretions and bronchoalveolar lavage fluid for the laboratory diagnosis of equine multinodular pulmonary fibrosis. *Equine Vet J* **2017**, *49*, 34-38, doi:10.1111/evj.12545.

61. Easton-Jones, C.A.; Madigan, J.E.; Barnum, S.; Maxwell, L.K.; Taylor, S.D.; Arnesen, T.; Pusterla, N. Effect of valacyclovir on EHV-5 viral kinetics in horses with equine multinodular pulmonary fibrosis. *Journal of Veterinary Internal Medicine* **2018**, *32*, 1763-1767, doi:https://doi.org/10.1111/jvim.15230.

62. Winterbottom, C.J.; Shah, R.J.; Patterson, K.C.; Kreider, M.E.; Panettieri, R.A., Jr.; Rivera-Lebron, B.; Miller, W.T.; Litzky, L.A.; Penning, T.M.; Heinlen, K.; et al. Exposure to Ambient Particulate Matter Is Associated With Accelerated Functional Decline in Idiopathic Pulmonary Fibrosis. *Chest* **2018**, *153*, 1221-1228, doi:10.1016/j.chest.2017.07.034.

63. Johannson, K.A.; Vittinghoff, E.; Morisset, J.; Wolters, P.J.; Noth, E.M.; Balmes, J.R.; Collard, H.R. Air Pollution Exposure Is Associated With Lower Lung Function, but Not Changes in Lung Function, in Patients With Idiopathic Pulmonary Fibrosis. *Chest* **2018**, *154*, 119-125, doi:10.1016/j.chest.2018.01.015.

64. Goobie, G.C.; Carlsten, C.; Johannson, K.A.; Khalil, N.; Marcoux, V.; Assayag, D.; Manganas, H.; Fisher, J.H.; Kolb, M.R.J.; Lindell, K.O.; et al.

Association of Particulate Matter Exposure With Lung Function and Mortality Among Patients With Fibrotic Interstitial Lung Disease. *JAMA Internal Medicine* **2022**, *182*, 1248-1259, doi:10.1001/jamainternmed.2022.4696.

65. Tomos, I.; Dimakopoulou, K.; Manali, E.D.; Papiris, S.A.; Karakatsani, A. Long-term personal air pollution exposure and risk for acute exacerbation of idiopathic pulmonary fibrosis. *Environmental Health* **2021**, *20*, 99, doi:10.1186/s12940-021-00786-z.

66. Kim, V.; Criner, G.J. Chronic Bronchitis and Chronic Obstructive Pulmonary Disease. *American Journal of Respiratory and Critical Care Medicine* **2013**, *187*, 228-237, doi:10.1164/rccm.201210-1843CI.

67. Suki, B.; Lutchen, K.R.; Ingenito, E.P. On the Progressive Nature of Emphysema. *American Journal of Respiratory and Critical Care Medicine* **2003**, *168*, 516-521, doi:10.1164/rccm.200208-908PP.

68. McManus, T.E.; Marley, A.-M.; Baxter, N.; Christie, S.N.; Elborn, J.S.; O'Neill, H.J.; Coyle, P.V.; Kidney, J.C. High levels of Epstein–Barr virus in COPD. *European Respiratory Journal* **2008**, *31*, 1221-1226, doi:10.1183/09031936.00107507.

69. Polosukhin, V.V.; Cates, J.M.; Lawson, W.E.; Zaynagetdinov, R.; Milstone, A.P.; Massion, P.P.; Ocak, S.; Ware, L.B.; Lee, J.W.; Bowler, R.P.; et al. Bronchial Secretory Immunoglobulin A Deficiency Correlates With Airway Inflammation and Progression of Chronic Obstructive Pulmonary Disease. *American Journal of Respiratory and Critical Care Medicine* **2011**, *184*, 317-327, doi:10.1164/rccm.201010-1629OC.

70. Wang, M.; Aaron, C.P.; Madrigano, J.; Hoffman, E.A.; Angelini, E.; Yang, J.; Laine, A.; Vetterli, T.M.; Kinney, P.L.; Sampson, P.D.; et al. Association Between Long-term Exposure to Ambient Air Pollution and Change in Quantitatively Assessed Emphysema and Lung Function. *JAMA* **2019**, *322*, 546-556, doi:10.1001/jama.2019.10255.

71. Liu, S.; Zhou, Y.; Liu, S.; Chen, X.; Zou, W.; Zhao, D.; Li, X.; Pu, J.; Huang, L.; Chen, J.; et al. Association between exposure to ambient particulate matter and chronic obstructive pulmonary disease: results from a cross-sectional study in China. *Thorax* **2017**, *72*, 788-795, doi:10.1136/thoraxjnl-2016-208910.

72. Beasley, R.; Semprini, A.; Mitchell, E.A. Risk factors for asthma: is prevention possible? *The Lancet* **2015**, *386*, 1075-1085, doi:10.1016/S0140-6736(15)00156-7.

73. Choi, S.; Sohn, K.-H.; Jung, J.-W.; Kang, M.-G.; Yang, M.-S.; Kim, S.; Choi, J.-H.; Cho, S.-H.; Kang, H.-R.; Yi, H. Lung virome: New potential biomarkers for asthma severity and exacerbation. *Journal of Allergy and Clinical Immunology* **2021**, *148*, 1007-1015.e1009, doi:https://doi.org/10.1016/j.jaci.2021.03.017.

74. Kowalski, M.L.; Wardzynska, A.; Studzinska, M.; Pawelczyk, M.; Lesnikowski, Z.J.; Paradowska, E. Cytomegalovirus DNA is highly prevalent in the blood of patients with asthma and is associated with age and asthma traits. *Allergy* **2017**, *72*, 2035-2038, doi:https://doi.org/10.1111/all.13233.

75. Houtsma, A.; Bedenice, D.; Pusterla, N.; Pugliese, B.; Mapes, S.; Hoffman, A.M.; Paxson, J.; Rozanski, E.; Mukherjee, J.; Wigley, M.; et al. Association between inflammatory airway disease of horses and exposure to respiratory viruses: a case control study. *Multidisciplinary Respiratory Medicine* **2015**, *10*, 33, doi:10.1186/s40248-015-0030-3.

76. Tétreault, L.-F.; Doucet, M.; Gamache, P.; Fournier, M.; Brand, A.; Kosatsky, T.; Smargiassi, A. Childhood Exposure to Ambient Air Pollutants and the Onset of Asthma: An Administrative Cohort Study in Québec. *Environmental Health Perspectives* **2016**, *124*, 1276-1282, doi:doi:10.1289/ehp.1509838.

77. Lavigne, E.; Donelle, J.; Hatzopoulou, M.; Van Ryswyk, K.; van Donkelaar, A.; Martin, R.V.; Chen, H.; Stieb, D.M.; Gasparrini, A.; Crighton, E.; et al. Spatiotemporal Variations in Ambient Ultrafine Particles and the Incidence of Childhood Asthma. *American Journal of Respiratory and Critical Care Medicine* **2019**, *199*, 1487-1495, doi:10.1164/rccm.201810-1976OC.

78. Bouazza, N.; Foissac, F.; Urien, S.; Guedj, R.; Carbajal, R.; Tréluyer, J.-M.; Chappuy, H. Fine particulate pollution and asthma exacerbations. *Archives of Disease in Childhood* **2018**, *103*, 828-831, doi:10.1136/archdischild-2017-312826.

79. Tétreault, L.-F.; Doucet, M.; Gamache, P.; Fournier, M.; Brand, A.; Kosatsky, T.; Smargiassi, A. Severe and Moderate Asthma Exacerbations in Asthmatic Children and Exposure to Ambient Air Pollutants. *International Journal of Environmental Research and Public Health* **2016**, *13*, 771.

80. Orellano, P.; Quaranta, N.; Reynoso, J.; Balbi, B.; Vasquez, J. Effect of outdoor air pollution on asthma exacerbations in children and adults: Systematic review and multilevel meta-analysis. *PLoS One* **2017**, *12*, e0174050, doi:10.1371/journal.pone.0174050.

81. Wilhelm, M.; Meng, Y.Y.; Rull, R.P.; English, P.; Balmes, J.; Ritz, B. Environmental public health tracking of childhood asthma using California health interview survey, traffic, and outdoor air pollution data. *Environ Health Perspect* **2008**, *116*, 1254-1260, doi:10.1289/ehp.10945.

82. Lung, M.L.; So, S.Y.; Chan, K.H.; Lam, W.K.; Lam, W.P.; Ng, M.H. Evidence that respiratory tract is major reservoir for Epstein-Barr virus. *The Lancet* **1985**, *325*, 889-892, doi:https://doi.org/10.1016/S0140-6736(85)91671-X.

83. Gómez-Román, J.J.; Martínez, M.N.; Fernández, S.L.; Val-Bernal, J.F. Epstein–Barr virus-associated adenocarcinomas and squamous-cell lung carcinomas. *Modern Pathology* **2009**, *22*, 530-537, doi:https://doi.org/10.1038/modpathol.2009.7.

84. Kasai, K.; Sato, Y.; Kameya, T.; Inoue, H.; Yoshimura, H.; Kon, S.; Kikuchi, K. Incidence of latent infection of Epstein-Barr virus in lung cancers--an analysis of EBER1 expression in lung cancers by in situ hybridization. *J Pathol* **1994**, *174*, 257-265, doi:10.1002/path.1711740405.

85. Jafarian, A.H.; Omidi-Ashrafi, A.; Mohamadian-Roshan, N.; Karimi-Shahri, M.; Ghazvini, K.; Boroumand-Noughabi, S. Association of Epstein Barr virus deoxyribonucleic acid with lung carcinoma. *Indian J Pathol Microbiol* **2013**, *56*, 359-364, doi:10.4103/0377-4929.125290.

86. Kheir, F.; Zhao, M.; Strong, M.J.; Yu, Y.; Nanbo, A.; Flemington, E.K.; Morris, G.F.; Reiss, K.; Li, L.; Lin, Z. Detection of Epstein-Barr Virus Infection in Non-Small Cell Lung Cancer. *Cancers (Basel)* **2019**, *11*, doi:10.3390/cancers11060759.

87. Turner, M.C.; Krewski, D.; Pope, C.A.; Chen, Y.; Gapstur, S.M.; Thun, M.J. Long-term Ambient Fine Particulate Matter Air Pollution and Lung Cancer in a Large Cohort of Never-Smokers. *American Journal of Respiratory and Critical Care Medicine* **2011**, *184*, 1374-1381, doi:10.1164/rccm.201106-1011OC.

88. Liu, X.; Mubarik, S.; Wang, F.; Yu, Y.; Wang, Y.; Shi, F.; Wen, H.; Yu, C. Lung Cancer Death Attributable to Long-Term Ambient Particulate Matter (PM2.5) Exposure in East Asian Countries During 1990–2019. *Front Med (Lausanne)* **2021**, *8*, doi:10.3389/fmed.2021.742076.

89. Lo, W.-C.; Ho, C.-C.; Tseng, E.; Hwang, J.-S.; Chan, C.-C.; Lin, H.-H. Long-term exposure to ambient fine particulate matter (PM2.5) and associations with cardiopulmonary diseases and lung cancer in Taiwan: a nationwide longitudinal cohort study. *International Journal of Epidemiology* **2022**, *51*, 1230-1242, doi:10.1093/ije/dyac082.

90. Huang, H.-L.; Chuang, Y.-H.; Lin, T.-H.; Lin, C.; Chen, Y.-H.; Hung, J.-Y.; Chan, T.-C. Ambient Cumulative PM2.5 Exposure and the Risk of Lung Cancer Incidence and Mortality: A Retrospective Cohort Study. *International Journal of Environmental Research and Public Health* **2021**, *18*, 12400.

91. Guo, H.; Li, W.; Wu, J. Ambient PM2.5 and Annual Lung Cancer Incidence: A Nationwide Study in 295 Chinese Counties. *International Journal of Environmental Research and Public Health* **2020**, *17*, 1481.

92. Ciabattini, M.; Rizzello, E.; Lucaroni, F.; Palombi, L.; Boffetta, P. Systematic review and meta-analysis of recent high-quality studies on exposure to particulate matter and risk of lung cancer. *Environmental Research* **2021**, *196*, 110440, doi:https://doi.org/10.1016/j.envres.2020.110440.

93. Setti, L.; Passarini, F.; De Gennaro, G.; Barbieri, P.; Licen, S.; Perrone, M.G.; Piazzalunga, A.; Borelli, M.; Palmisani, J.; Di Gilio, A.; et al. Potential role of particulate matter in the spreading of COVID-19 in Northern Italy: first observational study based on initial epidemic diffusion. *BMJ Open* **2020**, *10*,

e039338, doi:10.1136/bmjopen-2020-039338.

94. Jerrett, M.; Nau, C.L.; Young, D.R.; Butler, R.K.; Batteate, C.M.; Su, J.; Burnett, R.T.; Kleeman, M.J. Air pollution and meteorology as risk factors for COVID-19 death in a cohort from Southern California. *Environment International* **2023**, *171*, 107675, doi:https://doi.org/10.1016/j.envint.2022.107675.

95. Frontera, A.; Cianfanelli, L.; Vlachos, K.; Landoni, G.; Cremona, G. Severe air pollution links to higher mortality in COVID-19 patients: The "double-hit" hypothesis. *J Infect* **2020**, *81*, 255-259, doi:10.1016/j.jinf.2020.05.031.

96. Konstantinoudis, G.; Padellini, T.; Bennett, J.; Davies, B.; Ezzati, M.; Blangiardo, M. Long-term exposure to air-pollution and COVID-19 mortality in England: A hierarchical spatial analysis. *Environ Int* **2021**, *146*, 106316, doi:10.1016/j.envint.2020.106316.

97. Pozzer, A.; Dominici, F.; Haines, A.; Witt, C.; Münzel, T.; Lelieveld, J. Regional and global contributions of air pollution to risk of death from COVID-19. *Cardiovascular Research* **2020**, *116*, 2247-2253, doi:10.1093/cvr/cvaa288.

98. Marchetti, S.; Colombo, A.; Saibene, M.; Bragato, C.; La Torretta, T.; Rizzi, C.; Gualtieri, M.; Mantecca, P. Shedding light on the cellular mechanisms involved in the combined adverse effects of fine particulate matter and SARS-CoV-2 on human lung cells. *Science of The Total Environment* **2024**, *952*, 175979, doi:https://doi.org/10.1016/j.scitotenv.2024.175979.

99. Hsiao, T.-C.; Cheng, P.-C.; Chi, K.H.; Wang, H.-Y.; Pan, S.-Y.; Kao, C.; Lee, Y.-L.; Kuo, H.-P.; Chung, K.F.; Chuang, H.-C. Interactions of chemical components in ambient PM2.5 with influenza viruses. *Journal of Hazardous Materials* **2022**, *423*, 127243, doi:https://doi.org/10.1016/j.jhazmat.2021.127243.

100. Dong, Z.; Ma, J.; Qiu, J.; Ren, Q.; Shan, Q.e.; Duan, X.; Li, G.; Zuo, Y.Y.; Qi, Y.; Liu, Y.; et al. Airborne fine particles drive H1N1 viruses deep into the lower respiratory tract and distant organs. *Science Advances* **2023**, *9*, eadf2165, doi:doi:10.1126/sciadv.adf2165.

101. Chen, G.; Zhang, W.; Li, S.; Zhang, Y.; Williams, G.; Huxley, R.; Ren, H.; Cao, W.; Guo, Y. The impact of ambient fine particles on influenza transmission and the modification effects of temperature in China: A multi-city study. *Environ Int* **2017**, *98*, 82-88, doi:10.1016/j.envint.2016.10.004.

102. Lindner-Cendrowska, K.; Bröde, P. Impact of biometeorological conditions and air pollution on influenza-like illnesses incidence in Warsaw. *International Journal of Biometeorology* **2021**, *65*, 929-944, doi:10.1007/s00484-021-02076-2.

103. Chau, T.-T.; Wang, K.-Y. An association between air pollution and daily most frequently visits of eighteen outpatient diseases in an industrial city. *Scientific Reports* **2020**, *10*, 2321, doi:10.1038/s41598-020-58721-0.

104. Lu, B.; Wang, Y.; Zhu, Z.; Zhang, Z.; Dong, T.; Li, F.; Gao, Y.; Du, X.; Qu, Z. Epidemiological and genetic characteristics of influenza virus and the effects of air pollution on laboratory-confirmed influenza cases in Hulunbuir, China, from 2010 to 2019. *Epidemiology and Infection* **2020**, *148*, e159, doi:10.1017/S0950268820001387.

105. Nenna, R.; Evangelisti, M.; Frassanito, A.; Scagnolari, C.; Pierangeli, A.; Antonelli, G.; Nicolai, A.; Arima, S.; Moretti, C.; Papoff, P.; et al. Respiratory syncytial virus bronchiolitis, weather conditions and air pollution in an Italian urban area: An observational study. *Environmental Research* **2017**, *158*, 188-193, doi:https://doi.org/10.1016/j.envres.2017.06.014.

106. Karr, C.J.; Rudra, C.B.; Miller, K.A.; Gould, T.R.; Larson, T.; Sathyanarayana, S.; Koenig, J.Q. Infant exposure to fine particulate matter and traffic and risk of hospitalization for RSV bronchiolitis in a region with lower ambient air pollution. *Environmental Research* **2009**, *109*, 321-327, doi:https://doi.org/10.1016/j.envres.2008.11.006.

107. Wrotek, A.; Badyda, A.; Czechowski, P.O.; Owczarek, T.; Dąbrowiecki, P.; Jackowska, T. Air Pollutants' Concentrations Are Associated with Increased Number of RSV Hospitalizations in Polish Children. *J Clin Med* **2021**, *10*, doi:10.3390/jcm10153224.

108. Li, M.; Chen, W.-J.; Yang, J.; Charvat, H.; Xie, S.-H.; Li, T.; Ling, W.; Lu, Y.-Q.; Liu, Q.; Hong, M.-H.; et al. Association between solid fuel use and seropositivity against Epstein-Barr virus in a high-risk area for nasopharyngeal carcinoma. *Environmental Pollution* **2022**, *304*, 119184, doi:https://doi.org/10.1016/j.envpol.2022.119184.

109. Hou, L.; Barupal, J.; Zhang, W.; Zheng, Y.; Liu, L.; Zhang, X.; Dou, C.; McCracken, J.P.; Díaz, A.; Motta, V.; et al. Particulate Air Pollution Exposure and Expression of Viral and Human MicroRNAs in Blood: The Beijing Truck Driver Air Pollution Study. *Environmental Health Perspectives* **2016**, *124*, 344-350, doi:doi:10.1289/ehp.1408519.

110. Steer, B.; Adler, B.; Jonjic, S.; Stewart, J.P.; Adler, H. A Gammaherpesvirus Complement Regulatory Protein Promotes Initiation of Infection by Activation of Protein Kinase Akt/PKB. *PLOS ONE* **2010**, *5*, e11672, doi:10.1371/journal.pone.0011672.

111. Stoeger, T.; Takenaka, S.; Frankenberger, B.; Ritter, B.; Karg, E.; Maier, K.; Schulz, H.; Schmid, O. Deducing in vivo toxicity of combustion-derived nanoparticles from a cell-free oxidative potency assay and metabolic activation of organic compounds. *Environ Health Perspect* **2009**, *117*, 54-60, doi:10.1289/ehp.11370.

112. Salaets, T.; Tack, B.; Gie, A.; Pavie, B.; Sindhwani, N.; Jimenez, J.; Regin, Y.; Allegaert, K.; Deprest, J.; Toelen, J. A semi-automated method for unbiased alveolar morphometry: Validation in a bronchopulmonary dysplasia model. *PLoS*

One **2020**, *15*, e0239562, doi:10.1371/journal.pone.0239562.

113. Ershov, D.; Phan, M.-S.; Pylvänäinen, J.W.; Rigaud, S.U.; Le Blanc, L.; Charles-Orszag, A.; Conway, J.R.W.; Laine, R.F.; Roy, N.H.; Bonazzi, D.; et al. TrackMate 7: integrating state-of-the-art segmentation algorithms into tracking pipelines. *Nature Methods* **2022**, *19*, 829-832, doi:10.1038/s41592-022-01507-1.

114. Cox, G.W.; Mathieson, B.J.; Gandino, L.; Blasi, E.; Radzioch, D.; Varesio, L. Heterogeneity of hematopoietic cells immortalized by v-myc/v-raf recombinant retrovirus infection of bone marrow or fetal liver. *J Natl Cancer Inst* **1989**, *81*, 1492-1496, doi:10.1093/jnci/81.19.1492.

115. Lee, J.H.; Kim, J.; Gludish, D.; Roach, R.R.; Saunders, A.H.; Barrios, J.; Woo, A.J.; Chen, H.; Conner, D.A.; Fujiwara, Y.; et al. Surfactant protein-C chromatin-bound green fluorescence protein reporter mice reveal heterogeneity of surfactant protein C-expressing lung cells. *Am J Respir Cell Mol Biol* **2013**, *48*, 288-298, doi:10.1165/rcmb.2011-0403OC.

116. De Zio, D.; Cianfanelli, V.; Cecconi, F. New insights into the link between DNA damage and apoptosis. *Antioxid Redox Signal* **2013**, *19*, 559-571, doi:10.1089/ars.2012.4938.

117. Kastlmeier, M.T.; Guenther, E.M.; Stoeger, T.; Voss, C. Lung Organoids for Hazard Assessment of Nanomaterials. *International Journal of Molecular Sciences* **2022**, *23*, 15666.

118. Duncker, H.-R. Vertebrate lungs: structure, topography and mechanics: A comparative perspective of the progressive integration of respiratory system, locomotor apparatus and ontogenetic development. *Respiratory Physiology & Neurobiology* **2004**, *144*, 111-124, doi:https://doi.org/10.1016/j.resp.2004.07.020.

119. Fountain, J.H.; Kaur, J.; Lappin, S.L. *Physiology, Renin Angiotensin System*; StatPearls Publishing, Treasure Island (FL): 2023.

120. Park, J.; Choi, S.; Takatoh, J.; Zhao, S.; Harrahill, A.; Han, B.-X.; Wang, F. Brainstem control of vocalization and its coordination with respiration. *Science* **2024**, *383*, eadi8081, doi:doi:10.1126/science.adi8081.

121. McFadden, E.R. Respiratory heat and water exchange: physiological and clinical implications. *Journal of Applied Physiology* **1983**, *54*, 331-336, doi:10.1152/jappl.1983.54.2.331.

122. Hughes, D.J.; Kipar, A.; Sample, J.T.; Stewart, J.P. Pathogenesis of a model gammaherpesvirus in a natural host. *J Virol* **2010**, *84*, 3949-3961, doi:10.1128/JVI.02085-09.

123. Yuan, X.; Nie, W.; He, Z.; Yang, J.; Shao, B.; Ma, X.; Zhang, X.; Bi, Z.; Sun, L.; Liang, X.; et al. Carbon black nanoparticles induce cell necrosis through lysosomal membrane permeabilization and cause subsequent inflammatory

response. *Theranostics* **2020**, *10*, 4589-4605, doi:10.7150/thno.34065.

124. Stoeger, T.; Reinhard, C.; Takenaka, S.; Schroeppel, A.; Karg, E.; Ritter, B.; Heyder, J.; Schulz, H. Instillation of six different ultrafine carbon particles indicates a surface area threshold dose for acute lung inflammation in mice. *Environ Health Perspect* **2006**, *114*, 328-333, doi:10.1289/ehp.8266.

125. Andre, E.; Stoeger, T.; Takenaka, S.; Bahnweg, M.; Ritter, B.; Karg, E.; Lentner, B.; Reinhard, C.; Schulz, H.; Wjst, M. Inhalation of ultrafine carbon particles triggers biphasic pro-inflammatory response in the mouse lung. *Eur Respir J* **2006**, *28*, 275-285, doi:10.1183/09031936.06.00071205.

126. Danielsen, P.H.; Bendtsen, K.M.; Knudsen, K.B.; Poulsen, S.S.; Stoeger, T.; Vogel, U. Nanomaterial- and shape-dependency of TLR2 and TLR4 mediated signaling following pulmonary exposure to carbonaceous nanomaterials in mice. *Part Fibre Toxicol* **2021**, *18*, 40, doi:10.1186/s12989-021-00432-z.

127. Thompson, A.B.; Daughton, D.; Robbins, R.A.; Ghafouri, M.A.; Oehlerking, M.; Rennard, S.I. Intraluminal Airway Inflammation in Chronic Bronchitis: Characterization and Correlation with Clinical Parameters. *American Review of Respiratory Disease* **1989**, *140*, 1527-1537, doi:10.1164/ajrccm/140.6.1527.

128. Donaldson, G.C.; Seemungal, T.A.; Patel, I.S.; Bhowmik, A.; Wilkinson, T.M.; Hurst, J.R.; Maccallum, P.K.; Wedzicha, J.A. Airway and systemic inflammation and decline in lung function in patients with COPD. *Chest* **2005**, *128*, 1995-2004, doi:10.1378/chest.128.4.1995.

129. WENZEL, S.E.; SZEFLER, S.J.; LEUNG, D.Y.M.; SLOAN, S.I.; REX, M.D.; MARTIN, R.J. Bronchoscopic Evaluation of Severe Asthma. *American Journal of Respiratory and Critical Care Medicine* **1997**, *156*, 737-743, doi:10.1164/ajrccm.156.3.9610046.

130. JATAKANON, A.; UASUF, C.; MAZIAK, W.; LIM, S.; CHUNG, K.F.; BARNES, P.J. Neutrophilic Inflammation in Severe Persistent Asthma. *American Journal of Respiratory and Critical Care Medicine* **1999**, *160*, 1532-1539, doi:10.1164/ajrccm.160.5.9806170.

131. Tecchio, C.; Cassatella, M.A. Neutrophil-derived chemokines on the road to immunity. *Semin Immunol* **2016**, *28*, 119-128, doi:10.1016/j.smim.2016.04.003.

132. Stewart, C.L.; Hook, A.L.; Zelzer, M.; Marlow, M.; Piccinini, A.M. Cellular and microenvironmental cues that promote macrophage fusion and foreign body response. *Frontiers in Immunology* **2024**, *15*, doi:10.3389/fimmu.2024.1411872.

133. Klopfleisch, R.; Jung, F. The pathology of the foreign body reaction against biomaterials. *Journal of Biomedical Materials Research Part A* **2017**, *105*, 927-940, doi:https://doi.org/10.1002/jbm.a.35958.

134. Prieditis, H.; Adamson, I.Y. Alveolar macrophage kinetics and multinucleated giant cell formation after lung injury. *J Leukoc Biol* **1996**, *59*, 534-538, doi:10.1002/jlb.59.4.534.

135. van der Strate, B.W.A.; Postma, D.S.; Brandsma, C.-A.; Melgert, B.N.; Luinge, M.A.; Geerlings, M.; Hylkema, M.N.; van den Berg, A.; Timens, W.; Kerstjens, H.A.M. Cigarette Smoke–induced Emphysema. *American Journal of Respiratory and Critical Care Medicine* **2006**, *173*, 751-758, doi:10.1164/rccm.200504-594OC.

136. Polverino, F.; Cosio, B.G.; Pons, J.; Laucho-Contreras, M.; Tejera, P.; Iglesias, A.; Rios, A.; Jahn, A.; Sauleda, J.; Divo, M.; et al. B Cell–Activating Factor. An Orchestrator of Lymphoid Follicles in Severe Chronic Obstructive Pulmonary Disease. *American Journal of Respiratory and Critical Care Medicine* **2015**, *192*, 695-705, doi:10.1164/rccm.201501-0107OC.

137. Pagán, A.J.; Ramakrishnan, L. The Formation and Function of Granulomas. *Annual Review of Immunology* **2018**, *36*, 639-665, doi:https://doi.org/10.1146/annurev-immunol-032712-100022.

138. Guest, I.C.; Sell, S. Bronchial lesions of mouse model of asthma are preceded by immune complex vasculitis and induced bronchial associated lymphoid tissue (iBALT). *Laboratory Investigation* **2015**, *95*, 886-902, doi:https://doi.org/10.1038/labinvest.2015.72.

139. Neyt, K.; GeurtsvanKessel, C.H.; Deswarte, K.; Hammad, H.; Lambrecht, B.N. Early IL-1 Signaling Promotes iBALT Induction after Influenza Virus Infection. *Frontiers in Immunology* **2016**, *7*, doi:10.3389/fimmu.2016.00312.

140. Hughes, D.J.; Kipar, A.; Leeming, G.H.; Bennett, E.; Howarth, D.; Cummerson, J.A.; Papoula-Pereira, R.; Flanagan, B.F.; Sample, J.T.; Stewart, J.P. Chemokine Binding Protein M3 of Murine Gammaherpesvirus 68 Modulates the Host Response to Infection in a Natural Host. *PLOS Pathogens* **2011**, *7*, e1001321, doi:10.1371/journal.ppat.1001321.

141. Foo, S.Y.; Phipps, S. Regulation of inducible BALT formation and contribution to immunity and pathology. *Mucosal Immunology* **2010**, *3*, 537-544, doi:https://doi.org/10.1038/mi.2010.52.

142. Marin, N.D.; Dunlap, M.D.; Kaushal, D.; Khader, S.A. Friend or Foe: The Protective and Pathological Roles of Inducible Bronchus-Associated Lymphoid Tissue in Pulmonary Diseases. *The Journal of Immunology* **2019**, *202*, 2519-2526, doi:10.4049/jimmunol.1801135.

143. Hogg, J.C.; Chu, F.; Utokaparch, S.; Woods, R.; Elliott, W.M.; Buzatu, L.; Cherniack, R.M.; Rogers, R.M.; Sciurba, F.C.; Coxson, H.O.; et al. The Nature of Small-Airway Obstruction in Chronic Obstructive Pulmonary Disease. *New England Journal of Medicine* **2004**, *350*, 2645-2653, doi:doi:10.1056/NEJMoa032158.

144. John-Schuster, G.; Hager, K.; Conlon, T.M.; Irmler, M.; Beckers, J.; Eickelberg, O.; Yildirim, A.Ö. Cigarette smoke-induced iBALT mediates macrophage activation in a B cell-dependent manner in COPD. *American Journal of Physiology-Lung Cellular and Molecular Physiology* **2014**, *307*, L692-L706, doi:10.1152/ajplung.00092.2014.

145. Barton, E.S.; White, D.W.; Cathelyn, J.S.; Brett-McClellan, K.A.; Engle, M.; Diamond, M.S.; Miller, V.L.; Virgin, H.W. Herpesvirus latency confers symbiotic protection from bacterial infection. *Nature* **2007**, *447*, 326-329, doi:10.1038/nature05762.

146. Furman, D.; Jojic, V.; Sharma, S.; Shen-Orr, S.S.; L. Angel, C.J.; Onengut-Gumuscu, S.; Kidd, B.A.; Maecker, H.T.; Concannon, P.; Dekker, C.L.; et al. Cytomegalovirus infection enhances the immune response to influenza. *Science Translational Medicine* **2015**, *7*, 281ra243-281ra243, doi:doi:10.1126/scitranslmed.aaa2293.

147. Hislop, A.D.; Annels, N.E.; Gudgeon, N.H.; Leese, A.M.; Rickinson, A.B. Epitope-specific evolution of human CD8(+) T cell responses from primary to persistent phases of Epstein-Barr virus infection. *J Exp Med* **2002**, *195*, 893-905, doi:10.1084/jem.20011692.

148. Tan, L.C.; Gudgeon, N.; Annels, N.E.; Hansasuta, P.; O'Callaghan, C.A.; Rowland-Jones, S.; McMichael, A.J.; Rickinson, A.B.; Callan, M.F.C. A Re-Evaluation of the Frequency of CD8+ T Cells Specific for EBV in Healthy Virus Carriers1. *The Journal of Immunology* **1999**, *162*, 1827-1835, doi:10.4049/jimmunol.162.3.1827.

149. Sylwester, A.W.; Mitchell, B.L.; Edgar, J.B.; Taormina, C.; Pelte, C.; Ruchti, F.; Sleath, P.R.; Grabstein, K.H.; Hosken, N.A.; Kern, F.; et al. Broadly targeted human cytomegalovirus-specific CD4+ and CD8+ T cells dominate the memory compartments of exposed subjects. *J Exp Med* **2005**, *202*, 673-685, doi:10.1084/jem.20050882.

150. Sandalova, E.; Laccabue, D.; Boni, C.; Tan, A.T.; Fink, K.; Ooi, E.E.; Chua, R.; Shafaeddin Schreve, B.; Ferrari, C.; Bertoletti, A. Contribution of herpesvirus specific CD8 T cells to anti-viral T cell response in humans. *PLoS Pathog* **2010**, *6*, e1001051, doi:10.1371/journal.ppat.1001051.

151. Doisne, J.-M.; Urrutia, A.; Lacabaratz-Porret, C.; Goujard, C.c.; Meyer, L.; Chaix, M.-L.; Sinet, M.; Venet, A. CD8+ T Cells Specific for EBV, Cytomegalovirus, and Influenza Virus Are Activated during Primary HIV Infection1. *The Journal of Immunology* **2004**, *173*, 2410-2418, doi:10.4049/jimmunol.173.4.2410.

152. Tuuminen, T.; Kekäläinen, E.; Mäkelä, S.; Ala-Houhala, I.; Ennis, F.A.; Hedman, K.; Mustonen, J.; Vaheri, A.; Arstila, T.P. Human CD8+ T Cell Memory Generation in Puumala Hantavirus Infection Occurs after the Acute Phase and Is Associated with Boosting of EBV-Specific CD8+ Memory T Cells1. *The Journal*

of Immunology **2007**, *179*, 1988-1995, doi:10.4049/jimmunol.179.3.1988.

153. Kim, J.; Chang, D.-Y.; Lee, H.W.; Lee, H.; Kim, J.H.; Sung, P.S.; Kim, K.H.; Hong, S.-H.; Kang, W.; Lee, J.; et al. Innate-like Cytotoxic Function of Bystander-Activated CD8+ T Cells Is Associated with Liver Injury in Acute Hepatitis A. *Immunity* **2018**, *48*, 161-173.e165, doi:https://doi.org/10.1016/j.immuni.2017.11.025.

154. Gaudreault, E.; Fiola, S.; Olivier, M.; Gosselin, J. Epstein-Barr Virus Induces MCP-1 Secretion by Human Monocytes via TLR2. *Journal of Virology* **2007**, *81*, 8016-8024, doi:doi:10.1128/jvi.00403-07.

155. Ariza, M.-E.; Glaser, R.; Kaumaya, P.T.P.; Jones, C.; Williams, M.V. The EBV-Encoded dUTPase Activates NF-κB through the TLR2 and MyD88-Dependent Signaling Pathway1. *The Journal of Immunology* **2009**, *182*, 851-859, doi:10.4049/jimmunol.182.2.851.

156. Michaud, F.; Coulombe, F.; Gaudreault, É.; Kriz, J.; Gosselin, J. Involvement of TLR2 in Recognition of Acute Gammaherpesvirus-68 Infection. *PLOS ONE* **2010**, *5*, e13742, doi:10.1371/journal.pone.0013742.

157. Raué, H.P.; Brien, J.D.; Hammarlund, E.; Slifka, M.K. Activation of virus-specific CD8+ T cells by lipopolysaccharide-induced IL-12 and IL-18. *J Immunol* **2004**, *173*, 6873-6881, doi:10.4049/jimmunol.173.11.6873.

158. Raué, H.P.; Beadling, C.; Haun, J.; Slifka, M.K. Cytokine-mediated programmed proliferation of virus-specific CD8(+) memory T cells. *Immunity* **2013**, *38*, 131-139, doi:10.1016/j.immuni.2012.09.019.

159. Kim, T.-S.; Shin, E.-C. The activation of bystander CD8+ T cells and their roles in viral infection. *Experimental & Molecular Medicine* **2019**, *51*, 1-9, doi:10.1038/s12276-019-0316-1.

160. Janeway CA Jr, T.P., Walport M, et al. The distribution and functions of immunoglobulin isotypes. In *Immunobiology: The Immune System in Health and Disease.*, 5 ed.; Garland Science: New York, 2001.

161. Tsuji, T.; Aoshiba, K.; Nagai, A. Alveolar Cell Senescence in Patients with Pulmonary Emphysema. *American Journal of Respiratory and Critical Care Medicine* **2006**, *174*, 886-893, doi:10.1164/rccm.200509-1374OC.

162. Kanazawa, H.; Yoshikawa, J. Elevated Oxidative Stress and Reciprocal Reduction of Vascular Endothelial Growth Factor Levels With Severity of COPD. *Chest* **2005**, *128*, 3191-3197, doi:https://doi.org/10.1378/chest.128.5.3191.

163. Calabrese, F.; Giacometti, C.; Beghe, B.; Rea, F.; Loy, M.; Zuin, R.; Marulli, G.; Baraldo, S.; Saetta, M.; Valente, M. Marked alveolar apoptosis/proliferation imbalance in end-stage emphysema. *Respiratory Research* **2005**, *6*, 14, doi:10.1186/1465-9921-6-14.

164. KASAHARA, Y.; TUDER, R.M.; COOL, C.D.; LYNCH, D.A.; FLORES, S.C.; VOELKEL, N.F. Endothelial Cell Death and Decreased Expression of Vascular Endothelial Growth Factor and Vascular Endothelial Growth Factor Receptor 2 in Emphysema. *American Journal of Respiratory and Critical Care Medicine* **2001**, *163*, 737-744, doi:10.1164/ajrccm.163.3.2002117.

165. Nel, A.; Xia, T.; Mädler, L.; Li, N. Toxic Potential of Materials at the Nanolevel. *Science* **2006**, *311*, 622-627, doi:doi:10.1126/science.1114397.

166. Li, N.; Hao, M.; Phalen, R.F.; Hinds, W.C.; Nel, A.E. Particulate air pollutants and asthma: A paradigm for the role of oxidative stress in PM-induced adverse health effects. *Clinical Immunology* **2003**, *109*, 250-265, doi:https://doi.org/10.1016/j.clim.2003.08.006.

167. Bortz, E.; Wu, T.-T.; Patel, P.; Whitelegge, J.P.; Sun, R. Proteomics of Bronchoalveolar Lavage Fluid Reveals a Lung Oxidative Stress Response in Murine Herpesvirus-68 Infection. *Viruses* **2018**, *10*, 670.

168. Yue, J.; López, J.M. Understanding MAPK Signaling Pathways in Apoptosis. *International Journal of Molecular Sciences* **2020**, *21*, 2346.

169. Rex, V.; Zargari, R.; Stempel, M.; Halle, S.; Brinkmann, M.M. The innate and T-cell mediated immune response during acute and chronic gammaherpesvirus infection. *Frontiers in Cellular and Infection Microbiology* **2023**, *13*, doi:10.3389/fcimb.2023.1146381.

170. Feng, P.; Moses, A.; Früh, K. Evasion of adaptive and innate immune response mechanisms by γ-herpesviruses. *Current Opinion in Virology* **2013**, *3*, 285-295, doi:https://doi.org/10.1016/j.coviro.2013.05.011.

171. Adler, H.; El-Gogo, S.; Guggemoos, S.; Zimmermann, W.; Beauchemin, N.; Kammerer, R. Perturbation of lytic and latent gammaherpesvirus infection in the absence of the inhibitory receptor CEACAM1. *PLoS One* **2009**, *4*, e6317, doi:10.1371/journal.pone.0006317.

172. Kahan, S.M.; Wherry, E.J.; Zajac, A.J. T cell exhaustion during persistent viral infections. *Virology* **2015**, *479-480*, 180-193, doi:https://doi.org/10.1016/j.virol.2014.12.033.

173. Liang, C.; Oh, B.-H.; Jung, J.U. Novel functions of viral anti-apoptotic factors. *Nature Reviews Microbiology* **2015**, *13*, 7-12, doi:10.1038/nrmicro3369.

174. Paris, A.J.; Guo, L.; Dai, N.; Katzen, J.B.; Patel, P.N.; Worthen, G.S.; Brenner, J.S. Using selective lung injury to improve murine models of spatially heterogeneous lung diseases. *PLOS ONE* **2019**, *14*, e0202456, doi:10.1371/journal.pone.0202456.

175. Valipour, A.; Shah, P.L.; Gesierich, W.; Eberhardt, R.; Snell, G.; Strange, C.; Barry, R.; Gupta, A.; Henne, E.; Bandyopadhyay, S.; et al. Patterns of

Emphysema Heterogeneity. *Respiration* **2015**, *90*, 402-411, doi:10.1159/000439544.

176. Idiopathic Pulmonary Fibrosis: Diagnosis and Treatment. *American Journal of Respiratory and Critical Care Medicine* **2000**, *161*, 646-664, doi:10.1164/ajrccm.161.2.ats3-00.

177. Yang, L.; Liu, Q.; Kumar, P.; Sengupta, A.; Farnoud, A.; Shen, R.; Trofimova, D.; Ziegler, S.; Davoudi, N.; Doryab, A.; et al. LungVis 1.0: an automatic AI-powered 3D imaging ecosystem unveils spatial profiling of nanoparticle delivery and acinar migration of lung macrophages. *Nature Communications* **2024**, *15*, 10138, doi:10.1038/s41467-024-54267-1.

178. Misharin, A.V.; Morales-Nebreda, L.; Mutlu, G.M.; Budinger, G.R.S.; Perlman, H. Flow Cytometric Analysis of Macrophages and Dendritic Cell Subsets in the Mouse Lung. *American Journal of Respiratory Cell and Molecular Biology* **2013**, *49*, 503-510, doi:10.1165/rcmb.2013-0086MA.

179. Minkah, N.; Macaluso, M.; Oldenburg, D.G.; Paden, C.R.; White, D.W.; McBride, K.M.; Krug, L.T. Absence of the uracil DNA glycosylase of murine gammaherpesvirus 68 impairs replication and delays the establishment of latency in vivo. *J Virol* **2015**, *89*, 3366-3379, doi:10.1128/jvi.03111-14.

180. Mu, Y.; Plummer, J.B.; Zelazowska, M.A.; Paul, S.; Dong, Q.; Chen, Z.; Krug, L.T.; McBride, K.M. A Recombinant Antibody For Tracking Murine Gammaherpesvirus 68 Uracil DNA Glycosylase Expression. *bioRxiv* **2023**, doi:10.1101/2023.05.17.541089.

181. Cheng, P.; Chen, Y.; Wang, J.; Han, Z.; Hao, D.; Li, Y.; Feng, F.; Duan, X.; Chen, H. PM2.5 induces a senescent state in mouse AT2 cells. *Environmental Pollution* **2024**, *347*, 123686, doi:https://doi.org/10.1016/j.envpol.2024.123686.

182. Wu, X.; Ciminieri, C.; Bos, I.S.T.; Woest, M.E.; D'Ambrosi, A.; Wardenaar, R.; Spierings, D.C.J.; Königshoff, M.; Schmidt, M.; Kistemaker, L.E.M.; et al. Diesel exhaust particles distort lung epithelial progenitors and their fibroblast niche. *Environmental Pollution* **2022**, *305*, 119292, doi:https://doi.org/10.1016/j.envpol.2022.119292.

183. Yu, H.; Lin, Y.; Zhong, Y.; Guo, X.; Lin, Y.; Yang, S.; Liu, J.; Xie, X.; Sun, Y.; Wang, D.; et al. Impaired AT2 to AT1 cell transition in PM2.5-induced mouse model of chronic obstructive pulmonary disease. *Respiratory Research* **2022**, *23*, 70, doi:10.1186/s12931-022-01996-w.

184. Choi, S.; Kim, E.-M.; Kim, S.-Y.; Choi, Y.; Choi, S.; Cho, N.; Park, H.-J.; Kim, K.K. Particulate matter exposure exacerbates cellular damage by increasing stress granule formation in respiratory syncytial virus-infected human lung organoids. *Environmental Pollution* **2022**, *315*, 120439, doi:https://doi.org/10.1016/j.envpol.2022.120439.

185. Issa, R.; Lozano, N.; Kostarelos, K.; Vranic, S. Functioning human lung organoids model pulmonary tissue response from carbon nanomaterial exposures. *Nano Today* **2024**, *56*, 102254, doi:https://doi.org/10.1016/j.nantod.2024.102254.

VIII. LIST OF PUBLICATIONS

Kastlmeier, M.T.; Guenther, E.M.; Stoeger, T.; Voss, C. **Lung Organoids for Hazard Assessment of Nanomaterials**. *International Journal of Molecular Sciences* 2022, *23*, 15666.

Kastlmeier, M.T.; Gonzalez-Rodriguez, E.; Cabanis, P.; Guenther, E.M.; König, A.-C.; Han, L.; Hauck, S.M.; See, F.; Asgharpour, S.; Bukas, C.; et al. **Cytokine signaling converging on IL11 in ILD fibroblasts provokes aberrant epithelial differentiation signatures**. *Frontiers in Immunology* 2023, 14.

IX. ACKNOWLEDGEMENTS

Zuallererst möchte ich mich bei meinem Betreuer Dr. Tobias Stöger bedanken, dafür, dass ich in der AG Stöger so herzlich aufgenommen wurde, für die wirklich großartige Betreuung, die vielen hilfreichen Diskussionen, die stetige Unterstützung, Motivation und deine Begeisterung für die Thematik.

Ein großes Dankeschön geht auch an meinen Betreuer Prof. Dr. Heiko Adler. Vielen Dank für die herzliche Betreuung, die Möglichkeit, in deinem Labor zu arbeiten, die großartige Unterstützung, trotz der vielen Veränderungen, und die dauerhafte Erreichbarkeit für Diskussionen und Austausch.

Des Weiteren möchte ich mich bei Prof. Dr. Eckhard Wolf für die Betreuung meiner Doktorarbeit an der tierärztlichen Fakultät bedanken.

Vielen lieben Dank auch an die Unterstützung von Dr. Carola Voss. Danke, dass du mir die Welt der Organoide gezeigt hast, für deine stetige Hilfe bei den Experimenten und deine wertvollen Ideen.

A big thank you to all the members of “AG Stöger”. Thanks for the tremendous help, whenever it was needed, the fun birthday parties, the scientific discussions in the office and lovely activities outside. Thank you, Verena and Lianyong, for introducing me to this project and the constant help. Thanks David, for your help and support regarding all of the animal experiments and everything else in the lab. Thank you, Miriam, for your support and help in and beyond the lab. Thanks to Camille for your support regarding the organoids. Thanks to all members of this working group, Markus, Yasmin, Hongyu, Haiyun, Guo, Jiating, Osama, Chenxi and Qiongliang, I had such a good time with you in the past four years.

Ein besonderer Dank geht an meine Freunde, danke für die mentale Unterstützung, die schöne gemeinsame Zeit und Ablenkung, besonders Lucie, Birte und Pauline.

Ganz besonders möchte ich mich bei dir bedanken, Leo. Danke für deine wunderbare Unterstützung und dass ich mich auf dich verlassen kann.

Zu guter Letzt danke ich von ganzem Herzen meinen Eltern und meinen beiden Schwestern – danke, dass ihr mich immer unterstützt und für mich da seid. Dank euch habe ich das alles geschafft.